PACE
SYSTEMS

QUARTERLY REPORT NO.2
ROLLUP SUBSOLAR ARRAY

Prepared for: Jet Propulsion Laboratory

Prepared Under: Contract 952314
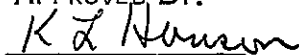
GENERAL ELECTRIC

ROLLUP SUBSOLAR ARRAY

QUARTERLY TECHNICAL REPORT NO. 2

1 JUNE 1969 TO 31 AUGUST 1969

PREPARED FOR:

JET PROPULSION LABORATORY
CALIFORNIA INSTITUTE OF TECHNOLOGY
PÁSADENA, CALIFORNIA

PREPARED UNDER UNDER: CONTRACT 952314
CONTRACTING OFFICER: E.C. FLARITY
PROJECT MANAGER: W.A. HASBACH

APPROVED BY:

K.L. HANSON,
PROJECT MGR.

GENERAL ELECTRIC

SPACE SYSTEMS ORGANIZATION
Valley Forge Space Center
P O Box 8555 • Philadelphia, Penna 19101

TABLE OF CONTENTS

TABLE OF CONTENTS (Cont'd)

LIST OF ILLUSTRATIONS

LIST OF ILLUSTRATIONS (Cont'd)

LIST OF TABLES

ABSTRACT

Results of the activities performed during the second quarter of the project to design and develop the technology of a 30 watt per pound rollup solar array are reported. The major effort during this quarter was devoted to the detailed design of component parts. Each component is described and the associated performance analysis in support of the design is presented. System test planning has been started and the design requirements for the supporting equipment are established along with preliminary implementation concepts.

SECTION 1

INTRODUCTION AND SUMMARY

A program to generate a detailed design, fabricate, assemble and test a 250 square foot roll-up subsolar array, capable of providing a minimum of 30 watts of electrical power per pound of subsolar array weight, was initiated March 5, 1969. The term subsolar array is used to indicate the item is one unit of a solar array system that utilizes four identical units to provide the electrical power requirements for an interplanetary spacecraft design concept. Each subsolar array is a complete subsystem with respect to spacecraft applications and the design requirements are intended to provide technology that applies to other mission applications. An extensive environmental test program is planned to establish the integrity of the design for spacecraft applications, to provide performance data, and to verify analysis techniques that will have application to large-area lightweight solar array designs based on the rollup concept.

The design of the rollup subsolar array is based on the concepts and technology developed in the Feasibility Study for a 30 Watts per Pound Rollup Solar Array (JPL Contract 951970) and was documented in Reference 1. For convenience, the 250 square foot rollup subsolar array unit will be referred to as the RA250.

This Second Quarterly Report describes the technical results achieved from June 1 through August 31, 1969. During this period, program emphasis was on the detailed design and supporting analyses of the RA250 system. Procurement of long lead items was continued and the design of support equipment initiated. Preliminary test planning was accomplished. The overall project schedule is shown in Figure 1-1.

A design description of each major system component is presented along with the associated drawings. A weight computation based on these design drawings has yielded a calculated weight of 80.02 pounds for the complete RA250 system. The resulting power-to-weight ratio is 31.2 watt/lb based on a specific power of 10 watt/ft^2 for 250 ft^2 of gross solar cell module area.

EVENTS	1969										1970			
	M 1	A 2	M 3	J 4	J 5	A 6	S 7	O 8	N 9	D 10	J 11	F 12	M 13	A 14
PROGRAM PLAN		◇▼												
ANALYSIS		◇ ▲					▽							
DETAIL ARRAY DESIGN		◇ ▲			▽									
JPL DESIGN REVIEWS		◇▼			▼					▽				
FABRICATION CYCLE						△	▲			▽				
SUPPORT EQUIPMENT DESIGN					▲		▽							
SUPPORT EQUIPMENT FABRICATION							△		▽				▽	
DETAILED TEST PLAN									▽					
DEVELOPMENT TESTS					▲				▽					
ARRAY TEST SEQUENCE											△			▽
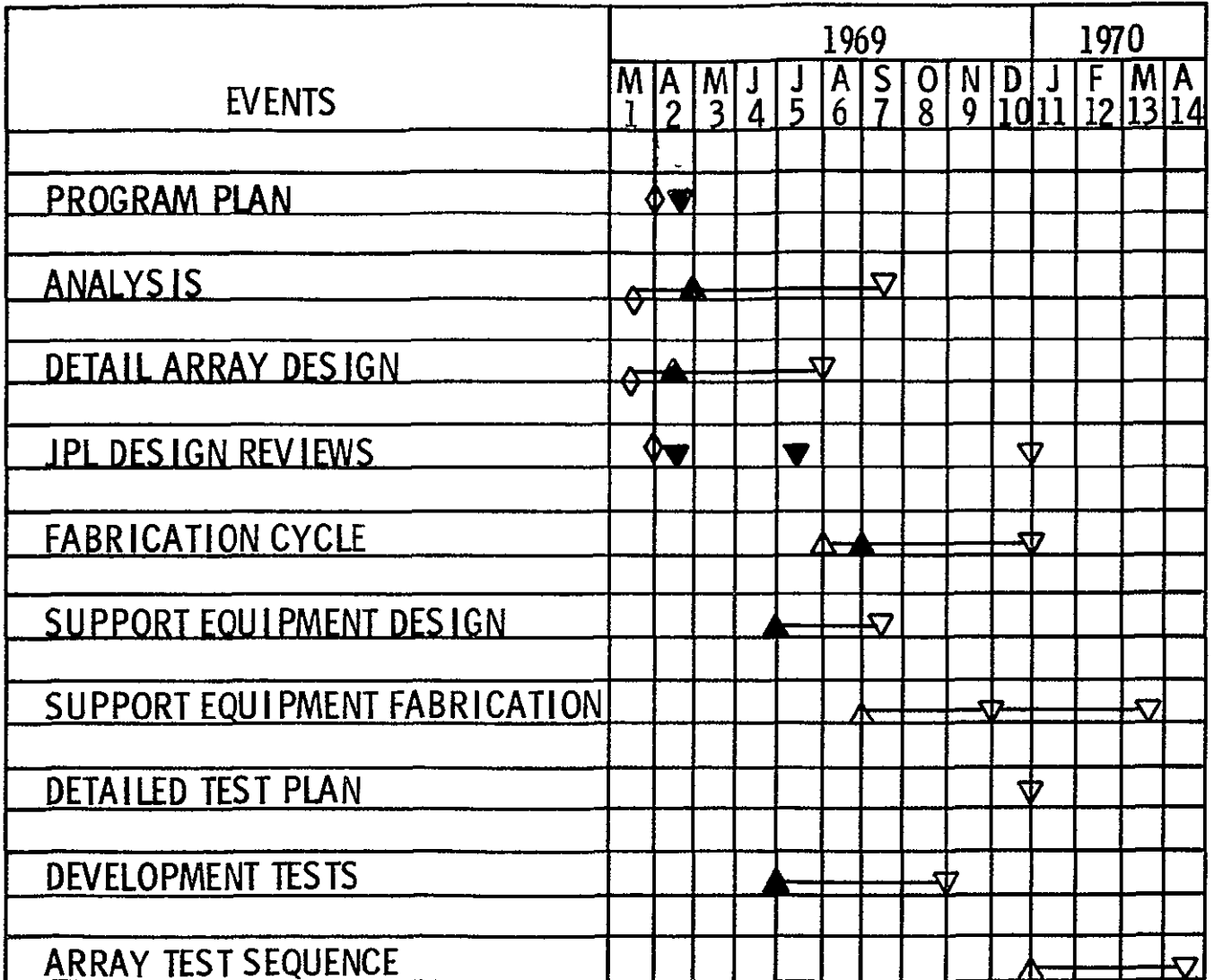
Figure 1-1. Master Schedule

Supporting performance analyses are included in the following areas: thermal, magnetic fields, deployed dynamics, stowed configuration dynamics and stress, reliability, and electrical performance.

The solar cell module interconnection soldering process has been developed and is being further refined in preparation for the assembly of the engineering prototype solar array blanket. The necessary tooling has been defined and is in the progress of design and fabrication.

The system test activity has been concerned with the preliminary planning and the definition of the support equipment requirements. The development testing has included a comparative evaluation of the bending stiffness of dummy solar cell module configurations with different types of simulated interconnections. Preliminary planning for a development test program to determine the thermal bending characteristics of the BI-STEM has been completed.

Support equipment design has been started. The approach to the upward deployment aid has been established.

SECTION 2
SYSTEM DESCRIPTION

2.1 CONFIGURATION AND FUNCTIONAL ARRANGEMENT

The RA250 Rollup Subsolar Array system provides 250 square foot of deployable solar
cell array which is stored on a drum during launch. The schematic arrangement of the
system in the deployed configuration is shown in Figure 2.1-1. Solar cells are mounted
on two flexible panels of Kapton-H film [each panel is 46.06 inches by 409.35 inches] .
Tension in this substrate is utilized to maintain the desirable single plane geometry and to
establish the natural frequency of the system slightly above the required 0.04 Hz. Six
major elements combine to form the RA250 power producing system: (1) the array blankets,
(2) the single BI-STEM solar panel actuator, (3) the storage drums, (4) the center support,
(5) the leading edge member, and (6) the outboard end supports. Figure 2.1-2 shows the
assembly of these various components to form the system.
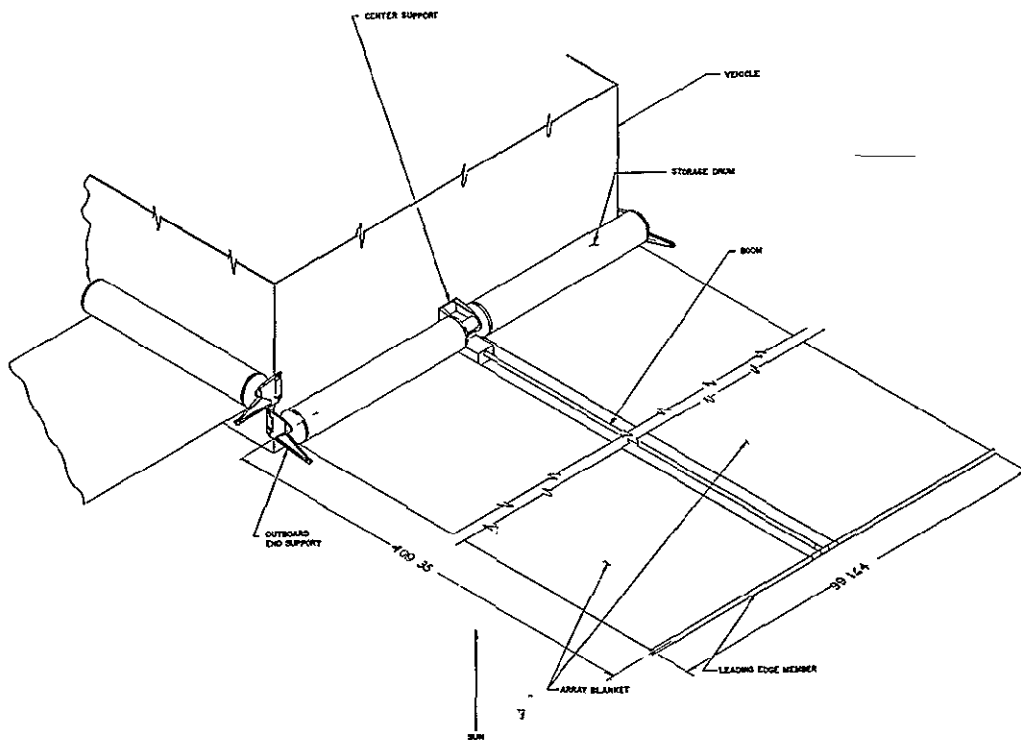
Figure 2.1-1. RA250 Deployed Configuration

2.1.1 SOLAR ARRAY BLANKETS

Each of the two solar cell array blankets accommodates six 102-volt circuits which feed to a common blanket mounted busbar. The power is transmitted along array-mounted busbars on the underneath side of the panel until it reaches the feedthrough interface on the drum skin. At the design operating point the current is 24.739 amps (power = 2523 watts) for the designated temperature of 55°C. The array blankets are the major weight influence on the system contributing 45.97 pounds of the total 80.02 pounds. Interlayer cushioning buttons of foamed RTV560 are bonded to the underside of the blankets to enable survival of the launch dynamics environments. Attachment to the drums is made by bonding. Attachment to the leading edge member is made by looping the Kapton substrate around it.

Fabrication of the array blanket proceeds by assembling modules (19 parallel by 20 or 22 cells in series) and installing them on the substrate which includes the busbars and the foamed rubber pads.

Interconnection of the solar cells is by soldering of a formed silver mesh interconnection. The soldering process employs an infrared lamp as the heat source. Precise control of the amount of solder is planned by preplating the interconnections, a method which provides control of solder position and quantity. Modules will be electrically tested before bonding on the substrate.

The substrate starts as a sheet of Copper Clad Kapton (Schjel-Clad L7510) which is etched to remove all copper, except that of the busbar network. Busbar insulation and jumper connections are installed and the foamed RTV cushioning buttons are installed before the final assembly operation during which the modules are installed and interconnected.

PLAN VIEW (ARRAY DEPLOYED)
SCALE 1/10

VIEW C (3X1)

SECTION AA (1/12)
SECTION ROTATED 90° CCW
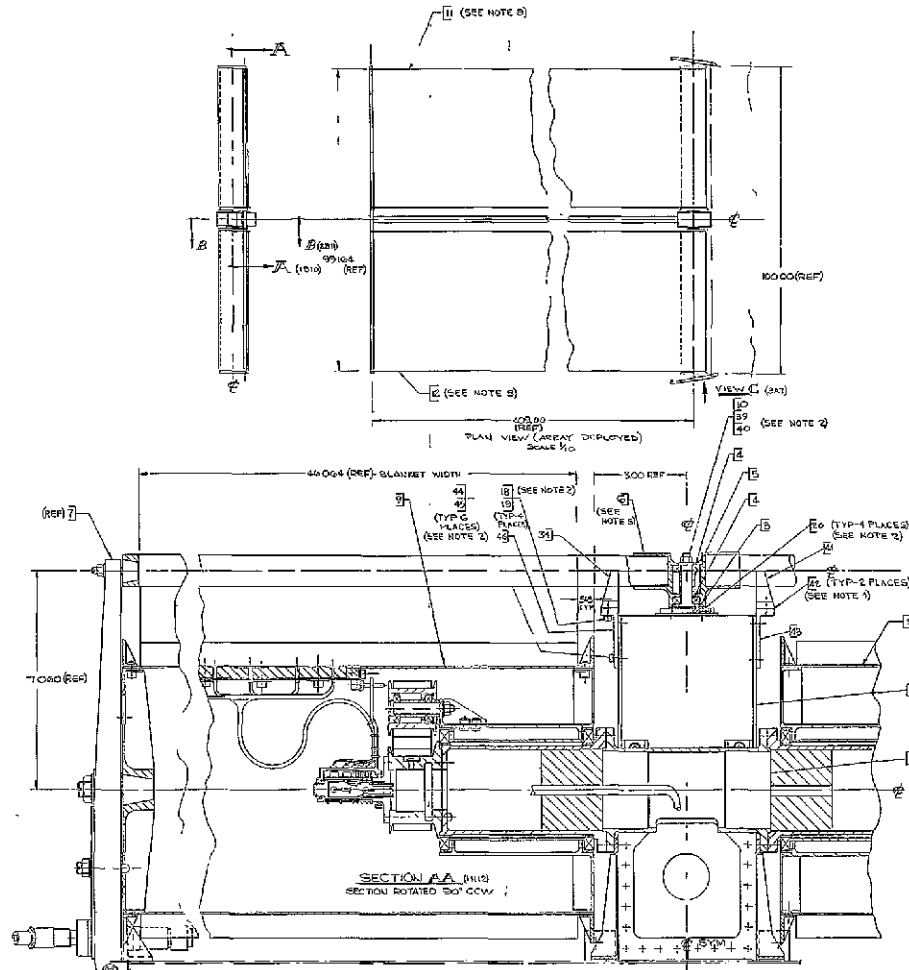
NOTES
1- INTERPRETATION OF DRAWING TERMS AND
   TOLERANCES PER 11BA1664
2- TORQUE FASTENERS AS FOLLOWS
   - 6-32- 7-8 IN-LBS   1/4-28-50-60 IN-LBS
   - 8-32- 12-15 IN LBS
   - 10-32- 30-35 IN LBS
   INSTALL ITEM 32 WITH 100 IN-LBS TORQUE
3- INSTALL CONNECTOR, ITEM 10, TO ACTUATOR LEADS
   PER 530028 USING LACING TAPE, ITEM 57
4- USE .050 SHIM, ITEM 12, INITIALLY, FOR SADDLE
   INSTALLATION
5- USING BOOM ACTUATOR, ITEM 9, UNDER POWER,
   REST LEADING EDGE, ITEM 6, ON SADDLES, ITEM 3&4&1
6- END SUPPORT INSTALLATION
   a- PREASSEMBLE THE FOLLOWING
        MOVEABLE ARMS   - ITEMS 7 & 25
        HINGE PINS   - ITEM 28
        HINGE BRACKETS - ITEMS 21 & 26
        SEPARATION BOLTS - BOLTS-ITEMS 8 & 35
        BOLT CATCHERS   - ITEM 33
        TAPER PLUGS   - ITEMS 30 & 31
        TORSION SPRINGS - ITEMS 27 & 36
   b- HINGE PIN, ITEM 28 SHALL BE CENTERED
      SUCH THAT AFTER INSTALLATION OF NUTS,
      ITEM 22, THREADED PORTION OF PIN SHALL
      NOT ENGAGE BRACKETS, ITEMS 21 & 26
      HINGE NUTS, ITEM 22, SHALL BE SNUG FIT
   c- ADJUST DRUM TAPER PLUGS, ITEM 30, SO THAT
      PIN IS PERPENDICULAR (VISUAL ORIENTATION) TO
      OUTBOARD END CAP AND SECURE HINGE
      BRACKETS, ITEMS 21 & 26
      CAUTION VERIFY THAT LOCATOR PINS, ITEM
      29, IS ENGAGED WITH THE OUTBOARD END
      CAP IT MAY BE NECESSARY TO ROTATE
      THE DRUM, ITEM 9, TO ACHIEVE PIN ENGAGE-
      MENT
      NOTE IT MAY BE NECESSARY TO HOLD
      LEADING EDGE DOWN TO ENGAGE TAPER
      PLUGS, ITEM 31 SECURE BOTH ENDS OF
      LEADING EDGE SIMULTANEOUSLY
   d- TORQUE DRUM TAPER PLUG, ITEM 30, TO
      100-110 IN-LBS
   e- SNUG FIT LEADING EDGE TAPER PLUGS, ITEM 31
7- IF AFTER COMPLETION OF 4,5&6 ABOVE, THE
   LEADING EDGE IS NOT FIRMLY SECURED, INCREASE
   SHIM, NOTE 4, AND REPEAT NOTES 5 & 6 DO
   NOT SHIM BEYOND .0150 THICKNESS
8- SOLDER ARRAY, ITEMS 11&12, TO DRUM ASSY, ITEM 9,
   USING ITEM 46 PER NASA SPEC NHB5300.4
   BOND ARRAY TO DRUM ASSY USING ITEM 49 PER
   ITEM 50
   CAUTION - PRIOR TO SOLDERING & BONDING,
   ALIGN ARRAY SO THAT MAX OVERLAP IN
   EITHER DIRECTION IS 0.100" IN ROLLED UP
   POSITION

THIS ASSEMBLY CONTAINS EXPLOSIVES

Figure 2.1-2. RA250 Assembly (Sheet 1 of 2)

Fold Out

6 (REF)

⊄ LEADING EDGE

1.308 (REF)

2.700 (REF)

15
13 (TYP-16 PLACES)
    SEE NOTE 2

(REF) 2

5.700 (REF)

(REF) 1

⊄ DRUM AND
  CENTER SUPPORT

11.000 (REF)

5.500 (REF)

16
47
(SEE NOTE 3)

9 (REF)

1 (REF)

⊄

13
14
(UND HD) 15
(TYP-2 PLACES)
SEE NOTE 2

SECTION "B B" (1H12)

(ROTATED 180°)
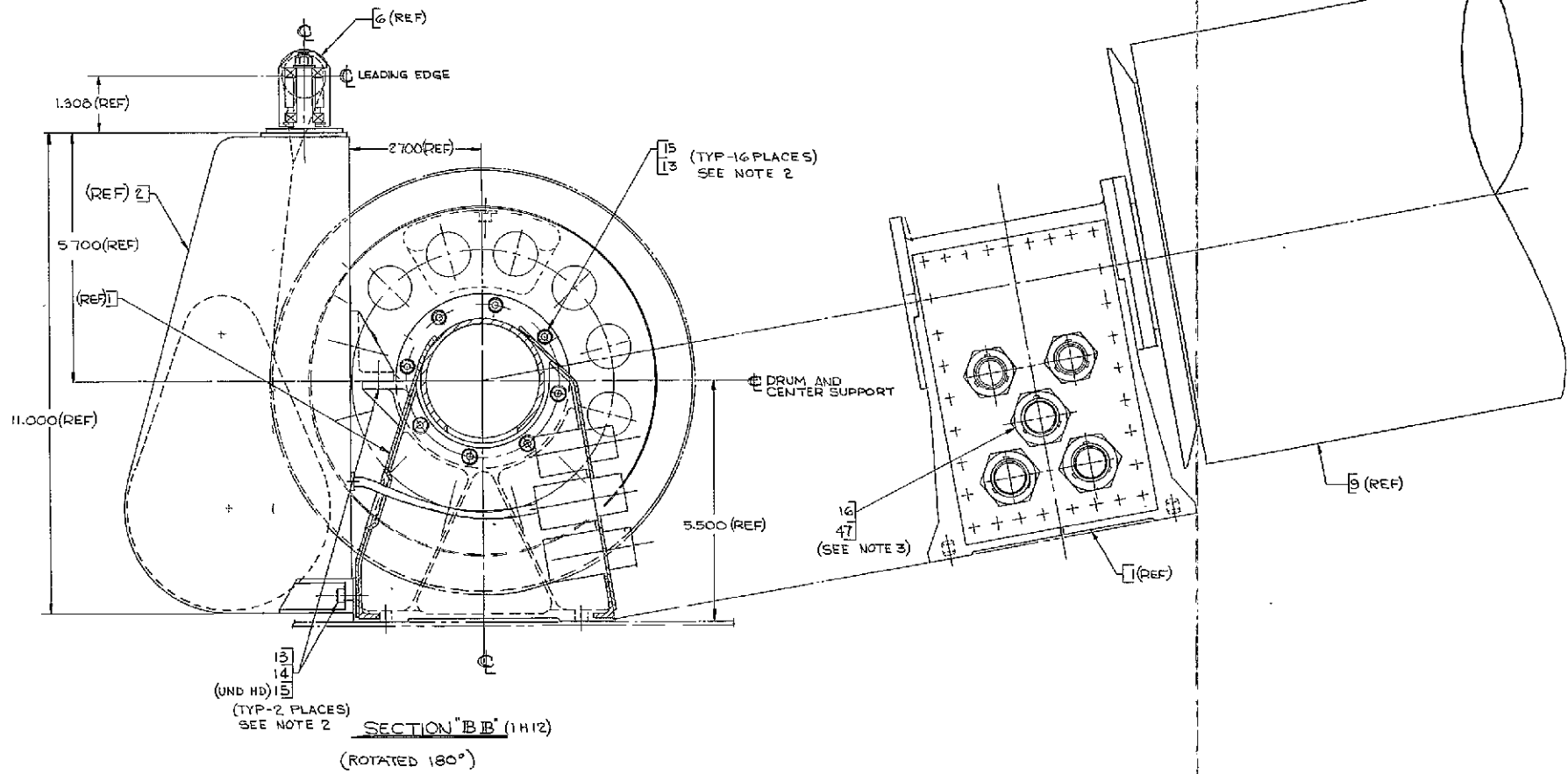
Figure 2.1-2. RA250 Assembly (Sheet 2 of 2)

Fold Out

2.1.2 BI-STEM SOLAR PANEL ACTUATOR

The backbone of the deployed configuration structure is the BI-STEM erection rod (1.34-inch-diameter, 0.007-inch-thick stainless steel) which provides the support strength and outboard end positioning control during the transition from stowed to deployed configurations. The rod strength is sufficient to overcome the tensioning forces transmitted through the array blanket throughout the 33.5 feet linear travel. Its strength is also sufficient to keep the out-of-plane geometry of the deployed configuration within ± 10 degrees from its basic position normal to the spacecraft centerline.

The BI-STEM operates as a pin-ended column for the space condition where the absence of a gravitational component results in a simple axial loading with the line of action passing through the ends. The compressive force is 4 pounds, which provides the blanket tension so the natural frequency will exceed the 0.04 Hz specified.

In the earth environment, the BI-STEM closely approximates a fixed-free column with respect to buckling. The rod strength is such that unaided deployments can be performed while supporting the combined tension load and leading edge member weight load, but not the blanket loads. Counterweighting to compensate for the blanket load with a deployment aid enables rod actuation of the array system in the 1-G environment.

2.1.3 STORAGE DRUMS

The principal function which establishes the storage drum configuration is that of supporting the solar cell blankets during launch. An 8-inch-diameter configuration has been established based on prior vibration and acoustic testing. Stress studies established that "simple support" at each end of the drum resulted in the overall lightest configuration. The drum lengths are 47.1 inches, an inch wider than the blankets in order to accommodate guide flanges for tracking during retraction. Additional features incorporated into the drum component are the blanket tensioning control through utilization of a Négator spring and power transfer through the rotary joint between the array blankets and the spacecraft. The feed-through consists of two harnesses and a slip ring assembly. Both power and telemetry signals are transmitted through the joint.

The inboard end assembly forms a major subassembly of the drum. This unit includes the stationary support shaft, on which are ground the bearing mounting diameters, the bearings, and the inboard end cap housing which rides on the bearing. In addition, the Negator spring take up spool and output spool are attached to the end cap and shaft, respectively, enabling inspection and test of this function at the subassembly stage. The slip ring and its feedthrough harnesses are also attached to the inboard end assembly allowing a complete electrical check of these components before their assembly into the drum.

The assembly sequence is to install the inboard assembly into the drum shell, and then to close the assembly with the installation of the outboard end cap. The array assembly is then mounted and connected to the drum with external operations.

2.1.4 CENTER SUPPORT

The single point interface between the deployed subarray system and the spacecraft is provided by the center support structural component. The unit provides the mounting and electrical interfaces for the major system components, the storage drums and the BI-STEM actuator. Construction is a magnesium riveted structure with pads for the two drums on opposite sides and pads for the BI-STEM at 90 degrees and in the same plane. Pass-through access for the electrical harnesses which pass through the drum shafts is accommodated by a hole in the center support shaft and the harness end connectors are mounted on the center support and become the spacecraft electrical interface.

2.1.5 LEADING EDGE MEMBER

Support of the outboard ends of the solar cell blankets is provided by the 1.0-inch diameter leading edge member. The leading edge mounts through bearings on the outer end of the BI-STEM, thereby maintaining torsional freedom between the rod and blankets and allowing the tensioning to maintain the array blanket in the plane of the tangent to the drum.

Construction of the leading edge is essentially that of a beryllium tube, the material choice being principally to achieve a lightweight, stiff member. Minimization of the droop deflection aids the uniformity of load distribution across the ends of the solar array blanket and ensures that the deployed dynamics characteristics are established.

2.1.6 OUTBOARD END SUPPORTS

The need for simple support of the drums and for caging of the outer ends of the blankets during launch is fulfilled by outboard end supports which are engaged only during the stowed configuration. These supports provide a direct structural tie to the spacecraft at the outboard ends of the drums and leading edge member. The attachment to the subarray components is by conical plug and socket joints to enable end plug release as the initial function in the deployment sequence. A spring-loaded hinge joint actuates the release following a pyrotechnic actuation of a separation nut used to secure the stowed configuration lock-up.

2.2 WEIGHT AND POWER SUMMARY

A detailed weight calculation has been performed based on the released design drawings. The results of this calculation are summarized in Table 2.2-1. The total RA250 subsolar array system weight is calculated to be 80.02 pounds which can be broken down into the following general categories:

	Weight (lb)	Fraction of Total Weight
• Structure	21.91	0.274
• Array Blankets	45.97	0.574
• BI-STEM Boom Actuator	12.14	0.152
	80.02	1.000

Table 2.2-1. Weight Summary

Nomenclature	Drawing No.	Unit Weight (lb)	Qty/Next Assy	Weight (lb)
Subsolar Array Assembly	47E214519			80.016
Center Support Assy	47E218547	1.590	1	1.590
Leading Edge Assy		0.800	1	0.800
Leading Edge	47D218544	0.620	1	
Post	47C218546	0.111	1	
Spacer	47B218545	0.009	1	
Bearing	47C218349	0.030	2	
Outboard End Support Assy		2.315	2	4.630
Moveable Arm	47E218539	0.532	1	
Bracket	47D218540	0.200	1	
Separation Nut	47C218327	0.425	1	
Bolt Catcher	47C218329	0.280	1	
Pressure Cartridge	47D218330	0.100	2	
Spring	47C218542	0.182	1	
Pin Locator	47B218536	0.044	1	
Hinge Pin	47B218529	0.133	1	
Taper Plug	47B218527	0.075	1	
Taper Plug	47B218526	0.193	1	
Bolt	47B218805	0.051	1	
Boom Actuator	47E214524	12.000	1	12.000
Connector	U54-14-19P-5037	0.140	1	0.140
Drum Assembly	47E218804	7.443	2	14.886
Drum Shell	47E218194	1.780	1	
Guide Flange	47E218535	0.285	2	
Stud	47B218802	0.004	1	
Stud Mtg Plate	47B218803	0.004	1	
Inboard End Cap Assy	47E218549	4.688	1	
Inboard End Cap	47E218194	1.190	1	
Support Shaft	47D218532	0.680	1	
Bearing	47C218344	0.260	2	
Brg Spacer	47C218533	0.220	1	
Slip Ring Assy	47B214689	0.620	1	
Negator Spring	47C218538	0.490	1	
Output Spool	47C218534	0.244	1	
Take-up Spool	47C218541	0.070	1	
Spacers	47B218548	0.004	1	
Power Feed Thru	47D218801	0.200	1	
Brg, Take-up Spool	47C218349	0.030	1	
Bolt, Take-up Spool	47C218800	0.060	1	
Connector	U54-14-5S-5073	0.140	1	
Connector	U54-12-10P-5073	0.120	1	
Harness		0.10	1	
Outboard End Cap	47E218194	0.397	1	
Array Blanket Assy	47J214517	22.985	2	45.970

The power summary for this system is presented in Table 2.2-2 to show the expected electrical power output at the center support interface connectors.

The power-to-weight ratio for the RA250 is calculated based on a specific output of 10 watt/ft^2 for 250 ft^2 of solar cell module area. Computed on this basis, the power-to-weight ratio is

$$\frac{2500}{80.02} = 31.24 \text{ watt/lb}$$

Table 2.2-2. Power Summary

	Power (watts)
● Array Raw Output	2523.
55°C Array Temperature	
10° Angle of Incidence	
6% Short-Circuit Current Loss	
● Array Bus Strip Loss at 55°C	50.
● Slip Ring and Harness Loss	12.
Net Power Available at Spacecraft Interface	2461.

SECTION 3

DESIGN OF SYSTEM ELEMENTS

3.1 ARRAY BLANKET

3.1.1 FLIGHT DESIGN

The flight design solar array consists of two blankets (or panels) each 46.06 inches wide by 402.3 inches long, with end leader pieces extending beyond the cells at both ends. Each blanket carries six circuits each of 242 cells in series by 19 cells in parallel. Each circuit is composed of twelve series-connected modules (eleven 20 series by 19 parallel and one 22 series by 19 parallel). Figure 3.1-1 shows the assembly drawing of one such blanket of the subsolar array. This drawing shows the six circuits arranged on the 2-mil Kapton-H film substrate. This substrate (shown in Figure 3.1-2) is fabricated from copper-clad Schjel-clad L-7510 which is photo-etched to form a conductor bus strip river-tributary system, with each circuit feeding into the main positive and negative bus which in turn connects to the power feed-through at the drum. Individual circuit diode isolation is not presently planned. Additional bus strip runs have been added to the substrate to enable installation of high-and-low temperature range thermistors on the panel. These also connect to the feedthrough section of the drum and the signal slip rings.

Figure 3.1-3 shows the bus strip connections for each individual circuit. Each circuit has been sketched separately to clarify the information contained on the drawing of Figure 3.1-1. Note that all connections from the cell side of the substrate to the bus strip system are around the edges rather than through holes in the substrate. These connections are made with Schjel-Clad L-7510 which is bonded to the Kapton substrate with SMRD-745 adhesive and soldered to the solar cell modules on the front and the bus strips on the rear. The exposed copper bus strips on the rear side of the substrate are covered with Kapton which is bonded in place with SMRD-745 adhesive.

Table 4.4-2. Ultimate Shear Load Summary

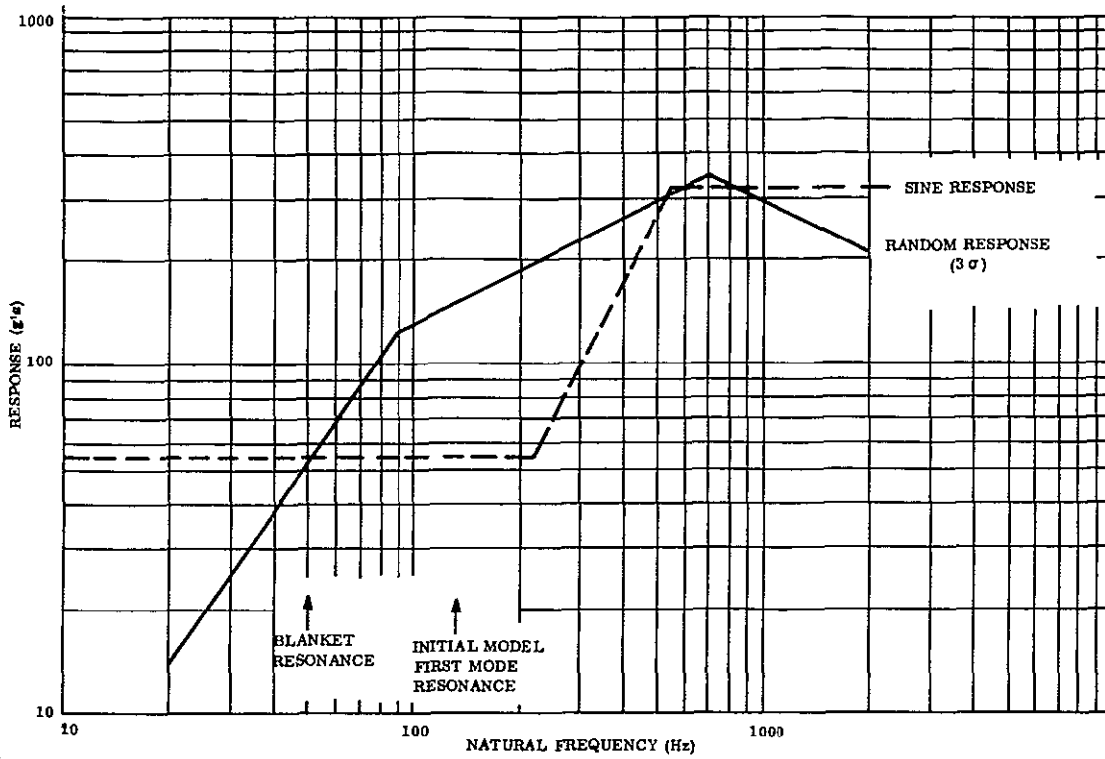| Mass Point	Symmetric Mode		Antisymmetric Mode		
	1	2	1	2	3
X_1		46			76
Y_1			501		
Z_1	111			181	
X_2		286			453
Y_2			643		
Z_2	402			526	
X_3		437			603
Y_3			638		
Z_3	562			648	
X_4		469			519
Y_4			629		
Z_4	574			530	
X_5		346			252
Y_5			512		
Z_5	409			245	
X_6		149			108
Y_6			213		
Z_6	176			105	
X_7		162		No Motions Allowed	
Y_7			303		
Z_7	190				

NOTE: All loads are in pounds force

Figure 4.4-2. Structural Response of a Single Degree of Freedom System as a
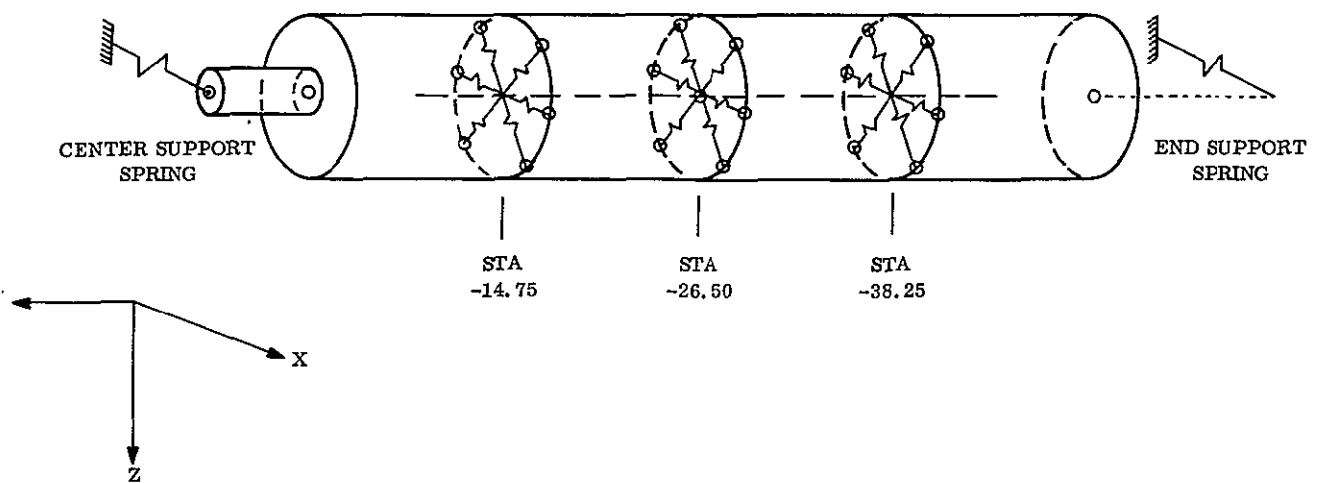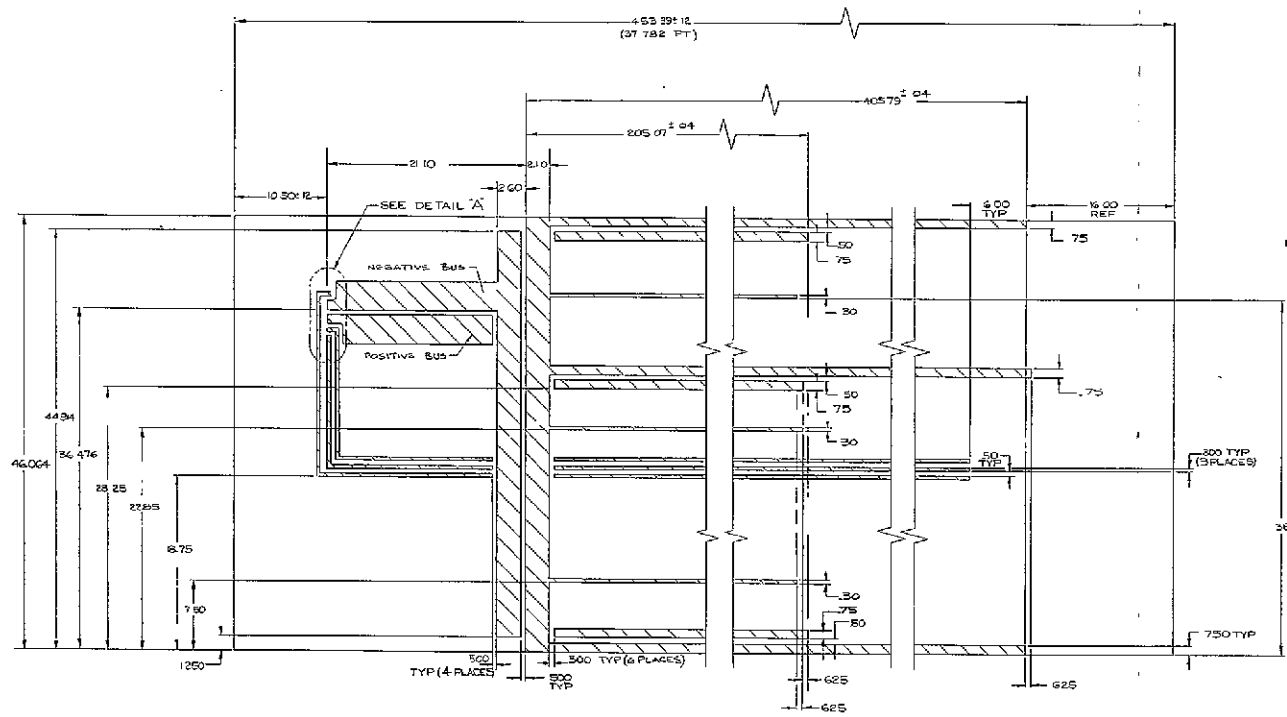Function of Natural Frequency (Q = 12)

Figure 4.4-3. Final Dynamic Model
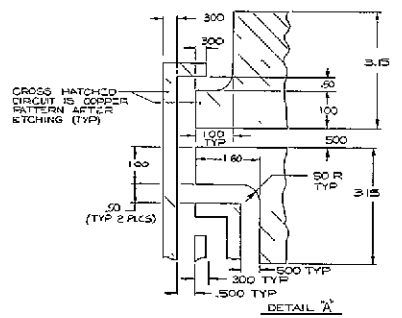
Figure 3.1-2. Array Substrate
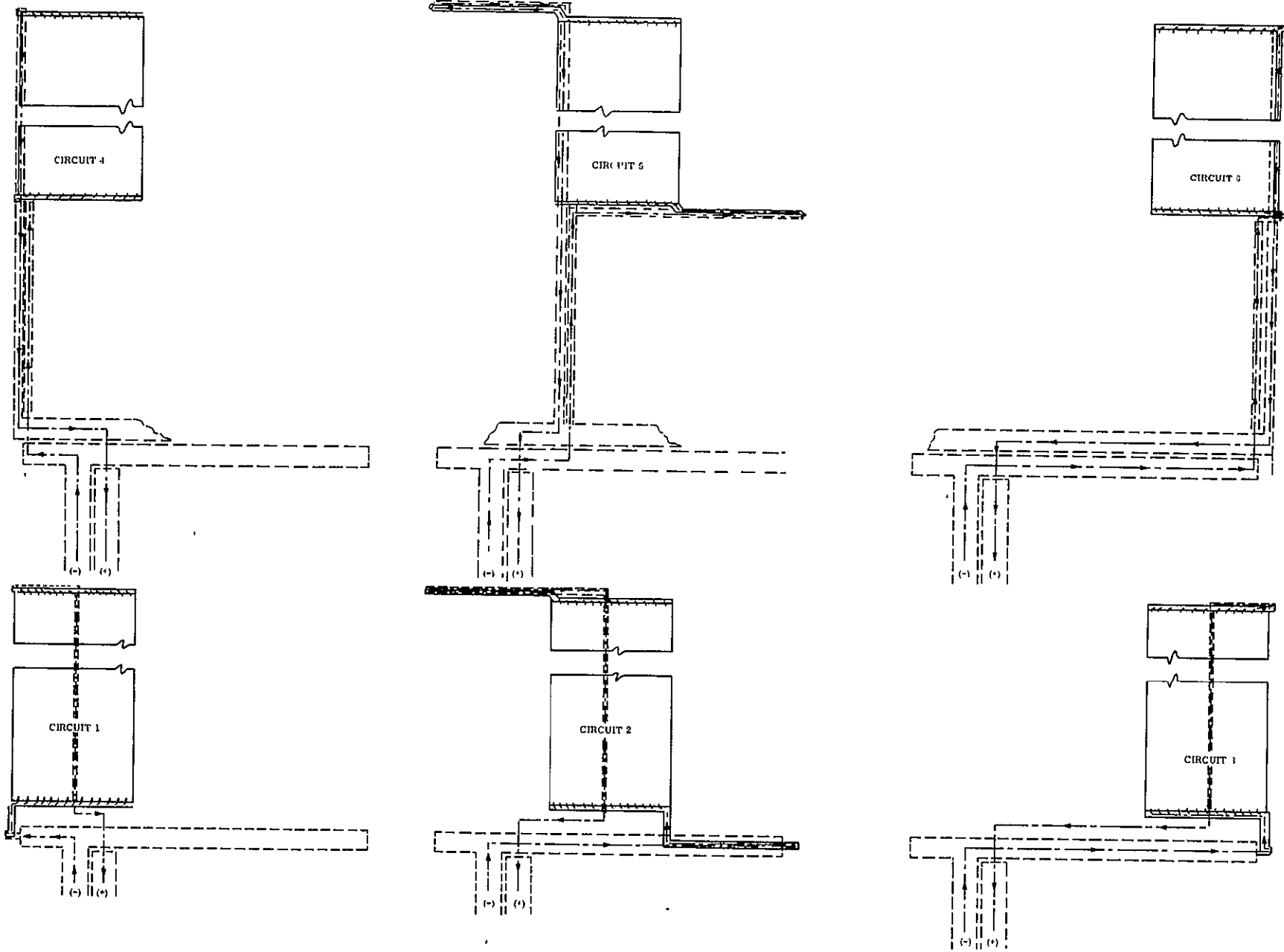
Figure 3.1-3. Individual Circuit Bus Strip Arrangement

Foamed RTV560 cushioning buttons are deposited on the rear side of the substrate at the •

corners of each solar cell. These buttons supply the required interlaying cushioning in the

stowed configuration. Each button is 0.188 inch in diameter by 0.040 inch high.

The solar cell module which forms the basic building block within each circuit is shown in

Figure 3.1-4. Within this module, the solar cells are interconnected using 2Ag5-5/0 flattened

silver expanded metal. It takes five interconnection segments to reach across the 19-cell

width of the module with the butt between interconnections occuring at the center of cells as

shown in Detail A of Figure 3.1-4. The coverglass is bonded to the solar cell with Sylgard

182.

3.1.2 PROTOTYPE DESIGN

The engineering prototype array blankets will be fabricated, for economic reasons, with only

10 percent active solar cell coverage. The remaining area will be covered with dummy glass

to simulate the mass properties of the solar cells. Figure 3.1-5 shows the planned arrange-

ments of active solar cell modules on the two prototype blanket assemblies. A total of fifteen

19 by 20 cell modules will be placed at selected locations on the blankets These locations

have been selected to yield a representative sampling of the various environments in the

wrapped configuration.

The dummy glass modules will be fabricated from 0.011 by 0.750 by 0.750 pieces of Corning

0211 Microsheet. This glass will be bonded directly to the Kapton substrate with SMRD 745.

Various techniques for simulating the stiffness of the expanded metal interconnections are

being evaluated for the dummy modules. Some preliminary test results are reported in

Section 6.1.1.
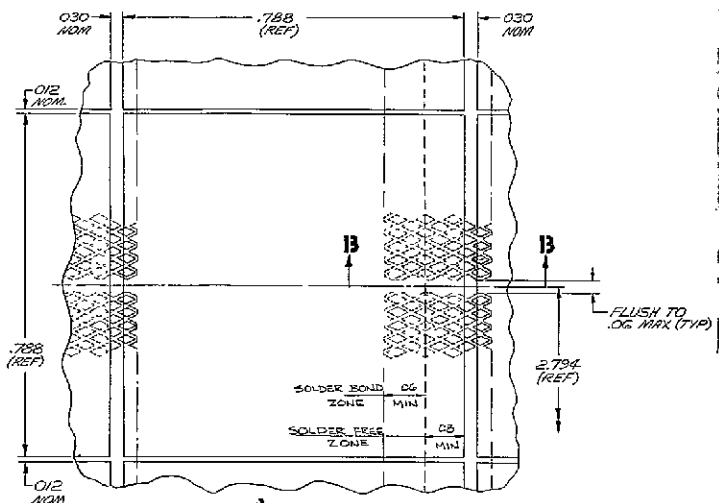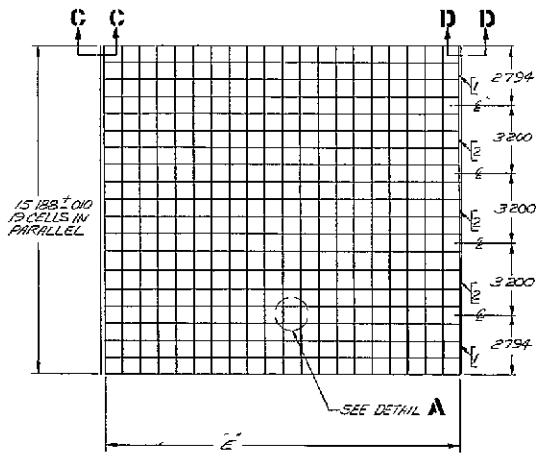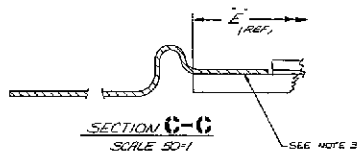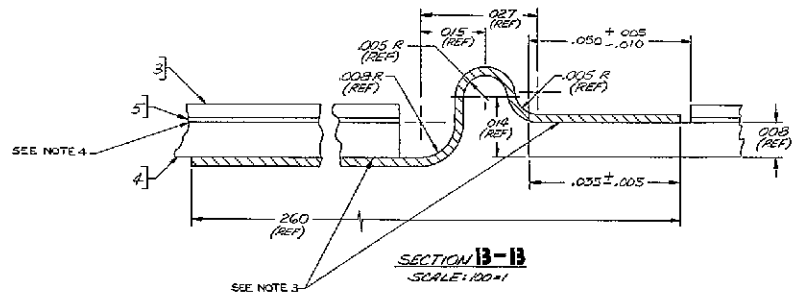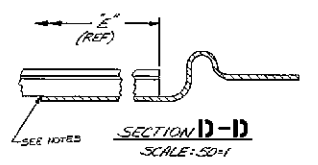
Figure 3.1-4. Solar Cell Module

ACTIVE MODULE (19P X 20S)

DUMMY GLASS MODULES

LEADING EDGE

¢ ROD

¢
STORAGE
DRUM

NUMBER OF 2 X 2 CM ACTIVE CELLS = 5700
NUMBER OF 2 X 2 CM DUMMY CELLS = 49476
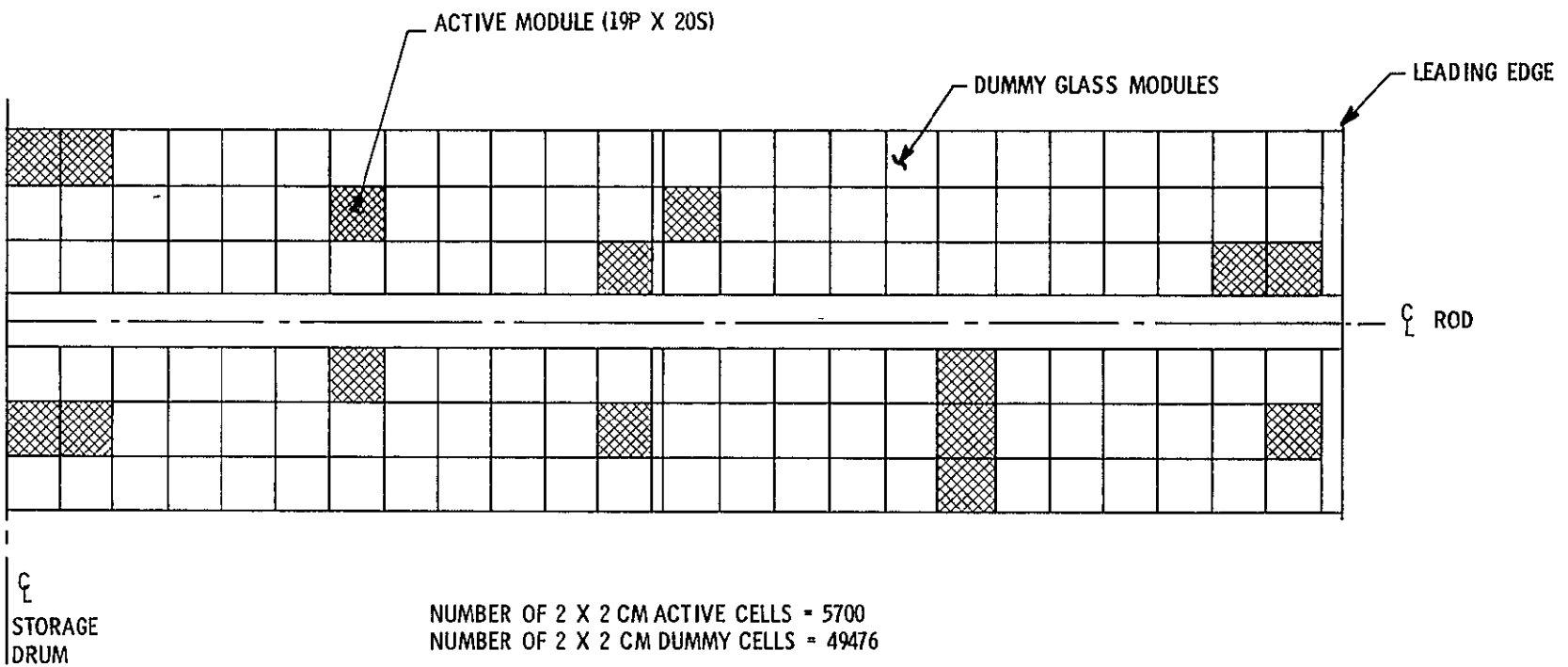
Figure 3. 1-5. Arrangement of Active Modules

3.2 STORAGE DRUM

The storage drum assembly consists of the following components:

1. Beryllium Drum Shell

2. Magnesium Outboard End Cap

3. Textolite Power Feedthrough

4. Inboard End Cap Assembly

5. Textolite Edge Guides

The beryllium drum shell is a 47. 10-inch-long, 0. 020-inch-thick sheet of beryllium rolled into an 8-inch-diameter cylinder which is closed with a lap-butt joint utilizing a 3/4-inch-wide strip of beryllium bonded with Epon 934. Figure 3.2-1 shows the assembly drawing of this shell. The outboard end cap and the inboard end cap are matched drilled from the drum shell hole pattern. Before this drilling, the centers of the two end caps are aligned to within 0. 005 inch to assist in reasonable accuracy of final assembly alignment (see Figure 3.2-2). To ensure that this alignment is maintained after any disassembly/reassembly, one hole in the match drill pattern is offset. There is no interchangeability of this subassembly.

The inboard end cap, which is the main bearing housing and load path from the drum shell to the bearings, is shown in Figure 3.2-3. This assembly consists of the following components:

1. Magnesium Inboard End Cap Housing

2. Bearings

3. Magnesium Support Shaft

4. Constant Torque Spring Motor Assembly

5. Slip Ring Assembly

3-12
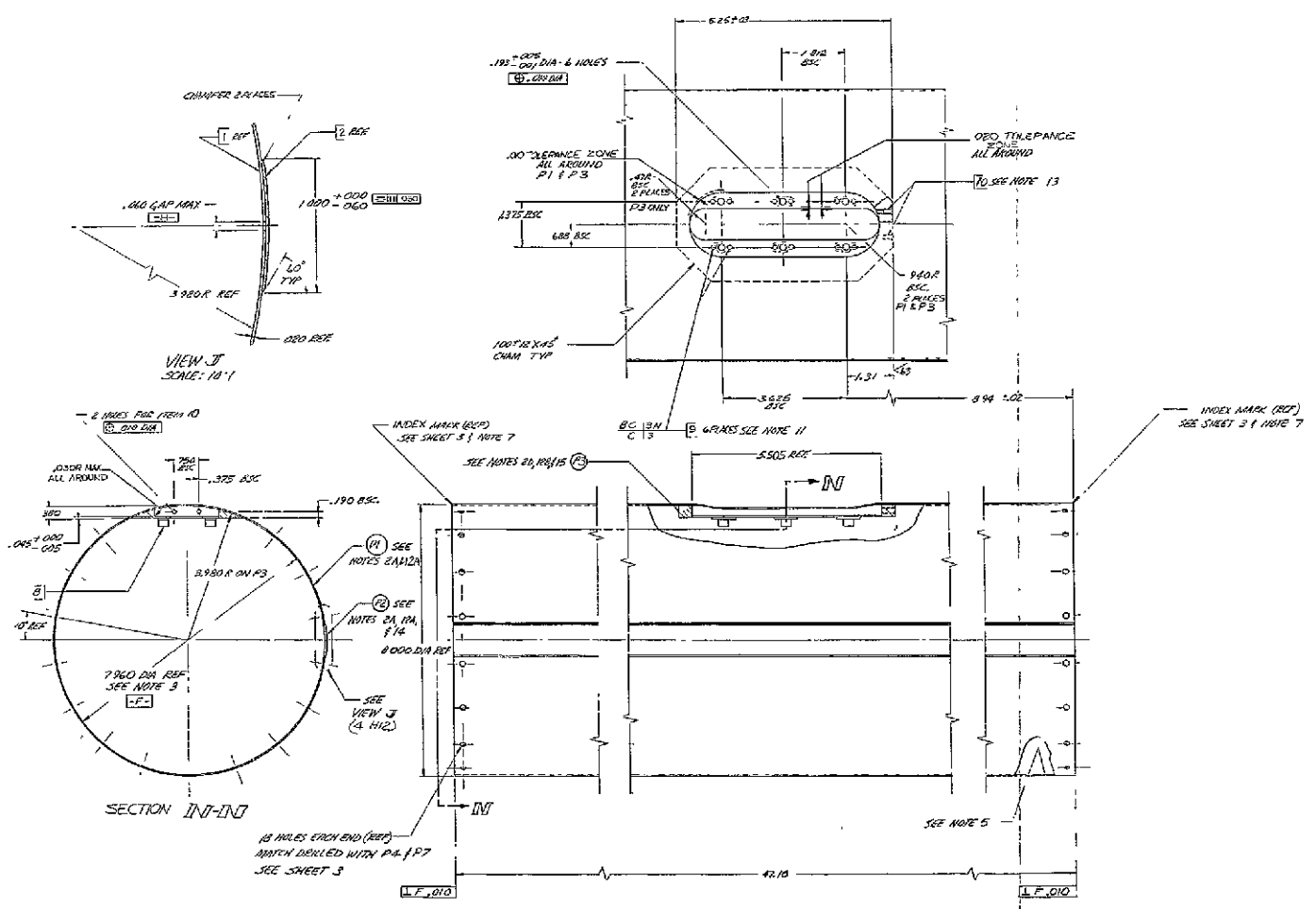
Figure 3.2-1. Storage Drum Shell
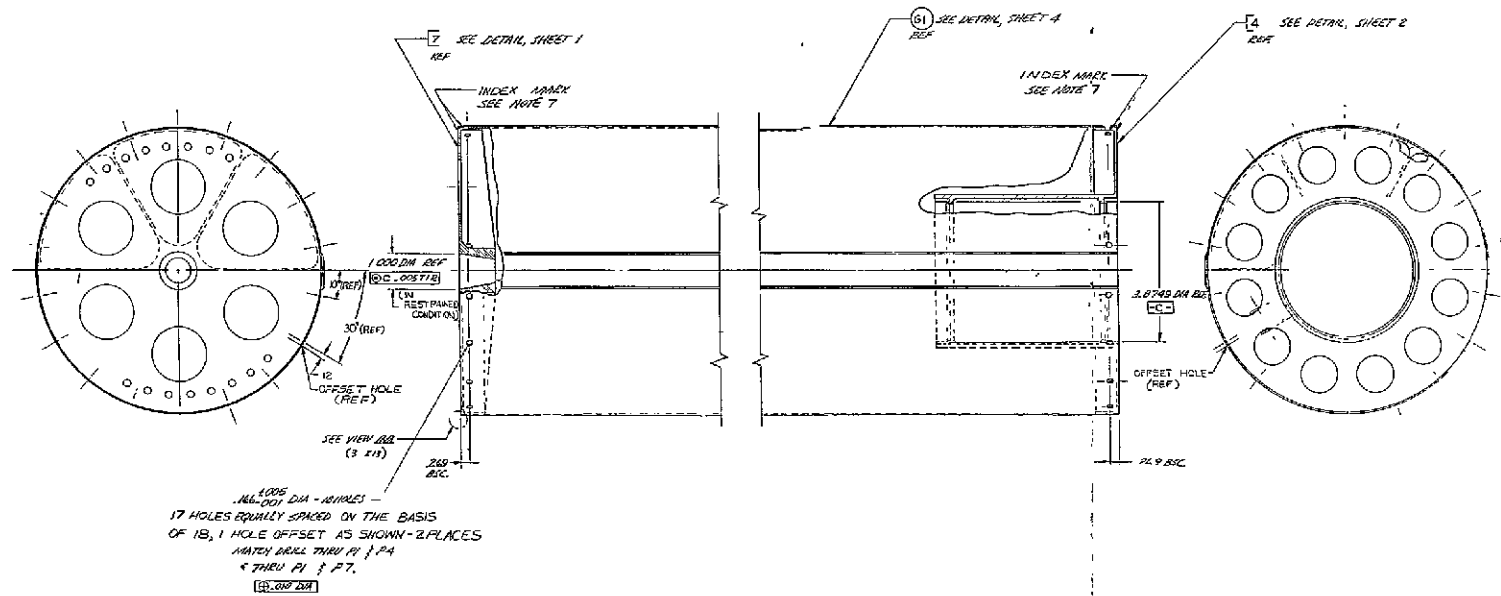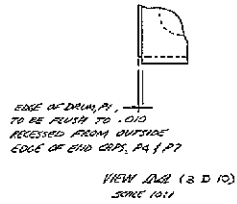
Figure 3.2-2. Storage Drum – Assembly of Inboard and Outboard End Caps
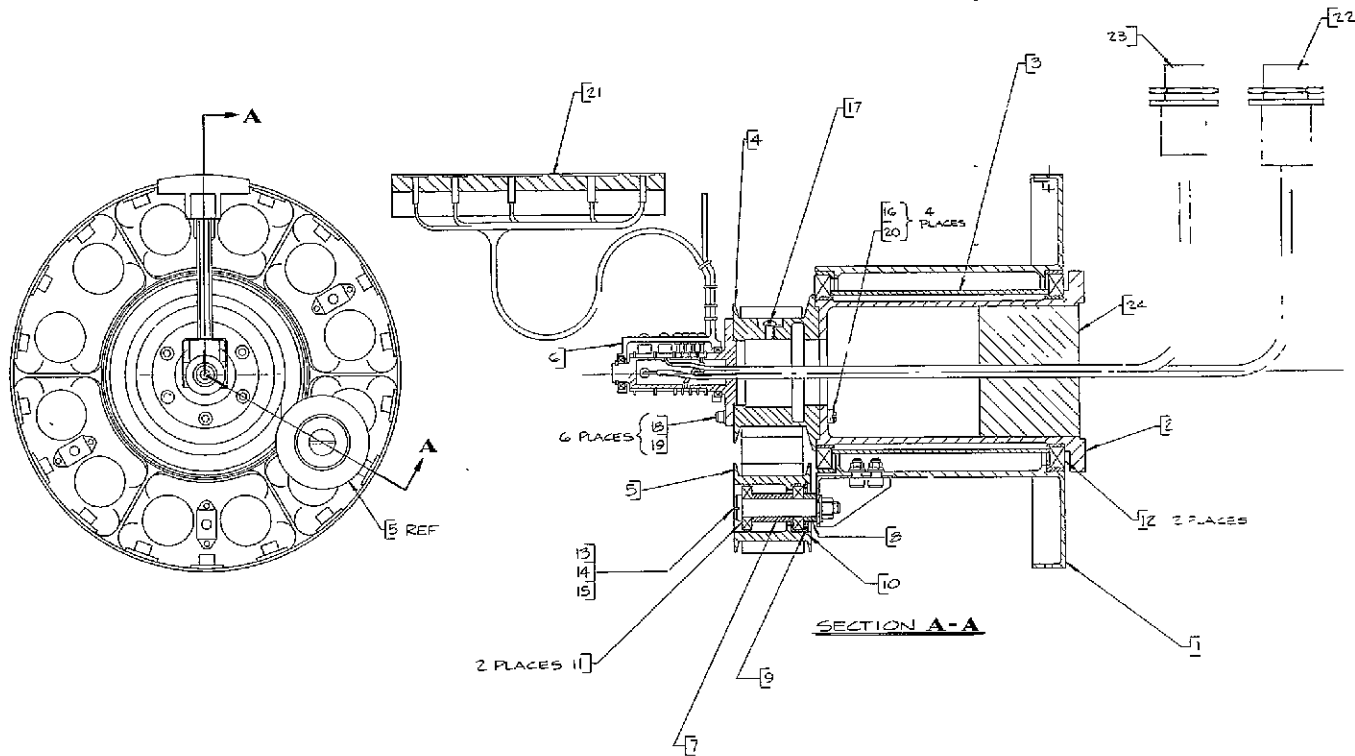
NOTES:
1. INTERPRETATION OF DWG TERMS & TOLERANCES PER 118A1664.

2. MARK 23991 - 47E218549 G _ " NUMBER AS APPLICABLE PER 118A1526 CL 17.

SECTION **A-A**

Figure 3.2-3. Inboard End Cap Assembly

The inboard end cap housing is shown in Figure 3.2-4. Note that interference fit steel inserts surround the bearings in the housing to protect against loads produced by differential expansion/contraction of magnesium and steel. The support shaft shown in Figure 3.2-5 is equipped with similar steel ring inserts. This shaft bolts directly to the center support. The main shaft bearings are matched angular contact bearings as shown in Figure 3.2-6. These bearings are manufactured by Split Ball Bearing Division of Miniature Precision Bearings, Inc., and are identified as part number 3TA049-62-46. Transfer film lubrication is obtained from Duroid 5813 toroid spacers.

The constant torque motor (Négator spring) assembly consists of a 136 inch by 1.25 inch by 0.010-inch stainless steel spring wound on a 2.18-inch-diameter magnesium output drum (attached to the stationary support shaft) and a 1.31-inch-diameter magnesium takeup drum (mounted to the rotating inboard end cap). The takeup drum free-wheels on instrument bearings that have a stainless steel shaft which mounts to the inboard end cap.

The slip ring assembly provides continuous electrical contact between relative rotating elements and transfers array power to the fixed harness which runs inside the spring motor output drum, support shaft through the center support tube and finally to the connector interface on the center support. The rotating element (brushes and brush supporting structure) of the slip ring assembly has an arm which is joined to the storage drum shell. The slip ring assembly is described in greater detail in Section 3.5.

The outboard end cap, which transfers loads from the storage drum shell to the outboard end support, is shown in Figure 3.2-7. The tapered hole in this end cap mates with a corresponding tapered plug in the outboard end support. The 0.187-inch-diameter holes mate with a pin in the outboard end support and function to prevent the drum from rotating in the stowed configuration. Both these holes and the larger tapered hole are coated with Lubri-Bond "A."

Figure 3.2-4. Inboard End Cap Housing

P2 MATL 303 STAINLESS STEEL COND.A, QQ-S-764
SEE NOTE 3 & 5B

P1 MATL: MAGNESIUM ZK60A-T5, QQ-M-31
SEE NOTE 5A

2.625 +.002 -.000 DIA -D-

90°   45°

.31 R
4 PLACES

.185 +.005 -.001 DIA   1.32 DIA
4 HOLES EQUALLY SPACED
ON 1.750 DIA BASIC B.C

⊕ D .010 DIA

8 HOLES FOR ITEM 3,
EQUALLY SPACED ON
3.500 DIA. BASIC B.C.

⊕ A B .010 DIA

.020

.010 R MAX

3.0622 +.0000 -.0004 DIA

⊕ A .002 T.I.R
B .002
C .005

.02X45° CHAM

.12 R

SEE VIEW A

.065

2.875 +.002 -.000 DIA   4.00 DIA

-A-

2.620 DIA   3.220 DIA

.30   .400

-C-

4.995 ±.002

5.18

5.395 REF

-.002 -B-

2.880 +.000 -.005 DIA.

2.902 DIA
2 PLACES
SEE NOTE 3

.32 R. PERMISSIBLE

.010X45°CHAM
TYP.

.12 +.01 -.00

.02 R MAX

.03X45°CHAM.

.010 R

REF

2 REF

.350

.020 MAX.

.40
2 PLACES

.63

3 SEE NOTE 2

G1

VIEW A
SCALE 4:1

NOTES

1. INTERPRETATION OF DRAWING TERMS &
   TOLERANCES PER 118A1664.
2. INSTALL HELICAL COIL INSERTS, ITEM 3,
   PER MS33646 CL.2B. INSTALL INSERT
   WET WITH ZINC CHROMATE PRIMER,
   MIL-P-8585 PER MIL-P-6808.
   REMOVE TANG
3. ITEM 2 TO HAVE .002 TO .003 INTER-
   FERENCE FIT WITH ITEM 1.
4. MARK 2339147D21B532G1 PER
   118A1526 CL. 17
5. FINISH PARTS AS FOLLOWS
   A. FINISH P1 PER MIL-M-45202, TYPE I
   CLASS C FINISH ELECTRICAL CONTACT
   AREA PER MIL-M-3171,TYPE VI AFTER
   ANODIZING IMMERSE PARTS FOR 15 MINUTES
   MINIMUM, IN SEALING SOLUTION OF 7 OZ/GAL
   SODIUM, TETRASILICATE IN DEMINERALIZED
   WATER, AT 200 TO 212°F. REMOVE AND
   RINSE THOROUGHLY IN COLD TAP WATER.

   B. FINISH P2 PER 118A1600 P228. NO FINISH
      REQUIRED AFTER FINAL MACHINING AT
      ASSEMBLY FOR P2

Figure 3.2-5. Support Shaft

SOURCE OF SUPPLY			
CL.PRFX	VENDOR PART NO.	VENDOR	CODE
P1	3TA049-62-46	MINIATURE PRECISION BEARINGS, INC., SPLIT BALL BEARING 'DIV LEBANON, NEW HAMPSHIRE	40920

3.8750 DIA

30625 DIA

(P1)

.312

.624
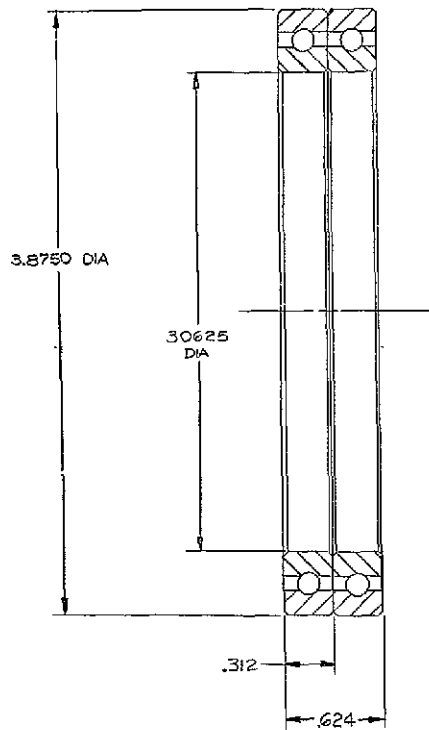
NOTES:

1. BEARING SHALL BE A PAIR OF MATCHED ANGULAR CONTACT BEARINGS, DB MOUNTING FROM ZERO PRELOAD ABEC7T TOLERANCE EXCEPT AS NOTED.

2. IN A RADIALLY UNRESTRAINED CONDITION, WITH THE MATING OUTER RACES FLUSH, NO MORE THAN 10 POUNDS SHALL BE APPLIED TO THE INNER RACE TO BRING THE INNER RING FACES FLUSH. BUT IN THE LAYING INNER RACES ARE FLUSH, THERE SHALL BE NO MORE THAN .0002 INS. INCH GAP BETWEEN MATING OUTER RING FACES. THESE VALUES ARE TO BE DETERMINED FROM THE OFFSET, MEASURED UNDER LOAD AND FROM THE MAXIMUM AND MINIMUM YIELD CURVES. SEND INSPECTION TEST DATA WITH BEARINGS.

3. RADIAL PLAY SHALL BE WITHIN .0016 FOR 0° CONTACT ANGLE WITH NO AXIAL LOAD.

4. BALLS AND RACES: CR. STL. AISI 440C.
   RETAINER: TOROID SPACERS, SELF LUBRICATING TEFLON COMPOSITION;
   DUROID 5813 - RODGERS CORP. (OR EQUIVALENT).

5. MARK EACH PT. GE47C218344 PER 118A1526, CL 4 OR 6. SERIALIZE EACH DUPLEX PAIR BY MARKING P1 - (SUFFIX LETTER AS APPLICABLE) & SERIAL NO. PER 118A1526 CL. 4 ON EACH BEARING.

6. THE BEARING SHALL BE ASSEMBLED & ALL INSPECTION PERFORMED IN A CLEAN ROOM MEETING THE REQUIREMENTS OF FED-STD-209, CLASS 10,000. AFTER ASSEMBLY & ANY SUBSEQUENT INSPECTIONS, THE BEARING SHALL BE PACKAGED TO MAINTAIN THE CLEAN CONDITION UNTIL ASSEMBLED INTO THE NEXT HIGHER ASSEMBLY.

SOURCE CONTROL DRAWING

ONLY THE ITEMS LISTED ON THIS DRAWING IN THE "SOURCE OF SUPPLY" TABULATION HAVE BEEN TESTED AND APPROVED BY MSD FOR USE ON SPACE EQUIPMENT. A SUBSTITUTE ITEM SHALL NOT BE USED WITHOUT PRIOR WRITTEN APPROVAL BY MSD.

NO CHANGES SHALL BE MADE TO THE DESIGN, CONFIGURATION, MATERIAL, PARTS OR MANUFACTURING PROCESSES WITHOUT PRIOR WRITTEN APPROVAL OF PURCHASING.

Figure 3.2-6. Main Shaft Ball Bearings

3-25/26

NOTES

Figure 3.2-7. Outboard End Cap

The edge guide flange shown in Figure 3.2-8 is attached to the storage drum at each end cap. These flanges are fabricated from Textolite and function to control the position of each blanket wrap during array retraction.

3.3 CENTER SUPPORT

The center support consists of a magnesium center tube (see Figure 3.3-1), two machined magnesium end fittings and two magnesium face sheets. As shown on the assembly drawing in Figure 3.3-2, the center tube is pinned to the end fittings and the face sheets are riveted to the tube end fittings. One face sheet provides for the electrical connector installation, and together with the other face sheet, transmits shear loads. The end fittings provide the interface pads for the vehicle structure and the solar panel actuator (BI-STEM). Tolerances on all interface surfaces were selected in order to achieve reasonable alignment between the storage drums, and the leading edge member and minimize end support vehicle interface adjustment at final installation. The center tube incorporates an access hole which allows either drum or the solar panel actuator to be disassembled from the center support without the removal of the connectors from the harness.

3.4 SOLAR PANEL ACTUATOR

The solar panel actuator is a BI-STEM deployable boom being designed and developed by the SPAR Aerospace Products Ltd. The interface drawing defining the outline dimensions, the mounting provisions, and the electrical interface of the actuator with the rest of the RA250 system is shown in Figure 3.4-1. The technical requirements on the performance of the system are defined in General Electric Specification SVS7552. Alignment and position with respect to the system are maintained by control of the dimensions and tolerances of the mounting brackets and their mating surfaces on the center support.

The boom element of the BI-STEM unit, the component which provides the actuation force for deployment and forms the primary structure in the deployed configuration, has a nominal outside diameter of 1.34 inches. It is made up of two 301 stainless steel strips, 4 inches wide and 0.007 inches thick, which are prestressed to form an overlapped tube in the deployed

position. The BI-STEM principle is shown in Figure 3.4-2. The boom is silver plated on its outside surfaces to reduce the temperature gradients in the boom when one side is exposed to solar radiation and the other side is in shadow. Properties of the boom element (as supplied by the vendor) are given in Table 3.4-1.
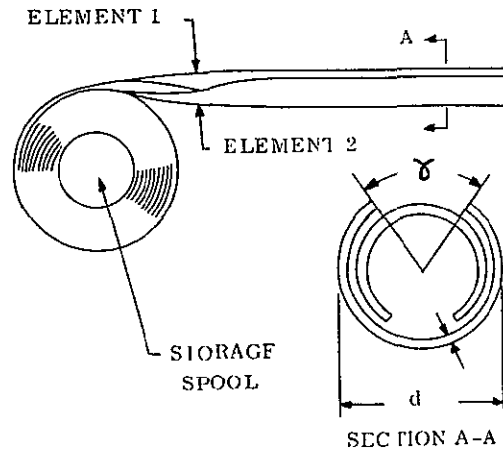
Figure 3.4-2. The BI-STEM Principle

Table 3.4-1. Properties of 1.34-Inch BI-STEM Element

Weight per Unit Length	(lb/in.)	0.01624
Bending Stiffness (EI)	(lb-in^2 min)	332,000
Bending Stiffness (EI)	(lb-in^2 max)	370,000
Column Torsional Instability	(lb)	22
Self Extension Force	(lb)	12.15

The boom actuator mechanism consists of a motor-driven storage spool mounted internal to a system of rollers which provide an external cassette for the stowed portion of the element and provide guidance to the root of the ploy section of the emerging boom. A guide is provided at the exit end of the mechanism to support the boom as it emerges from the actuator mechanism.

The drive motor is a 27 vdc unit manufactured by Clifton Precision Products and drives the storage spool through a gear train. The motor will be equipped with high altitude brushes and dry lubricants are used through the assembly. Microswitches provide control of the motor at the fully extended, the fully retracted, and at 6 inches from full retraction positions.

3.5 SLIP RING ASSEMBLY

The slip ring assembly is being designed and developed by Poly-Scientific Division of Litton Precision Products, Inc. The interface drawing defining the outline dimensions, the mounting provisions, and the electrical interface with the rest of the RA250 system is shown in Figure 3.5-1. The technical requirements on the performance are defined in General Electric Specification SVS7547. Alignment and position with respect to the slip ring installation in the system are controlled by the dimensions and tolerances on the shoulder on the mounting flange which fits into a pilot diameter on the adjoining subassembly.

Pertinent slip ring design data is shown in Table 3.5-1.

3.6 OUTBOARD END SUPPORT

The outboard end support shown in Figure 3.6-1 consists of the following major components:

1. Movable Arm Assembly

2. Hinge Bracket

3. Separation Nut

4. Bolt Catcher

5. Hinge Pin

6. Separation Bolt

7. Spring

.201 $^{+.005}_{-.001}$ DIA HOLE & RECESS
.375 $^{+.015}_{-.005}$ DIA -18 PLACES
17 HOLES EQUALLY SPACED ON THE
BASIS OF 18. 1 HOLE OFFSET AS SHOWN
⌖ .010 DIA

0°
20°
REF

A

60° REF

860 DIA. B.C.
BSC

9.86
DIA

.12
BSC

OFFSET HOLE
P1 ONLY

8.000
$^{+.004}_{-.000}$
DIA

95° BSC

.12
BSC

120° REF

OFFSET HOLE
P2 ONLY

P1 TEXTOLITE - GR 11682
P2 NEMA GR G-11 PER
MIL-P-18177 GEB
ROLLED TUBE STOCK

.06 R

23 40°

.015 R

.478
$^{+.002}_{-.005}$

.060 $^{+.000}_{-.005}$

5°
BSC

3 4 PLACES
SEE NOTE 3
FLUSH WITH
FAR SIDE
⌖ .020 DIA

SECTION A-A (ROTATED 70° CW)
SCALE 2:1

.269
BSC
TYP

G1
G2

NOTES:
1. INTERPRETATION OF DWG TERMS &
   TOLERANCES PER 118A1664.

2. MARK 2399/-47D218535G - " NUMBER
   AS APPLICABLE PER 118A1526 CL 17.

3. INSTALL HELICAL COIL INSERT PER MS33646
   CL 2B, REMOVE TANG AFTER ASSY.

Figure 3. 2-8. Edge Guide Flange

3-31/32

Figure 3.3-1. Center Support Tube

NOTES

1- DWG TERMS & TOLERANCES PER 11BA16G4

2- MARK 23551-47E218535G1 'PER 11BA1516CLIG

3- FINISH ALL SURFACES PER MIL M-45202,TYPE 1,
CLASS C FINISH ELECTRICAL CONTACT AREA
PER MIL-M-3171, TYPE III (P3 & P4 ONLY)

4- AFTER FINISHING, SEAL ALL SURFACES BY
IMMERSION OF ASS Y FOR 15 MINUTES IN A
SOLUTION OF 7 OUNCES OF SODIUM TETRABORI-
CATE PER GALLON OF DEMINERALIZED WATER
AT 200° TO 212° F RINSE THOROUGHLY IN
COLD WATER (P3 & P4 ONLY)

5- LIGHTENING HOLE CONFIGURATION PER RBA1834

6- INSTALL PINS ITEM 9 AT INDICATE LOCATIONS
TYPICAL BOTH ENDS HOLE SIZE TO BE
.1865±.0005 DIA PINS TO BE .010-.020
BELOW SURFACE OF TUBE, ITEM 5

P3 MATERIAL MAGNESIUM
HK31A-H24 PER MIL-M-26075
.063 THK

P4 MATERIAL MAGNESIUM
HK31A-H24 PER MIL-M-26075
.063 THK

Figure 3.3-2. Center Support Assembly

3-35/36

Figure 3.4-1. Solar Panel Actuator
Interface Drawings

Table 3. 5-1. Slip Ring Data

• Power rings per assembly	2
• Signal rings per assembly	4
• Structural material	303 stainless steel
• Ring material	Coin silver
• Ring diameter	0. 60 in.
• Brushes per signal ring	2
• Brushes per power ring	4
• Brush material	Silver/copper/niobium diselenide/ graphite
• Brush spring material	Ney Paliney 7
• Rated current per ring	
Power	15. 0 amp dc
Signal	1. 0 amp dc
• Brush contact force	
Power	0. 33 lb $\pm$ 10%
Signal	0. 12 lb $\pm$ 10%
• Starting torque	
Air	0. 7 in. –lb
Vacuum	0. 4 in. –lb
• Signal ring static contact resistance	0. 065 ohm
• Power ring static contact resistance	0. 020
• Rated current density/ring	
Power	188 amp/in.^{2}
Signal	83 amp/in.^{2}
• Anticipated power loss/assembly	6 watts
• Weight/assembly	0. 617 lb

Figure 3.5-1. Slip Ring Assembly
Interface Drawing
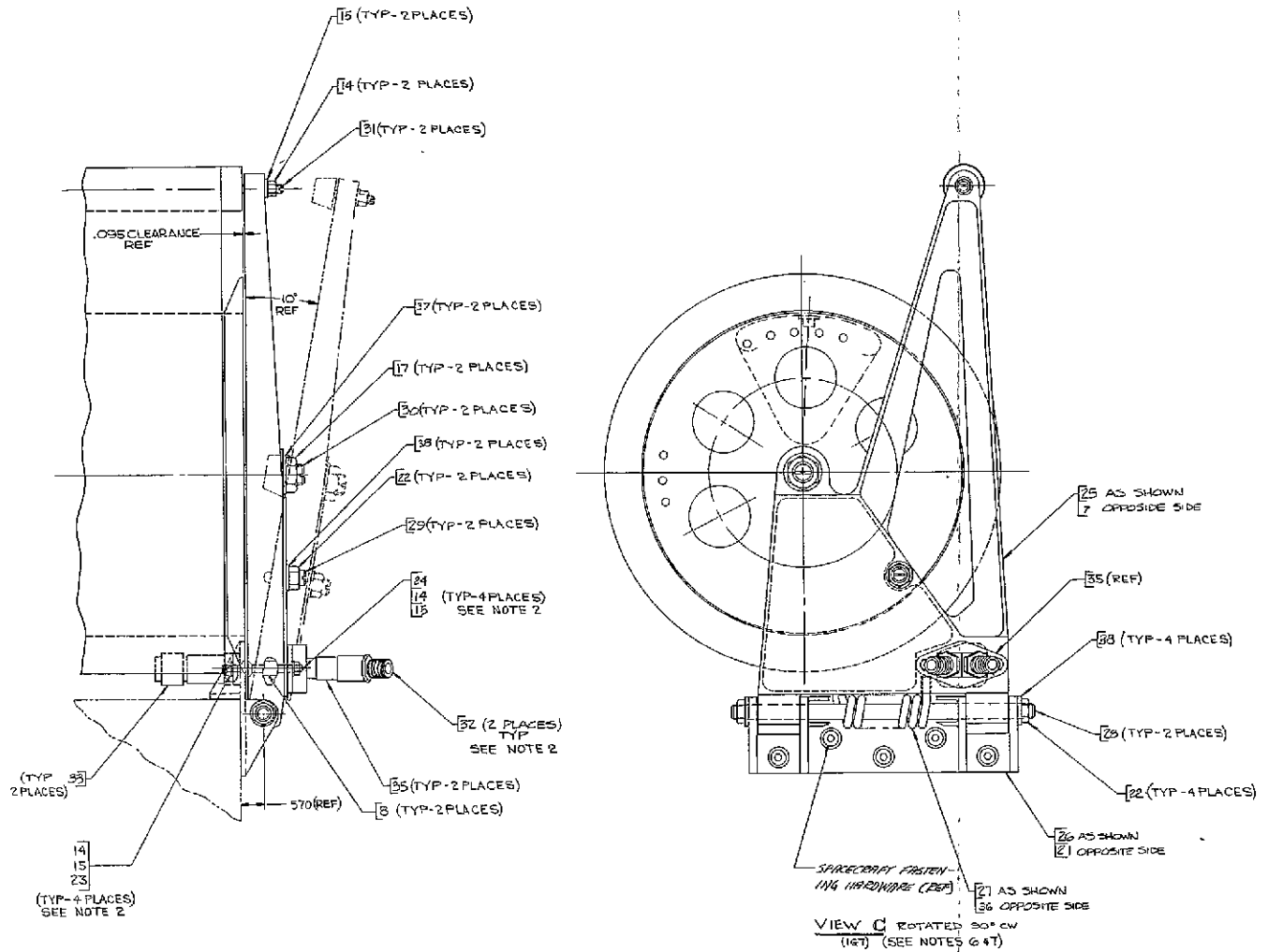
Figure 3.6-1. Outboard End Support

3-45/46

The movable arm assembly shown in Figure 3.6-2 is a machined magnesium weldment. This arm carries the stainless steel tapered plugs which interface with the outboard end cap and leading edge member. Attachment of the movable arm to the vehicle-mounted bracket is through a hinge joint. The hinge pin is titanium which is dry-film-lubricated. A torsion spring which mounts on the hinge pin furnishes 100 in.-lb of torque in the stowed configuration. The release of the support is accomplished by a separation nut/separation bolt/bolt catcher combination. The 3/8 -24 separation nut is attached to the movable arm and contains two electroexplosive pressure cartridges. Upon application of the required power pulse to the bridgewires of one or both of these cartridges, the nut will open and propel the separation bolt into the bolt catcher which is mounted on the stationary hinge bracket. The torsion spring forces the movable arm to rotate about the hinge pin through an angle of approximately 10 degrees. The storage drum and leading edge member are thus released to permit deployment of the BI-STEM actuator.

3.7 LEADING EDGE MEMBER

The leading edge member (LEM) is the restraining element on the outermost edge of the blanket. In the deployed configuration this member transmits the 4-pound blanket preload force from the array substrates to the boom tip. In the launch stowed configuration, the LEM functions to restrain the outer blanket wrap and to cage the BI-STEM boom element. The tips of the LEM are supported by the outboard end supports in the stowed configuration. The outer portion where the LEM attaches to the BI-STEM is supported from the actuator housing in two saddle-type brackets. Figure 3.7-1 shows the drawing for this assembly. With the exception of the stainless steel boom post, bearings, and associated spacers, all parts are made from beryllium. Each boom cylinder is a 50.1-inch-long by 0.020-inch-thick sheet of beryllium bonded with Epon 934. The two rod elements are inserted and bonded to the TEE fitting at the center. This TEE fitting also houses two instrument bearings, the shaft of which attaches to the actuator boom end. These bearings prevent array blanket rotation as a result of BI-STEM curl during deployment or retraction. No bearing inserts are required because the surrounding material is steel and beryllium whose coefficients of thermal expansion are nearly the same.
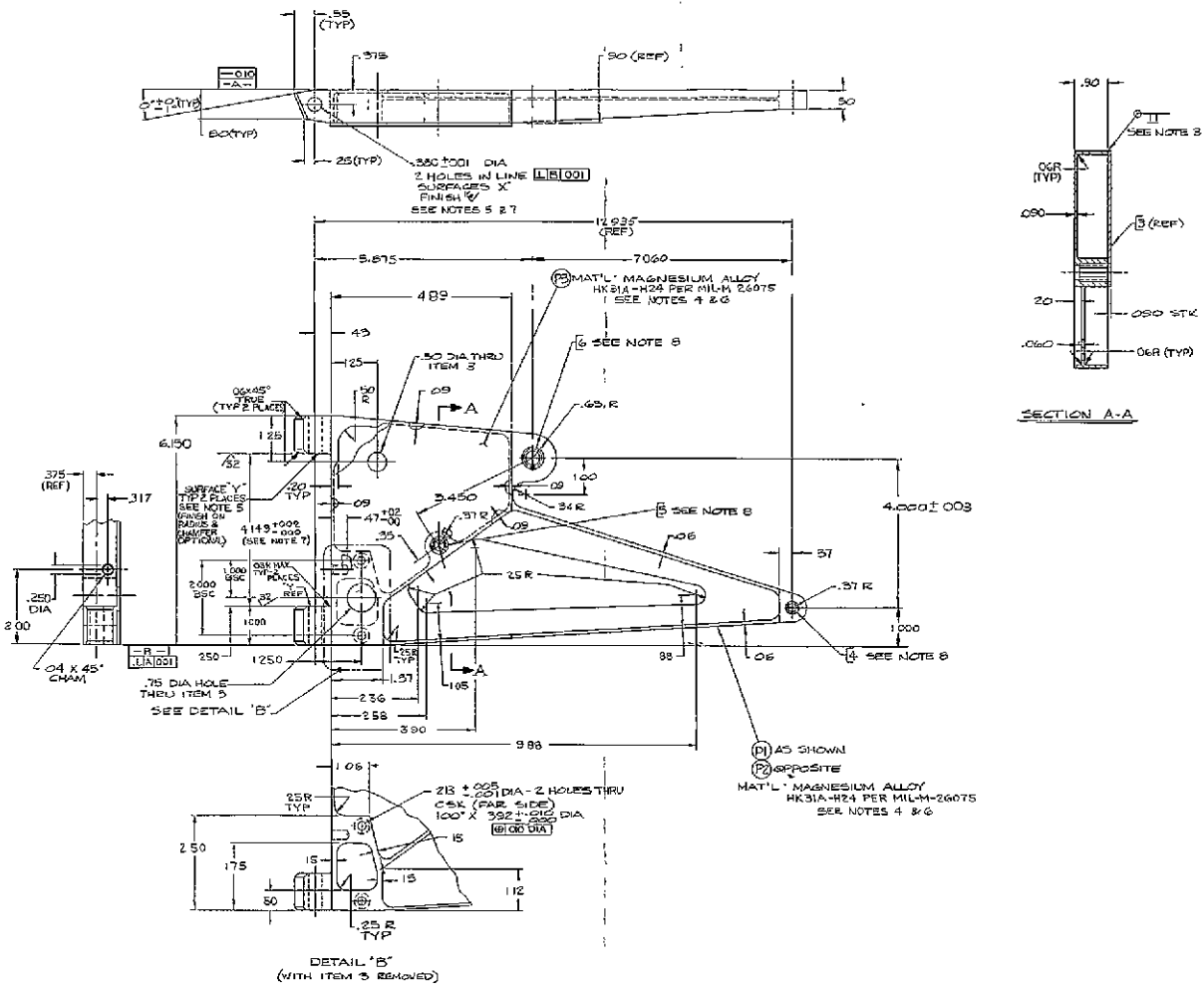
NOTES:
1. INTERPRETATION OF DWG TERMS & TOLERANCES PER 118A1664.

2. MARK "239SI-47E2IB533G__" NUMBER AS APPLICABLE PER 118A1526 CL 16.

3. WELD PER 171A4405, CLASS I MINIMUM PENETRATION .06. STRESS RELIEVE AFTER WELDING AT 275° TO 310°F FOR 1 HOUR

4. FINISH ALL SURFACES EXCEPT AREA ENCLOSED BY P3, PER MIL-M-45202, TYPE I, CLASS C PLUG .50 DIA HOLE BEFORE FINISHING. FINISH ALL INTERIOR SURFACES OF ENCLOSED AREA & ELECTRICAL CONTACT AREA PER MIL-M-3171, TYPE VI

5. SURFACES 'X' & 'Y' TO BE COATED WITH LUBRI-BOND "A" (ELECTROFILM INC NORTH HOLLYWOOD,CALIF) THICKNESS OF COATING TO BE .0002 TO .0005

6. AFTER FINISHING, SEAL ALL SURFACES EXCEPT 'X' & 'Y' AS FOLLOWS . IMMERSE ASSEMBLY FOR 15 MINUTES IN A SEALING SOLUTION OF 7 OUNCES OF SODIUM TETRASILICATE PER GALLON OF DEMINERALIZED WATER MAINTAINED AT 200° TO 212°F RINSE THOROUGHLY IN COLD WATER

7. NOTED DIMENSIONS TO APPLY AFTER COATING

8. INSTALL ITEMS 4, 5 & 6 PER MS33646 CL BB INSTALL INSERT WET WITH ZINC CHROMATE PRIMER, MIL-P-8585 PER MIL-P-6808 INSTALL AFTER FINISHING & SEALING. REMOVE TANG

Figure 3. 6-2.   Movable Arm Assembly
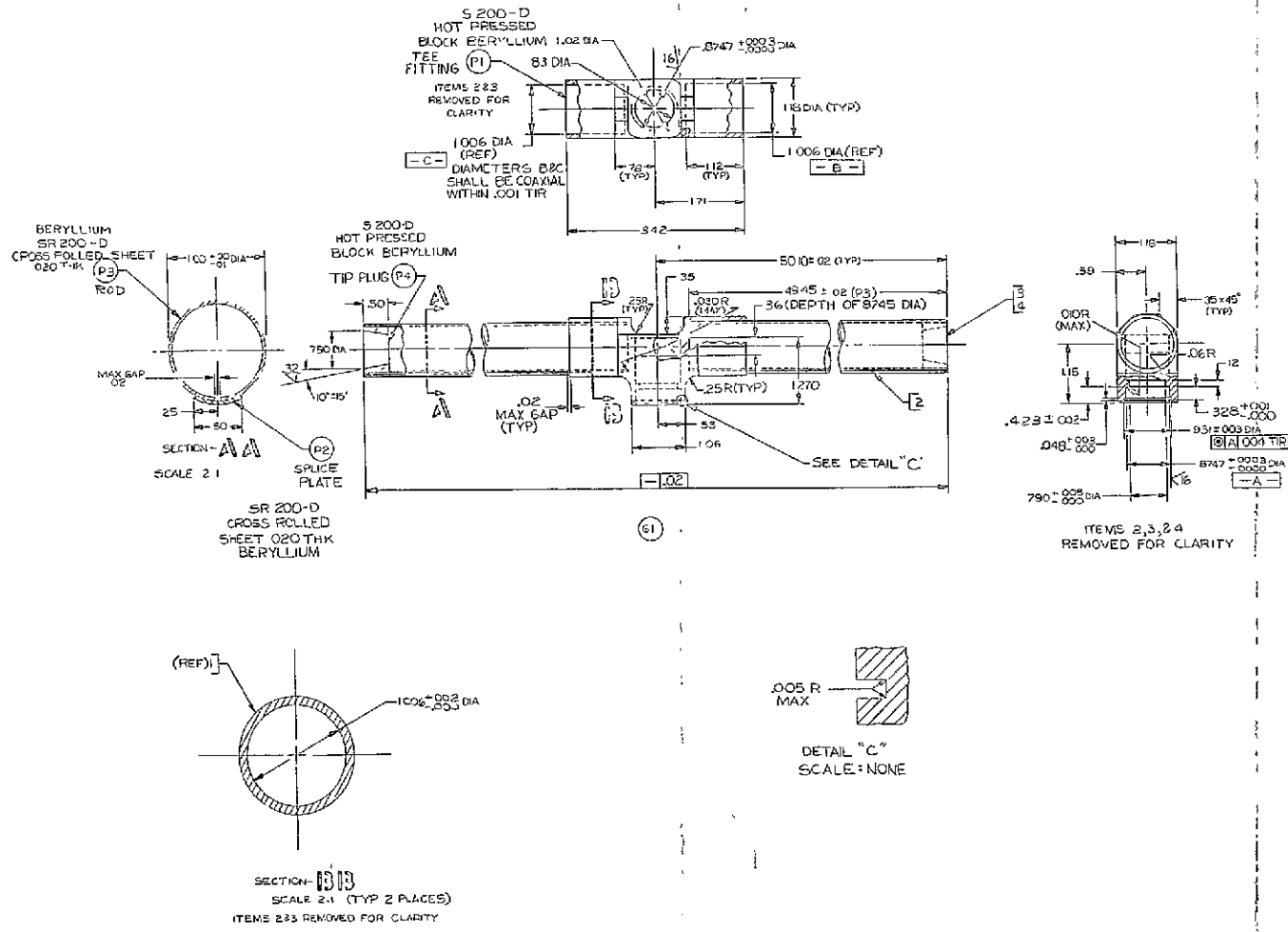
3-49/50

Figure 3.7-1. Leading Edge Member Assembly

SECTION 4

PERFORMANCE ANALYSIS

4.1 ELECTRICAL ANALYSIS

The RA250 solar array is required to generate 2500 watts while operating at 55°C, under
Air Mass Zero illumination and within $\pm$ 10 degree orientation with the sun at 1.0 AU.
Cell efficiency was specified indirectly by the area performance criteria of 10 watts/ft^2
The cell is specified as 8 mil thick, 2 by 2cm, with "bar contacts" (3.8 cm^2 active area
per cell). Figure 4.1-1 shows the nominal subsolar array I-V curve based on the published
performance of these cells. This curve represents the expected beginning-of-life array
performance and includes a 6 percent coverglass transmission loss.

The 7000 cells supplied by JPL for the prototype array were performance tested and graded
by the vendor in an Air Mass One equivalent illumination. The lot average current at the
0.470 volt test voltage is 0.0976 ampere at the standard test temperature of 28°C. The
cell performance which was used to formulate the array I-V curve of Figure 4.1-1 was
calculated for the Air Mass One illumination at 28°C. The resulting current at 0.470 volt is
0.0990 ampere, 1.43 percent higher than the average of the lot received.

4.2 THERMAL ANALYSIS

The thermal performance of the RA250 has been evaluated under numerous conditions. In
general, these analyses can be grouped into two categories: stowed configuration and de-
ployed configuration. In all cases the thermal analyses are based on the assumptions tabulat-
ed in Table 4.2-1. In addition, it was assumed that the maximum solar constant that the
array encounters is 363 mw/cm^2 (based on the specified maximum array temperature of
140°C and the assumed array optical properties), and that the spacecraft acts as an adiabatic
boundary in the steady state deployed cases.

4.2.1 STOWED CONFIGURATION

Aerodynamic heating of the stowed array is presented in Figure 4.2-1. The outer wrap
increases at a rate of 30°C/min from 30°C to 130°C and then is held at 130°C until the end
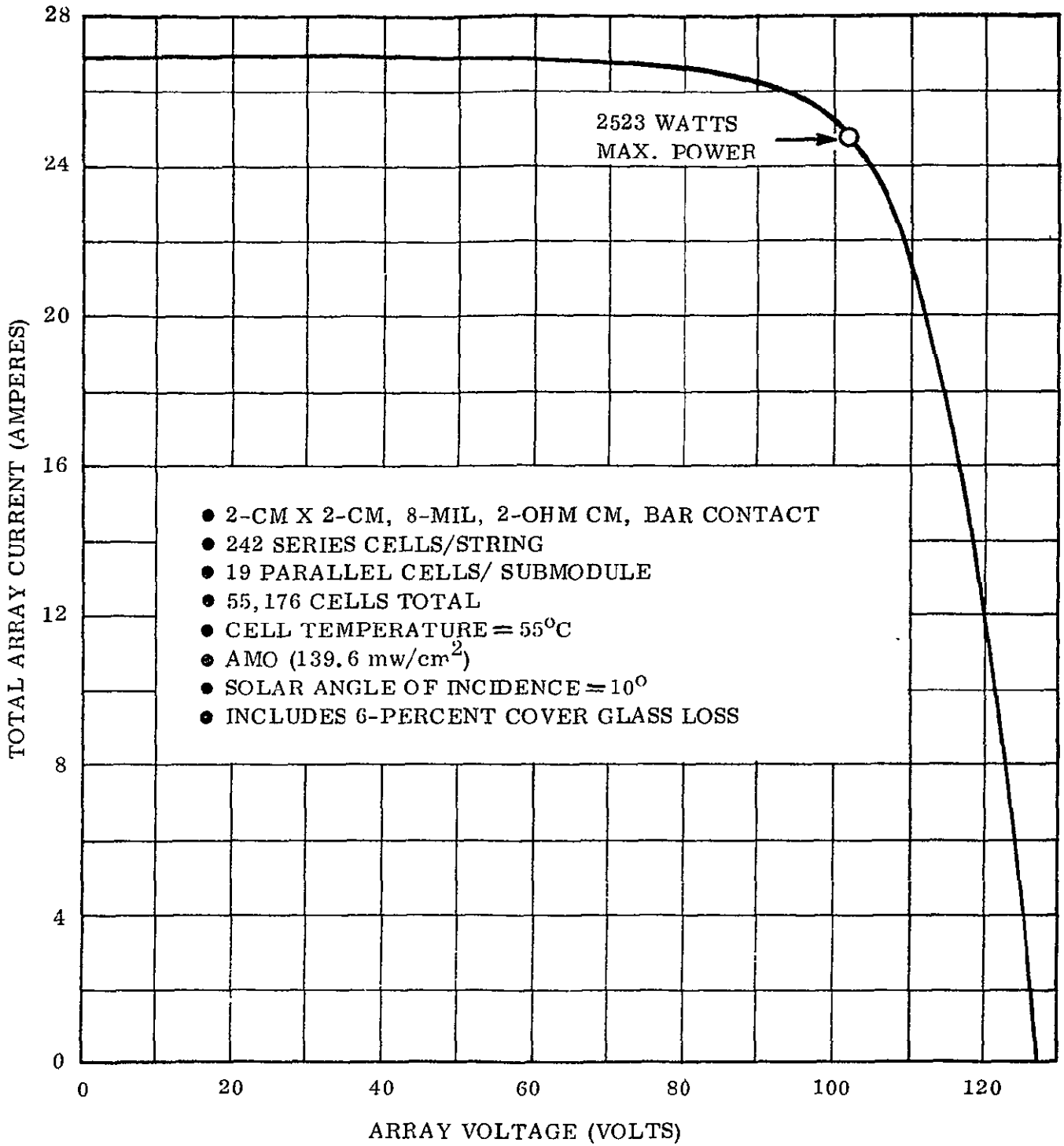
Figure 4.1-1. Nominal Subsolar Array I-V Curve

The figure shows a plot of TOTAL ARRAY CURRENT (AMPERES) on the vertical axis (0 to 28) versus ARRAY VOLTAGE (VOLTS) on the horizontal axis (0 to 120). A point labeled "2523 WATTS MAX. POWER" is marked on the curve near 100 volts and 25 amperes.

- 2-CM X 2-CM, 8-MIL, 2-OHM CM, BAR CONTACT
- 242 SERIES CELLS/STRING
- 19 PARALLEL CELLS/ SUBMODULE
- 55,176 CELLS TOTAL
- CELL TEMPERATURE = 55°C
- AMO (139.6 mw/cm^2)
- SOLAR ANGLE OF INCIDENCE = 10°
- INCLUDES 6-PERCENT COVER GLASS LOSS

Table 4.2-1. Thermal Properties of RA250

Optical Properties	α_s	ϵ_h
Solar Cell/Filter/Glass Composite	0.71	0.8
Inactive Array Surface	0.55	0.65
2-Mil Kapton Backed by Solar Cells	---	0.67
BI-STEM Rod	0.12	0.04
Drum, End Support, and End Cap	0.60	0.60
Mechanical Properties	.	
Drum Wall Thickness = 0.020 inch		
Weight of Array = 0.16 lb/ft^2		

of the 10-minute heating interval. The outboard end support and end plate radiate to a boundary whose temperature profile is identical to that of the outer wrap. An interesting point from these results is that the drum and parts internal to it (eg., bearing ass'y) are relatively unaffected by the aerodynamic heating.

Following the aerodynamic heating, solar flux was considered incident on the outboard end plate as shown in Figure 4.2-2. Again the drum temperature changes very slowly, while the outer wrap of the array has a short period of very rapid cooling since it is receiving no direct flux.

Thermal shock studies were performed with the assumption that the entire array assembly is at a uniform temperature of -202°F (-130°C) for the heating transient and 284°F (140°C) for the cooling transient. Figures 4.2-3 and 4.2-4 present the heating and cooling results for the stowed configuration. Again, it may be noted that the drum temperature responds very slowly to any major flux changes on the array outer wrap. This is particularly noticeable
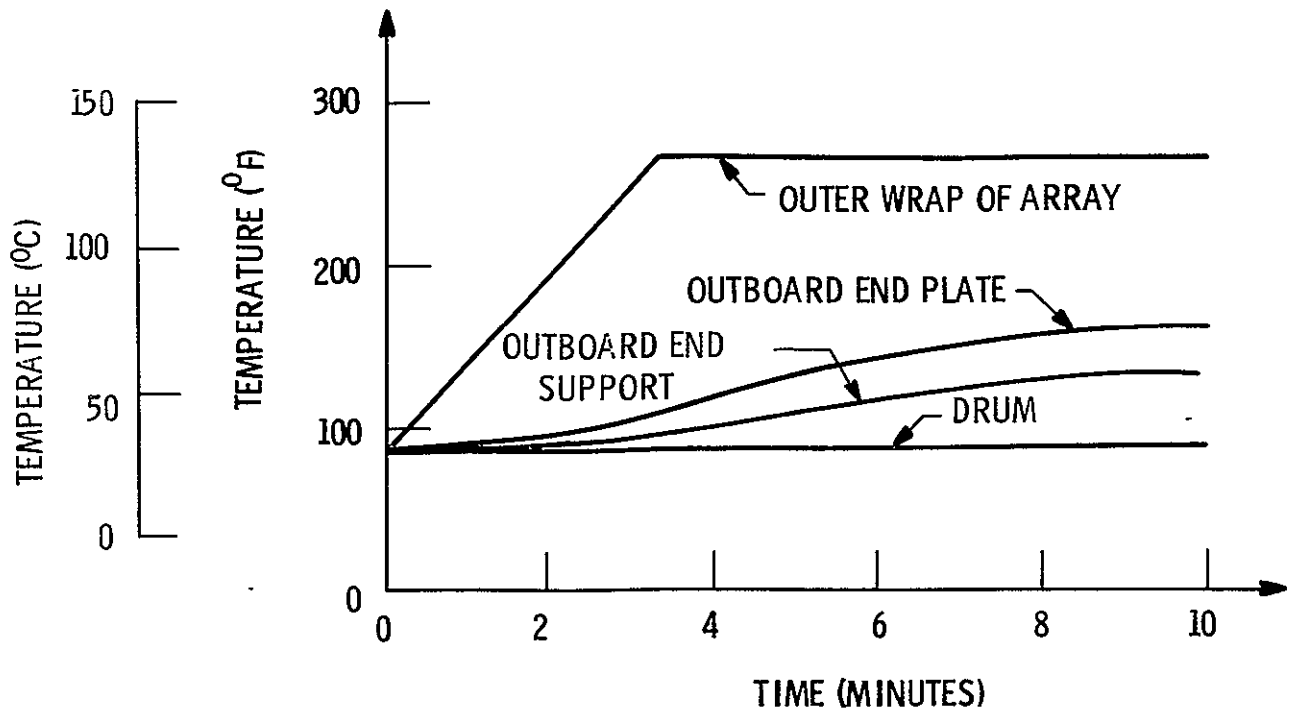
Figure 4.2-1. Aerodynamic Heating Analysis
of Stowed Configuration
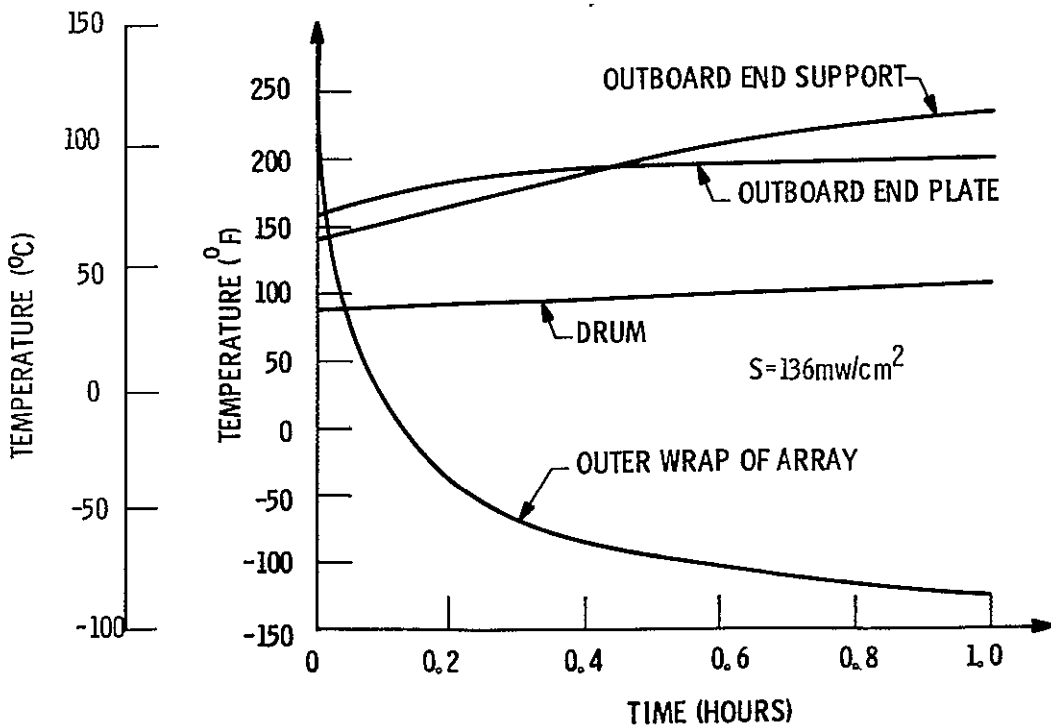
Figure 4.2-2. Solar Heating of End Cap After Initial
10 Minutes of Aerodynamic Heating
(Stowed Configuration)
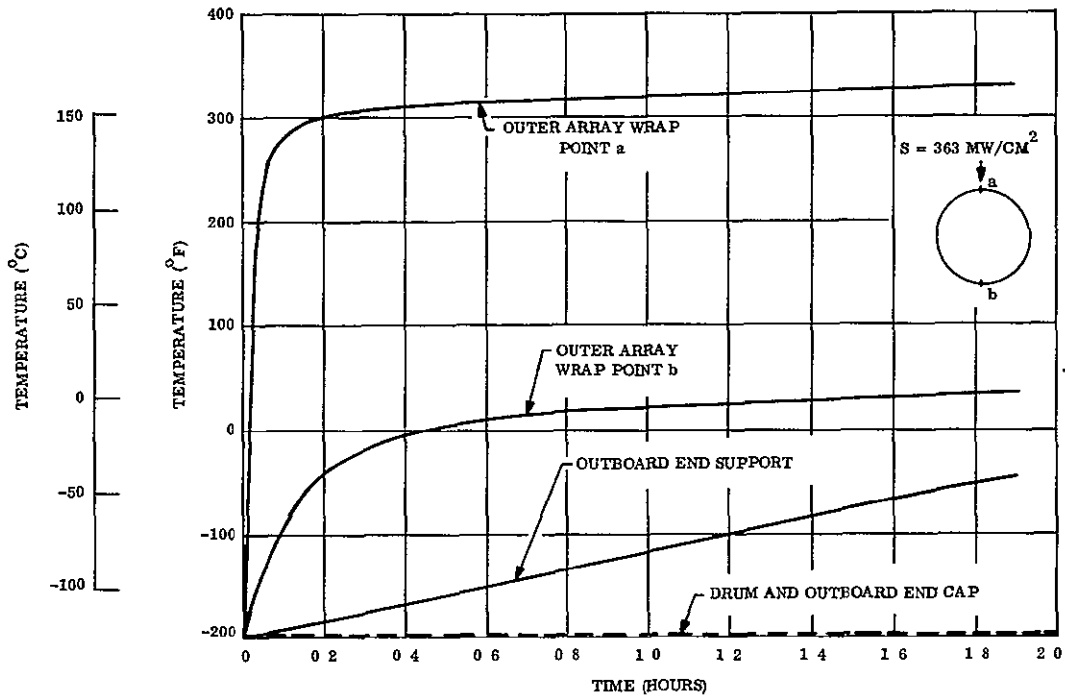
Figure 4.2-3. Thermal Shock Heating Transient from -200°F
(-130°C) (Stowed Configuration)
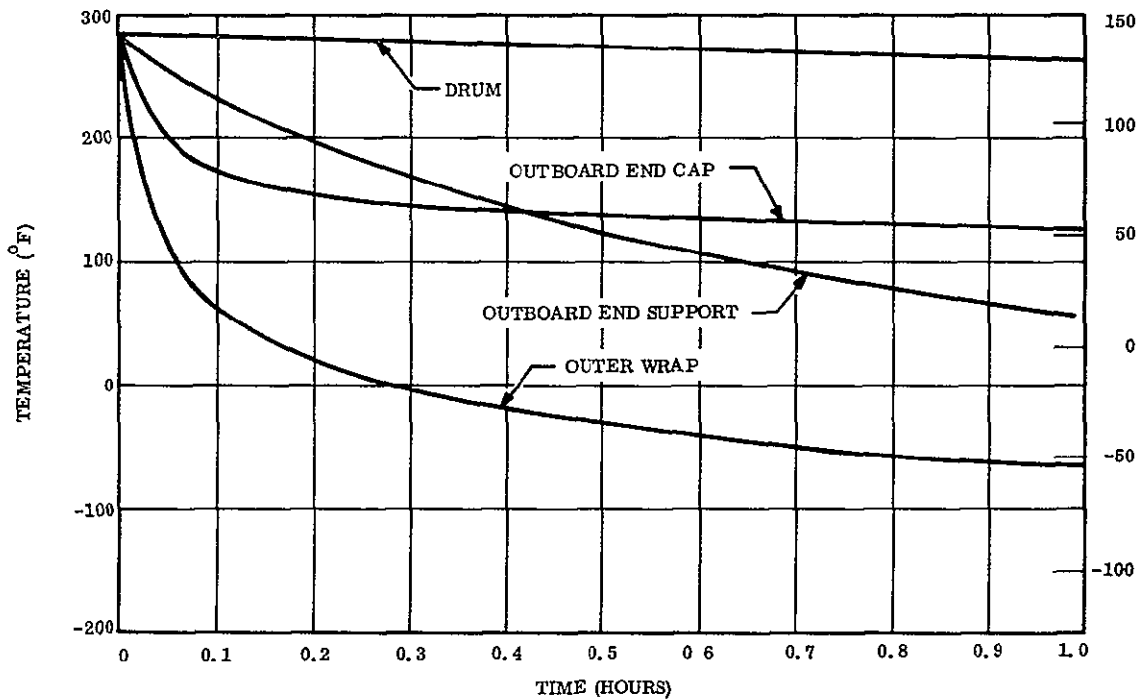
Figure 4.2-4. Thermal Shock Cooling Transient from 284°F
(140°C) (Stowed Configuration)

in heating case where the drum temperature has only increased a few degrees in two hours. This is due to the fact that the many wraps of the stowed array effectively insulate the drum. A steady state analysis of this stowed configuration yields an inner wrap and drum temperature of 148°F. An additional point to be considered from the heating studies is whether the rapid heating of point (a) on the outer wrap (and the adjacent area), from -200°F to $+200^{\circ}$F in approximately three minutes, would in any way damage the array.

4.2.2 DEPLOYED CONFIGURATION

Figures 4.2-5 and 4.2-6 present the thermal shock results for the deployed configuration. In this case, the drum responds rapidly to flux changes because it is directly exposed to these variations and has a low capacitance (WCp product). The inboard end cap and bearing assembly now respond slowest to flux changes. It should be noted that the spacecraft effect was not included in the transient analysis because the thermal characteristics of the spacecraft are not defined. A steady-state analysis of the deployed configuration yields an inboard end cap assembly, bearing assembly temperature of 231°F (111°C).

The steady-state tempature distribution of the BI-STEM rod was determined under the maximum solar flux condition of 363 mw/cm^2. The resulting inner and outer strip temperatures are shown in Figure 4.2-7.

The "hot spot" analysis contained in Reference 2 was refined to include the effects of conduction from the "hot spot" area to adjacent cells as well as radiant transfer from both sides of the array. Figure 4.2-8 shows the results of this study. The maximum temperature observed in the silicon was 287°F (142°C) for the case in which two cells within a submodule are affected, and 199°F (93°C) for the case in which a single cell within a submodule is affected. Both cases therefore result in temperatures below the solder melting range of 360°F to 400°F (182° to 204°C). The straight lines shown in Figure 4.2-7 represent the heating load of reverse biased cells within the affected submodule, one for each of the cases evaluated. With these load functions as inputs, all temperatures were calculated, considering conduction heat transfer to adjacent cells and radiation to space from both array faces. Resulting temperatures are shown by the dotted line in the figure;

NOTE SPACECRAFT NOT INCLUDED
IN MODEL

ARRAY

QUARTER DRUM WITH INCIDENT SOLAR = 363 mw/cm² (a)

OUTBOARD END CAP

DRUM SECTION SHADED FROM DIRECT SOLAR
AND HOT ARRAY FLUXES (b)

INBOARD END CAP, BEARING ASS'Y

TEMPERATURE (°C)

TEMPERATURE (°F)

TIME (HOURS)
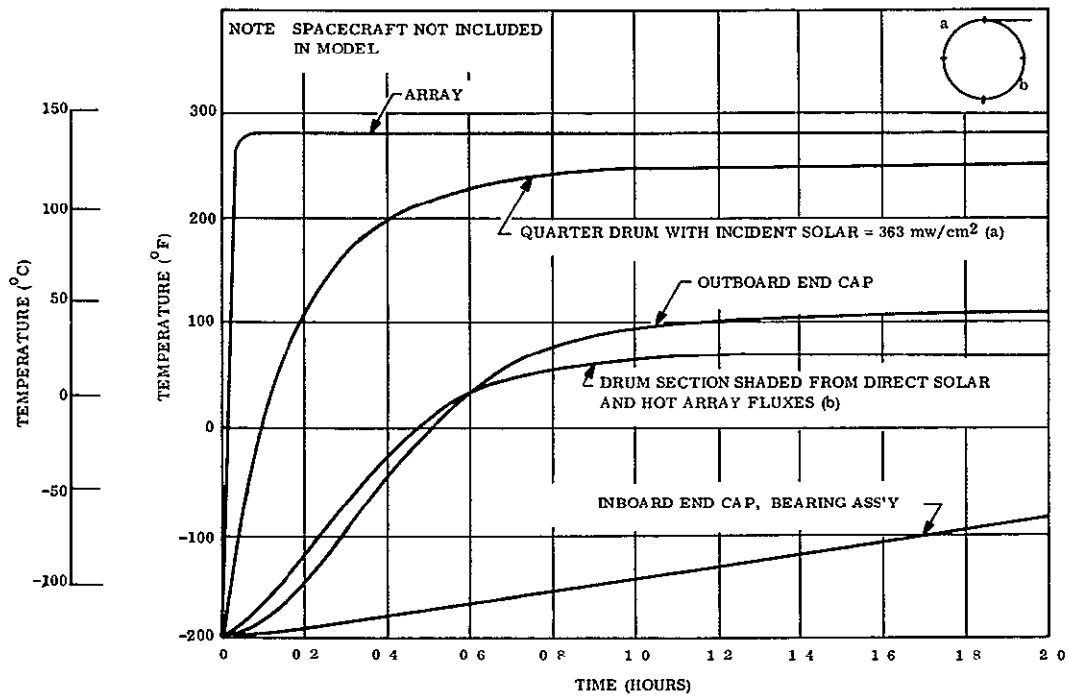
Figure 4.2-5. Thermal Shock Heating Transient from –200°F (–130°C) (Deployed Position)

INBOARD END CAP BEARING ASS'Y

OUTBOARD END PLATE

DRUM

ARRAY

TEMPERATURE (°C)

TEMPERATURE (°T)

TIME (HOURS)
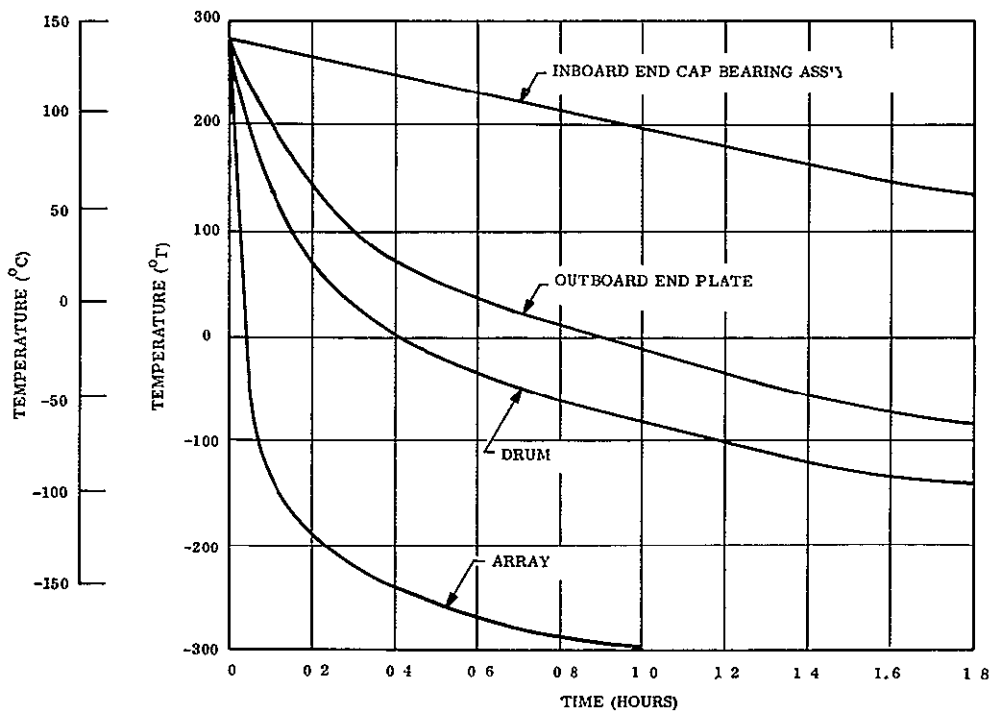
Figure 4.2-6. Thermal Shock Cooling Transient from 284°F (140°C) (Deployed Position)

$$S = 363 \ \text{MW/CM}^2$$

457°F   455°F   457°F

451°F   451°F

430°F   442°F   442°F   430°F

BASED ON SILVER
PLATING THICKNESS
OF 27 μIN.

436°F   436°F

414°F   414°F
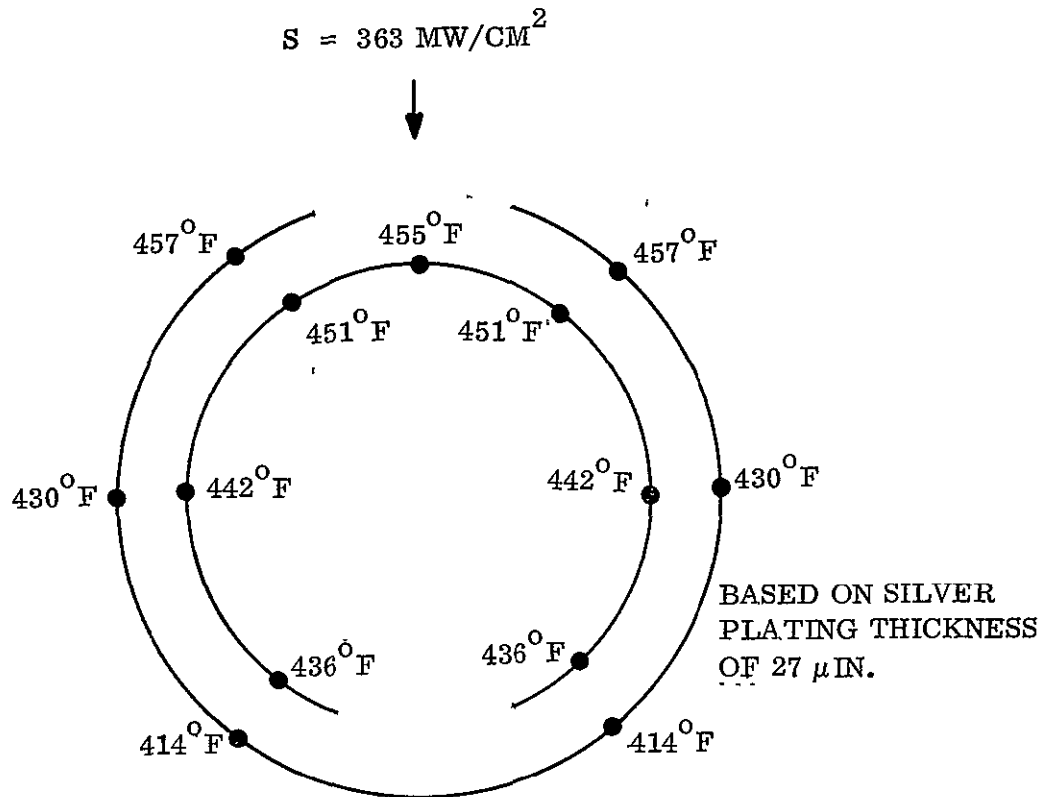
Figure 4.2-7. BI-STEM Rod Steady State Distribution

the improvement attributable to finning effects are clearly seen when comparing values on the dotted curve with those on the solid one where conduction is not included.

4.3 DEPLOYED DYNAMIC ANALYSIS

A stiffness matrix and mass matrix generator set up by Dr. R. Ross of JPL has been incorporated into the GE dynamic computing system.

The stiffness and mass matrices, as programmed by Dr. Ross, consist of assemblies of element stiffness and consistent mass matrices. The representation of the deployable boom and the leading edge member are essentially those of Archer (Reference 5). These mass and stiffness elements are shown in Figure 4.3-1. The element stiffnesses are modified for axial loads by the method of Martin (Reference 6). The form of this element is shown in Figure 4.3-2. The total beam stiffness is the sum of the bending stiffness and the effect of axial load. The solar cell blankets are represented as a membrane having only out-of-plane coordinates. The stiffness and mass matrices for the blanket elements are shown in Figure 4.3-3.
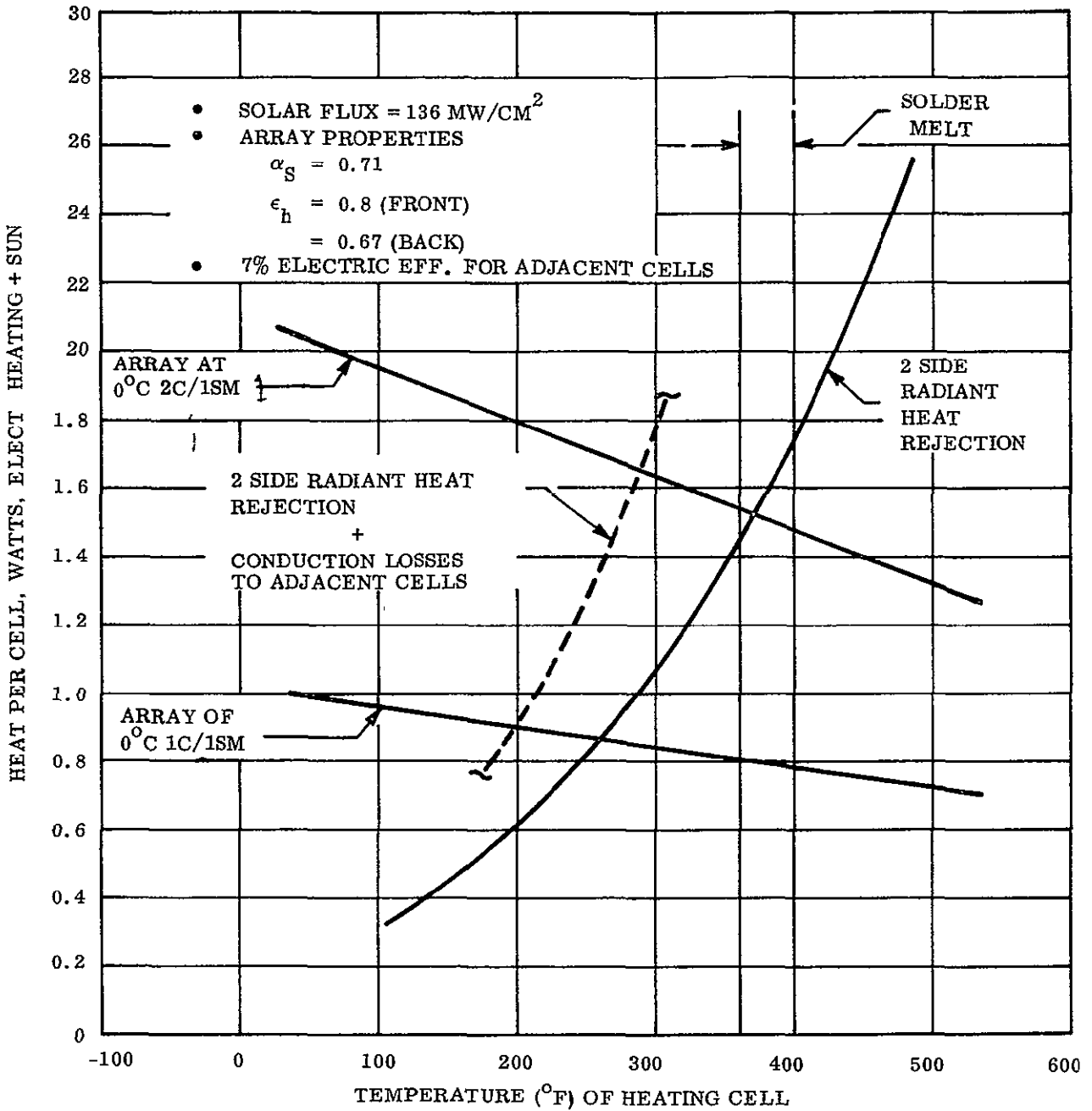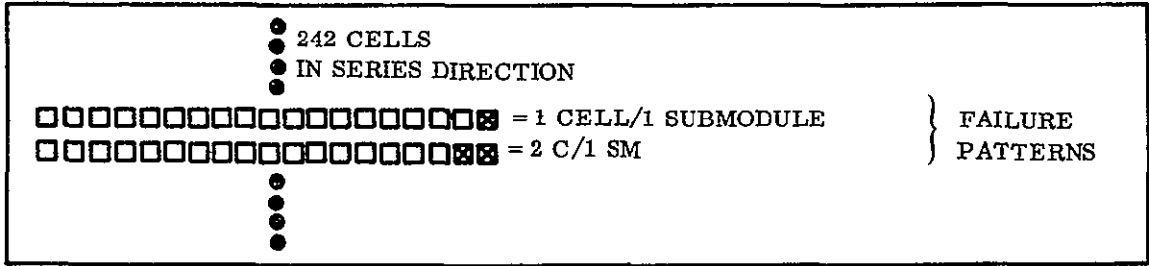
Figure 4.2-8. Array "Hot Spot" Thermal Study
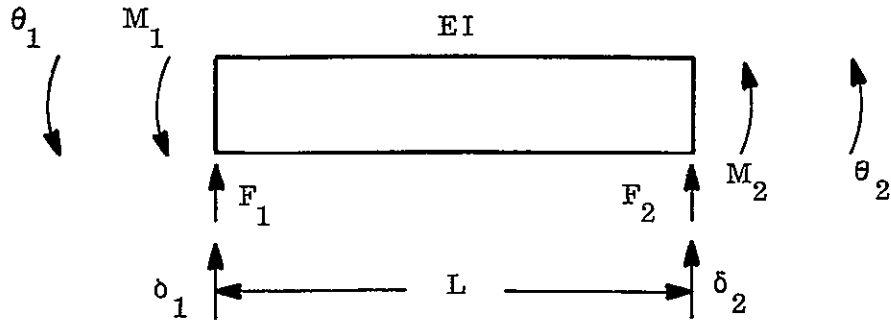
$$F = \begin{bmatrix} F_1 \\ M_1 \\ F_2 \\ M_2 \end{bmatrix} = K \begin{bmatrix} \delta_1 \\ \theta_1 \\ \delta_2 \\ \theta_2 \end{bmatrix} = KX$$

$$K = \frac{EI}{L^3} \begin{bmatrix} 12 & 6L & -12 & 6L \\ 6L & 4L^2 & -6L & 2L^2 \\ -12 & -6L & 12 & -6L \\ 6L & 2L^2 & -6L & 4L^2 \end{bmatrix}$$

$$F = M \begin{bmatrix} \ddot{\delta}_1 \\ \ddot{\theta}_1 \\ \ddot{\delta}_2 \\ \ddot{\theta}_2 \end{bmatrix} = M\ddot{X}$$

$$M = \frac{W}{32.2 \times 420} \begin{bmatrix} 156 & 22 & 54 & -13 \\ 22 & 4 & 13 & -3 \\ 54 & 13 & 156 & -22 \\ -13 & -3 & -22 & 4 \end{bmatrix}$$

W = TOTAL WEIGHT OF ELEMENT IN POUNDS

Figure 4.3-1. Stiffness and Mass of Beam Element Matrices
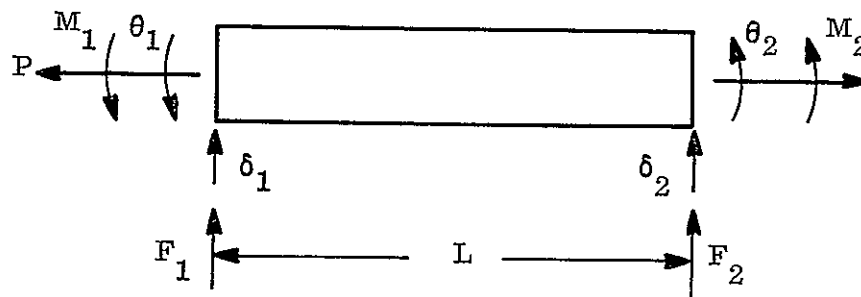
$$F = \begin{bmatrix} F_1 \\ M_1 \\ F_2 \\ M_2 \end{bmatrix} = K \begin{bmatrix} \delta_1 \\ \theta_1 \\ \delta_2 \\ \theta_2 \end{bmatrix} = KX$$

$$K = \frac{P}{30\,L} \begin{bmatrix} 36 & 3\,L & -36 & 3L \\ 3\,L & 1 & -3\,L & -1 \\ -36 & -36 & 36 & -3\,L \\ 3\,L & -1 & -36 & 4 \end{bmatrix}$$

Figure 4.3-2.   Beam Stiffness Due to Axial Load
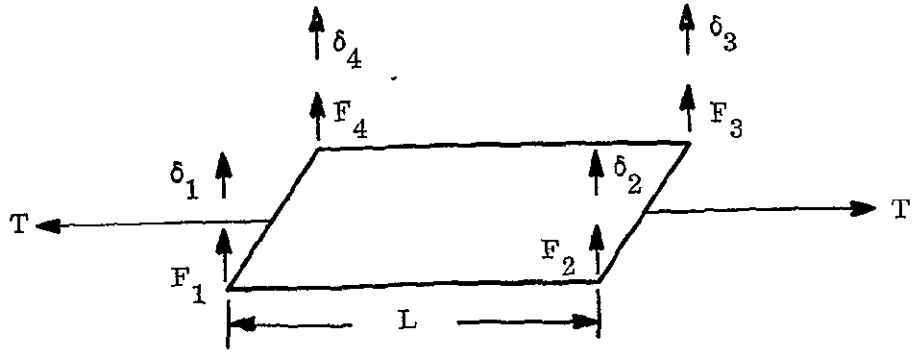
$$F = \begin{bmatrix} F_1 \\ F_2 \\ F_3 \\ F_4 \end{bmatrix} = K \begin{bmatrix} \delta_1 \\ \delta_2 \\ \delta_3 \\ \delta_4 \end{bmatrix} = KX$$

$$K = \frac{T}{6L} \begin{bmatrix} 2 & -2 & -1 & 1 \\ -2 & 2 & 1 & -1 \\ -1 & 1 & 2 & -2 \\ 1 & -1 & -2 & 2 \end{bmatrix}$$

$$F = \begin{bmatrix} F_1 \\ F_2 \\ F_3 \\ F_4 \end{bmatrix} = M \begin{bmatrix} \ddot{\delta}_1 \\ \ddot{\delta}_2 \\ \ddot{\delta}_3 \\ \ddot{\delta}_4 \end{bmatrix} = M\ddot{X}$$

$$M = \frac{W}{32.2 \times 36} \begin{bmatrix} 4 & 2 & 1 & 2 \\ 2 & 4 & 2 & 1 \\ 1 & 2 & 4 & 2 \\ 2 & 1 & 2 & 4 \end{bmatrix}$$

W = TOTAL WEIGHT OF ELEMENT IN POUNDS

Figure 4.3-3. Stiffness and Mass of Membrane Element

The computing routine provides an algorithm for dividing the total system into equal divisions along the span and across the half width, computes the element stiffnesses and masses according to the relations given in Figures 4.3-1, 4.3-2, 4.3-3, and assembles them into a total representation as indicated by Figure 4.3-4 and 4.3-5.

This representation permits a linear varying load to be applied separately to the boom and the blankets which allows consideration of the weight load due to gravity. It also permits a two dimensional representation of the blanket. This model appears to offer a sound basis for extension to include the plate bending stiffness and in-plane membrane stiffness. The in-plane membrane stiffness is considered to be of possible large significance, particularly in torsional modes. Samples of actual solar blankets have bending stiffness that is not obviously negligible or orthotropic. An analysis of blanket stiffness effects is needed. A discussion of qualitative tests of the stiffness of blanket samples is given in Section 6.

The results of computation using this stiffness representation substantiate previous analyses utilizing the string analogy for the first mode; however, the higher modes involve distortions across the membrane width. The incorporation of axial shortening correction has served to verify the "judgement" design choice which sized the blanket tension load on the extension boom to be one-fourth of the critical column load. It has been observed that the first mode frequency is almost unchanged whether axial shortening is considered or ignored when the axial load is in close proximity to the design value. If the axial load is increased, without a corresponding increase in boom section properties, the computed frequencies (for symmetrical modes) reduce significantly.

Some results of computations to evaluate the effects of varying the manner of dividing the system into discrete coordinates are shown in Table 4.3-1. These computations were done as a part of the preliminary studies to incorporate bending stiffness and in-plane flexibility into the model.

In order to incorporate these terms, additional coordinates are required for the system. (For example, incorporation of bending stiffness adds at least two coordinates at each
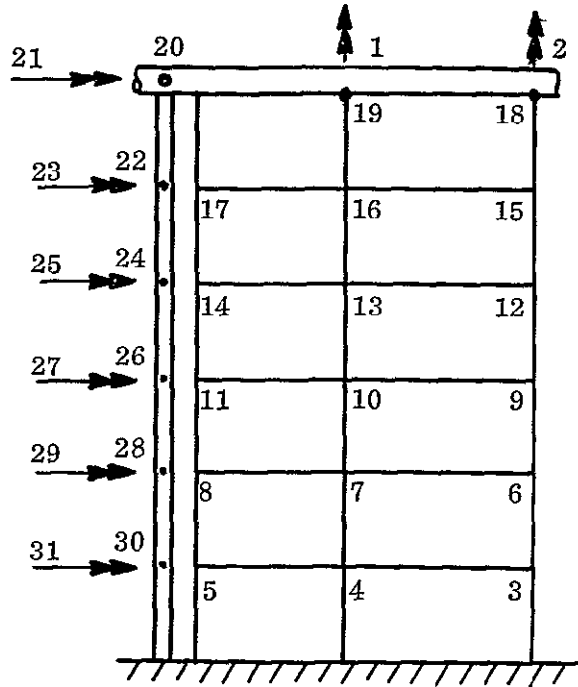
SAMPLE ORDER OF COORDINATE NUMBERING FOR
6 LENGTHWISE ELEMENTS AND 2 ELEMENTS IN A HALF-WIDTH

Figure 4.3-4. Order of Coordinates for Symmetric Case
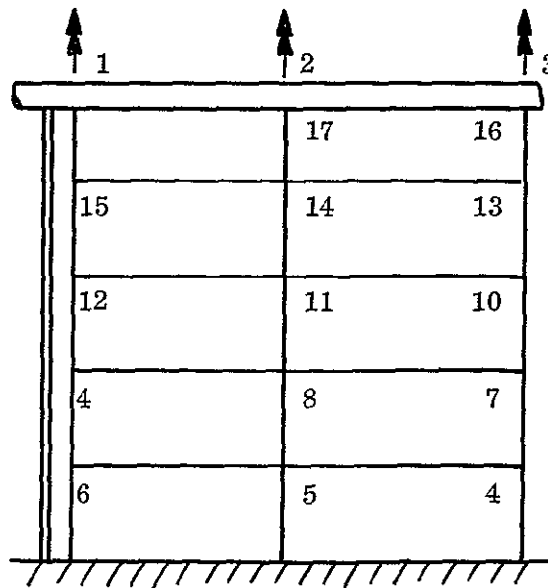
SAMPLE ORDER OF COORDINATE NUMBERING FOR
5 LENGTHWISE ELEMENTS AND 2 ELEMENTS IN A HALF-WIDTH

Figure 4.3-5. Sample Order of Coordinate Numbering for Lengthwise Elements
and Elements in a Half-Width

Table 4.3-1. Comparison of Natural Frequencies with Different System Elements

Number of Elements in Length		Frequency – Hz			
		10	5	10	5
Number of Elements in a Half Width		2	2	1	1
Symmetric	1	0.07715	0.07662	0.07655	0.07678
	2	0.1437	0.1455	0.1437	0.1455
	3	0.1437	0.1455	0.2081	0.2127
	4	0.2067	0.2127	0.2909	0.3052
	5	0.2909	0.3052	0.3482	0.3683
	6	0.2909	0.3683	0.4453	0.4909
	7	0.3474	0.4909	0.4964	0.5429
	8	0.4453	0.4909	0.6104	0.6876
	9	0.4653	0.5429	0.6550	0.7105
	10	0.4960	0.6875	0.7890	1.399
Anti-symmetric	1	0.0703	0.0707	0.06994	0.07014
	2	0.1437	0.1455	0.1437	0.1455
	3	0.1437	0.1455	0.2114	0.2166
	4	0.2115	0.2168	0.2910	0.3052
	5	0.2909	0.3052	0.3576	0.3811
	6	0.2909	0.3052	0.4534	0.4909
	7	0.3576	0.3812	0.5117	0.5654
	8	0.4454	0.4909	0.6104	0.6876
	9	0.4453	0.4909	0.6765	0.7284
	10	0.5117	0.5655	0.7890	1.009

panel point). Because most of the system coordinates are associated with the blanket, it can be seen that the order of the system can quickly grow beyond computational limits if a fine breakdown of the membrane is maintained.

Examination of Table 4.3-1 indicates little difference in natural frequencies through the first five modes for the symmetrical case, or the first six modes in the anti-symmetric, when the number of division across the solar blanket is the same. Reducing the fineness of division across the width, however, eliminates the repeated roots which appear with finer widthwise divisions of the blanket. Examination of the mode shapes associated with the repeated roots indicates a lateral rocking of the blanket in the modes which have integral longitudinal wave lengths (i.e., an odd number of inflection points) in the blanket. Reduction in the number of elements along the length does not appear to seriously affect either the frequency or nature of the lower modes. Present judgment would indicate then (especially because it is anticipated that the incorporation of in-plane flexibility will have its greatest effect on variations across the width of the blanket) that any reduction of elements below two across the width will lose some essential information, while a fairly large reduction in elements in the longitudinal direction (especially in the booms) can be reasonably made.

An analysis of the solar array panels using the Rayliegh Ritz technique and treating them as stretched membranes is presented in Appendix A. The present preferred approach is to treat the blanket as an assembly of interconnected elements and current efforts are directed toward incorporation of in-plane and bending stiffness through the methods described in Reference 7.

4.4 ANALYSIS OF STOWED CONFIGURATION

4.4.1 DYNAMIC ANALYSIS
The dynamic analysis discussion is divided into two separate parts. The first part consists of calculation of the inertial loads for use in design of the structure, while the second part consists of predicting the dynamic characteristics based on a more detailed mathematical model denoted herein as Model II.

The inertial loads used for sizing the RA250 primary structure are based on the environ-
ments specified in Reference 3 and are calculated based on the dynamic characteristics of
the initial mathematical model (Model I). The loads calculated from the math model are
modified to include the effects of the flexible blanket attached to the drum. The status of
the final dynamics mathematical model did not permit the use of the final mode shapes in
determining the loads for use in the design of the structure. However, the results of the
detailed modal analysis to date are presented.

4.4.1.1 Initial Mathematical Model (Model I)

The initial mathematical models for the symmetric and anti-symmetric analysis are presented
in Figure 4.4-1. The symmetric model consists of 33 degrees of freedom located at seven
mass points while the antisymmetric model consists of 32 degrees of freedom located at the
same seven mass points. The motions allowed at the plane of symmetry are x and z for the
symmetric model, and, y, θ_x and θ_z for the antisymmetric model as indicated in Figure
4.4-1. The θ_y coordinates have been eliminated from all mass points.

Beam properties are used to model the drum (mass point 1 through 5) and also the tube
carry through structure (mass points 6 through 7). The bearings are modeled through the
use of an equivalent spring, connecting points 5 and 6.

The stiffness of the center and end supports were obtained through the use of a structural
analysis computer program for the end support, and by hand calculations for the center
support.

The eigenvalues and eigenvectors are obtained utilizing the Jacobian-type iteration procedure.
The resultant mode shapes are normalized to a unit generalized mass. These mode shapes
and the system eigenvalues given in Table 4.4-1 are then used in determining the resultant
inertial loads.

The inertial loads are calculated for the random vibration input by calculating the sine
equivalent response at the resonant frequencies of the first modes (symmetric plus anti-
symmetric) of the system. The response to the sine equivalent input is taken as the same
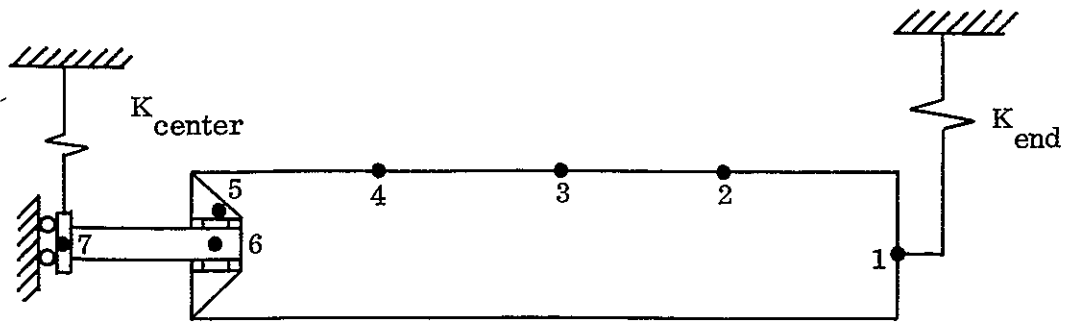
SYMMETRIC MODEL
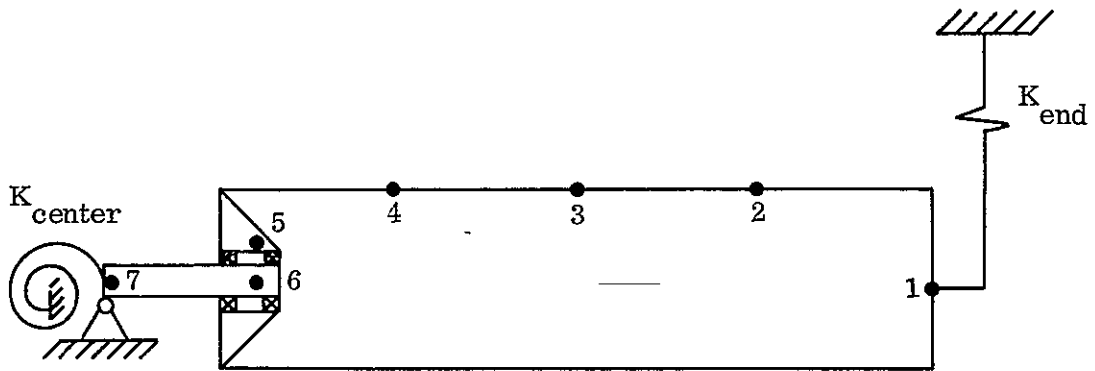
ANTISYMMETRIC MODEL
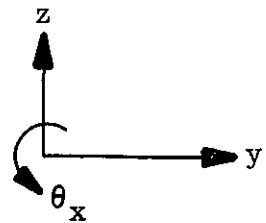
x - out of paper

Figure 4.4-1.   Initial Dynamic Model

Table 4.4-1. Stowed Configuration Frequency Summary

Be Drum (0.02 in Thickness)

Model	Frequency	Mode
Symmetric	145 Hz	Lateral Bending Z
Symmetric	149	Lateral Bending X
Antisymmetric	133	Axial Y
Antisymmetric	175	Lateral Bending Z
Antisymmetric	186	Lateral Bending X

magnitude as the 3-sigma response to the random input. The sine equivalent input is calculated as follows:

$$g_{in} = 3\sqrt{\frac{\pi f G_r}{2Q}}$$

where

g_{in} – sine equivalent input level g_{o-p}

Q   – Amplification Factor

f   – Frequency

G_r – random spectrum level – g^2/Hz

The response calculations are carried out using a Q of 12 for each of the modes. The response analysis as well as the determination of the dynamic characteristics are obtained, assuming that the solar cell blanket acts as a mass attached rigidly to the drum. This assumption results in a conservative loads analysis in that the flexibilities of the blanket wrapped around the drum are not included in the model.

Because these flexibilities are not included in the model, the first blanket mode frequency estimated to be at 50 Hz is not present. With the blanket flexibilities included, the present first mode frequency of 133 Hz would be split into a blanket mode of about 50 Hz, and a higher frequency drum mode. The response at the 50 Hz frequency is approximately one-third of the response at 133 Hz, as can be seen in Figure 4.4-2, where the response of a single degree-of-freedom system to the specified vibration environments is plotted as a function of frequency. Since 80 percent of the supported mass (drum plus blanket) is associated with the blanket, the inertial loads are greatest in the mode which consists primarily of blanket motion. Based on these considerations the inertial loads calculated with the blanket mass rigidly attached to the drum at 133 Hz are ratioed from the response at the resonant frequency to the response level at approximately 50 Hz. These loads are the limit loads to which a factor of 1.25 is applied, resulting in the ultimate loading condition. The ultimate inertial loads are tabulated in Table 4.4-2 for the first two symmetric and first three antisymmetric modes. Only the shear forces are presented as the moment loading is small.

4.4.1.2 Mathematical Model II

The second mathematical model includes a representation of the wrapped solar cell blanket flexibly attached to the drum. This model is shown pictorially in Figure 4.4-3. A conventional lumped mass and stiffness approach was used. From symmetry consideration, it was sufficient to model the stowed configuration from the plane of symmetry (at the center support) to an outboard end support. The stiffness matrix was generated by a general purpose structural analysis computer program. The model included 64 degrees of freedom assigned to 22 mass points. Only translational degrees of freedom were monitored at the mass points. To simulate symmetric drum motions, Y longitudinal motions and all

rotations are restricted at the plane of symmetry. The membrane was simulated by a longitudinal rod, lying along the centerline of the drum, connected to the drum as shown in Figure 4.4-3. This type modeling is equivalent to placing the membrane as a concentric cylinder outside the drum connected to it through the same system of springs. These springs were selected to provide a 50 Hz resonance of the membrane. This particular frequency was selected based on the test data of a rollup up solar cell blanket in Reference 4.

The mode shapes and frequencies were determined using a digital computer program. The dynamic matrix is obtained from matrix multiplication of the stiffness matrix and masses. Jacobi's method (diagonalization by successive rotations) was used to obtain the frequencies (eigenvalues) and mode shapes (eigenvectors).

The mode shapes have been normalized to a unit generalized mass. The first two modes are predominantly blanket modes with only small motions occurring in the drum and are not presented in the mode shape plots. The first five drum modes (system mode 3 through 7) are shown in Figure 4.4-4. The frequencies are summarized in Table 4.4-3. The first two drum modes approximate drum translations with no distortion. The third and fourth modes show drum distortion and are typical cylindrical shell modes, except that the order of the modes for a cylindrical shell would be reversed. The present order is attributed to the presence of the springs attaching the drum and the membrane. This more effectively couples points on the periphery of the drum.

4.4.2 STRESS ANALYSIS

Internal load distributions and member stresses and the stiffness matrix for the final dynamics model were determined through the use of the MASS Computer Program. This routine is capable of analyzing any three dimensional structure that is comprised of or can be approximated by straight and curved beams, tubes, springs, and panel elements for both static and dynamic effects. The program computes member stiffnesses from basic geometric and physical parameters. Using a deflection technique, a total stiffness matrix for the entire space structure is obtained. Substructures may also be used to build up the total system to enable the routine to handle very large structures. The routine sets
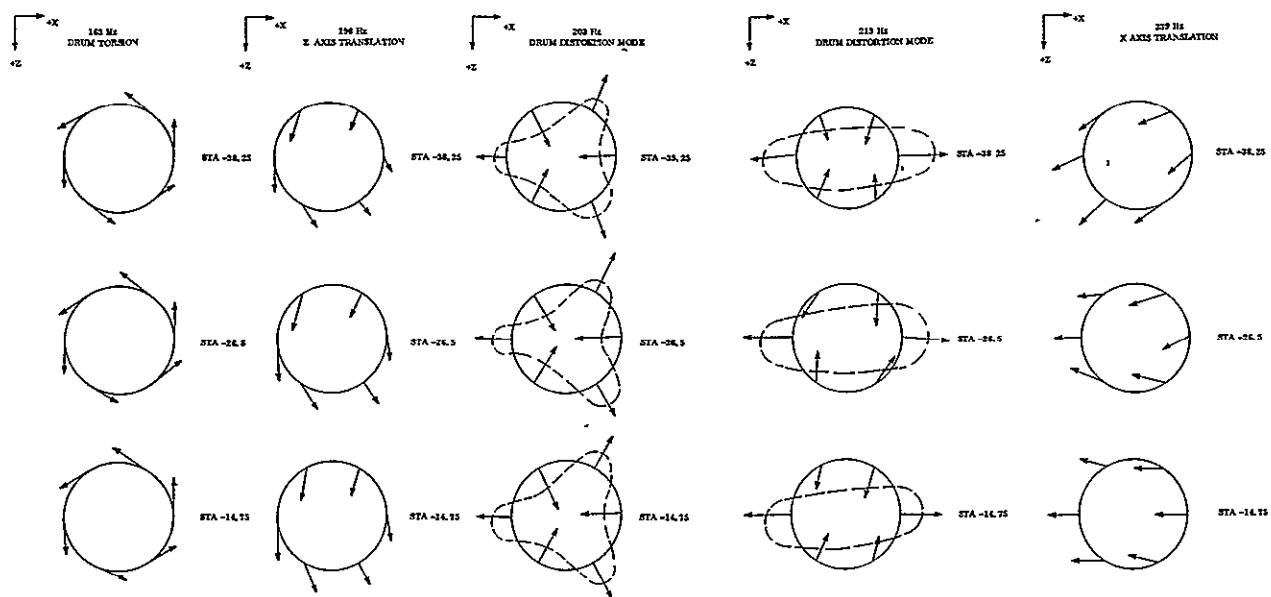
Figure 4.4-4. Storage Drum Mode Shapes

Table 4.4-3. Detailed Model Frequency Summary

(Symmetric)

Mode	Frequency	Description
1	48.4 Hz	Blanket translation – Z axis
2	49.5	Blanket translation – X axis
3	163.	Drum torsion
4	198.	Drum translation ∼ Z axis
5	203.	First drum distorsion mode
6	213.	Second drum distorsion mode
7	239.	Drum translation ∼ X axis

up force-deflection relationships which are then solved for internal loads, stresses, and deflections. Included is the capability to account for pinned and sliding connections anywhere in the structure, unsymmetrical bending, distributed mass, rotary inertia effects, rigid eccentric connections, shear distortion, variable section properties and loadings, thermal gradients, and flexible supports.

The structural model employed in the anlysis is depicted in Figure 4.4-5. The symmetry of the structure with respect to the X-Z plane permitted the consideration of only one-half of the total structure when appropriate boundary conditions are utilized. The center support is modeled as a system of connected flat plate elements with the center support tube represented by members 194-199 and 199-200. Spring 193-194 accounts for the flexibility of the bolted flange connection between the center support tube and the drum support shaft. Springs between joints 162 and 190, and also between 161 and 192, account for the flexibility in the bearings between the drum support shaft and the inboard end cap. Curved panel elements such as 131-136-137-125 are employed to represent the 0.02-inch-thick beryllium drum shell. The outboard support is modeled as a system of flat plates and beams with member 31-36 representing the tie-down bolt and joints 30 and 32 being the hinged reaction points.
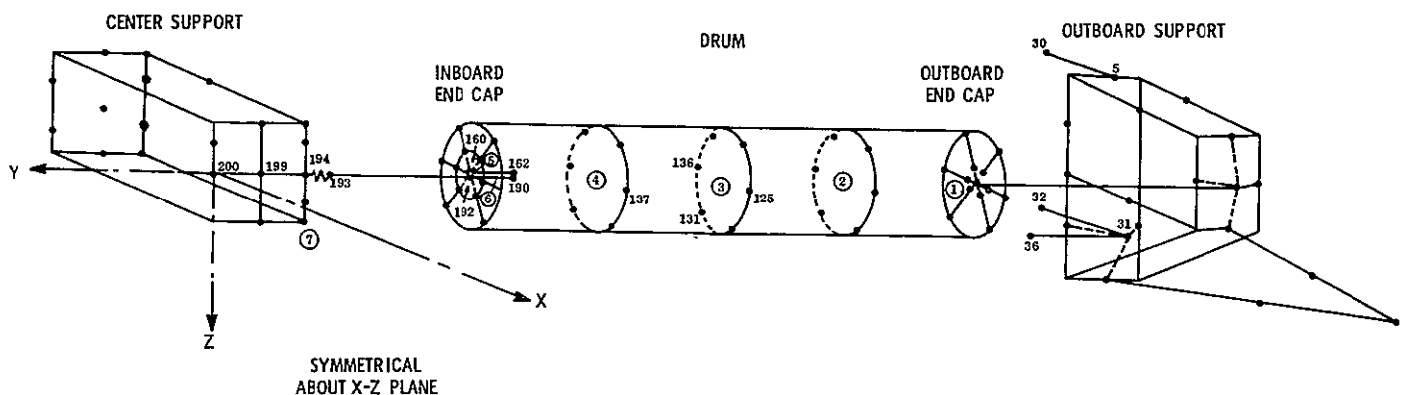
Figure 4.4-5. Structural Model

Static equivalent loads as determined by the dynamic response analysis (see Table 4.4-2) were applied at the seven locations as indicated in Figure 4.4-5. For the "Y" direction analysis, the loads associated with locations 2, 3 and 4, were distributed uniformly to the appropriate structural joints on the beryllium drum shell. In the case of lateral loading of the drum shell, the loads associated with these locations were applied in the same manner as an aerodynamic pressure loading acting on a 180 degree sector of the drum shell.

The drum shell and end caps were modeled with sufficient grid fineness such that the member loads and stresses, as computed by the MASS program, were adequate in themselves to determine margins of safety. No additional analysis is given except to quote stress levels for the critical condition and compute the applicable margins of safety. In other areas such as the center and end supports, center support tube, and drum support shaft, the structural complexity required that a number of members of equivalent stiffness be utilized in place of the actual elements. In these cases the resulting loads and reactions were taken from the program output and utilized for the formalized conventional stress analysis which is included in Appendix B. Margins of safety calculations for all fittings, joints, and attachments, are also given in Appendix B.

4.4.3 THERMAL STRESS ANALYSIS OF DRUM OUTBOARD END

A computerized analysis has been conducted to determine the interaction effects between the magnesium outboard end caps, the beryllium drum, and the textolite guide flange under the influence of a drop in temperature from 70 to -202°F. The modeling techniques are similar to those previously employed for the stress analysis of the entire assembly, except that a finer modeling grid has been utilized in order to determine the critical localized stresses at the bolted connections (joints 11, 13, 14, 16 of Figure 4.4-6). The drum assembly was considered to have sufficient symmetry so that only one-twelfth of the structure need be considered (with the proper symmetrical boundary conditions).

Because the magnesium end cap tends to shrink at a greater rate than either the drum shell or the guide flange, the restraining effect of these outer elements produces tension in the fasteners and subjects the skin flange of the end cap to point concentrated loads.
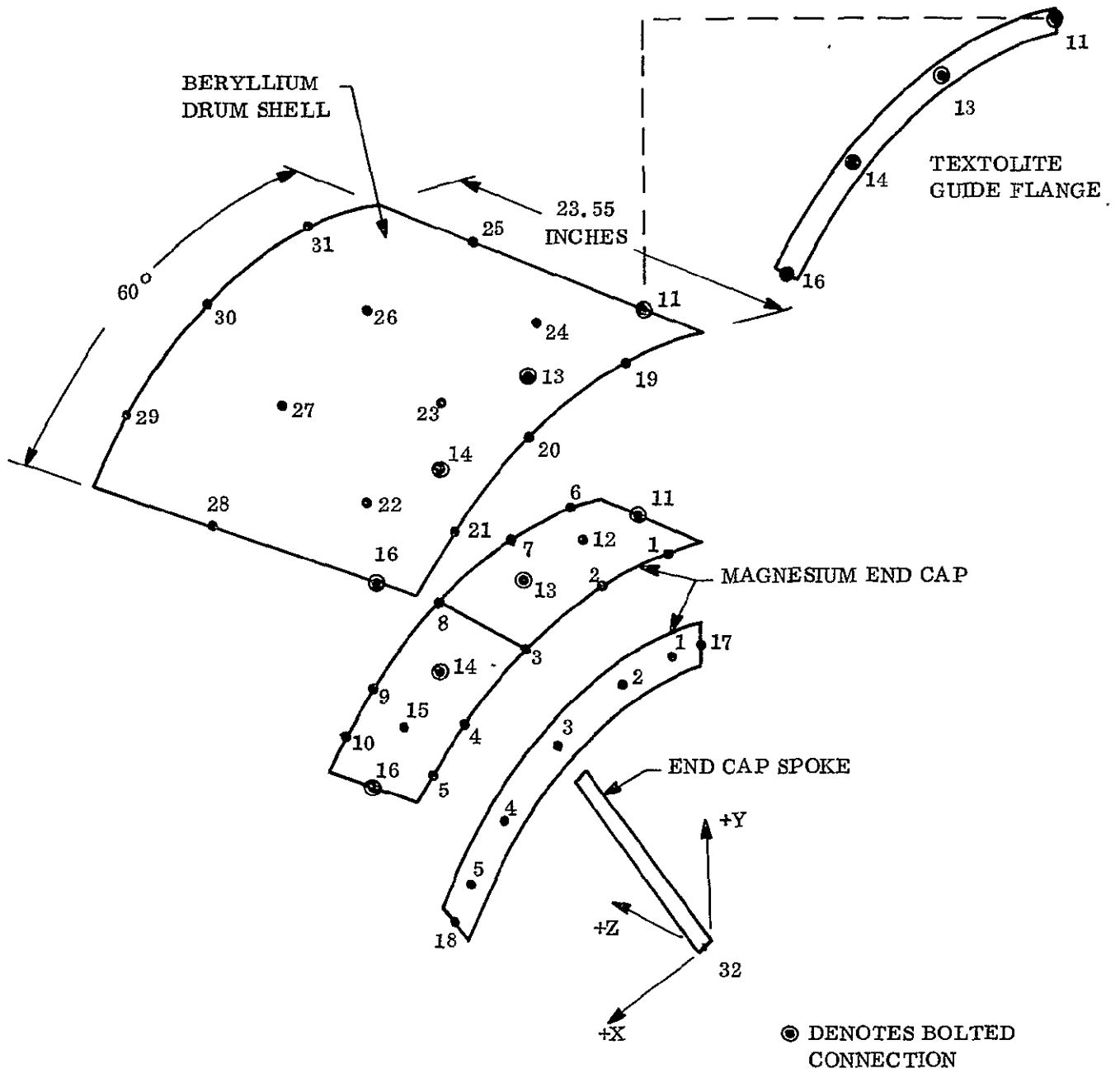
Figure 4.4-6. Drum Outboard End Structural Model

The skin flange of the end cap is represented by plate elements 1-6-12-11, 2-7-13-12, etc., while the cap flange normal to this is represented by beam elements 17-1, 1-2, etc. The "spoke" of the end cap is represented by member 3-32 and the gusseting effect at the juncture of the spoke with the outer flanges is accounted for by rigid connector 3-8. In a similar manner, the beryllium drum shell is represented by plate elements 19-24-13-11, 24-31-26-25, etc., and guide flange numbers run between joints 11-13, 13-14, and 14-16. The dissimilar structural elements are joined together only at bolt locations 11, 13, 14, and 16.

The guide flange develops negligible bending stresses of less than 1000 psi at locations 11 and 16. Bending stresses in the beryllium shell range between 5000 and 6000 psi at the bolt locations. The maximum bending stress in the skin flange of the end cap is 32,300 psi at joints 13 and 14. The yield stress of the ZK60A-T5 magnesium at this temperature is approximately 30,000 psi indicating that some slight local yielding may occur. Inasmuch as the number of cycles for such loading is anticpated to be very small, no ultimate failure can be envisioned.

4.4.4 STORAGE DRUM OPTIMIZATION STUDIES

Selection of a minimum weight storage drum design was based on the use of an existing computer program which has the capability of analyzing cylinders of various types of construction for minimum weight. The main purpose of this program is to compute entry and re-entry vehicle structural loads due to a number of loading conditions such as internal and external pressure, viscous drag, power boost loads, and single and multiple payloads with various support conditions. Taking these applied loads, the program calculates vehicle shear loads, axial loads, bending moments, and the shell hoop and axial membrane forces. From these loads, minimum weight calculations are made for a variety of materials and for the types of shell constructions shown in Table 4.4-4.

In order to utilize this program as a useful tool in the design of the storage drum, the drum was assumed to be simply supported at the ends and an axially uniform pressure distribution of the type shown in Figure 4.4-7 was applied along the drum.

4-28

Table 4.4-4. Comparison of Construction Approaches

Type of Construction	Weight (Lb/Ft^2)		
	Material		
	Al	Mg	Be
Monocoque	0.73	0.57	0.28
Honeycomb	0.54	0.68	0.35·
Waffle	0.45	0.71	0.36
Corregated	1.24	1.26	0.67
Corregated core	1.46	1.26	0.97
Ring-stiffened	0.63	0.57	0.29

ASSUMED SUPPORTS

q_o = 32.5 LB/IN.^{2}

q_o = 0

ASSUMED LOADING
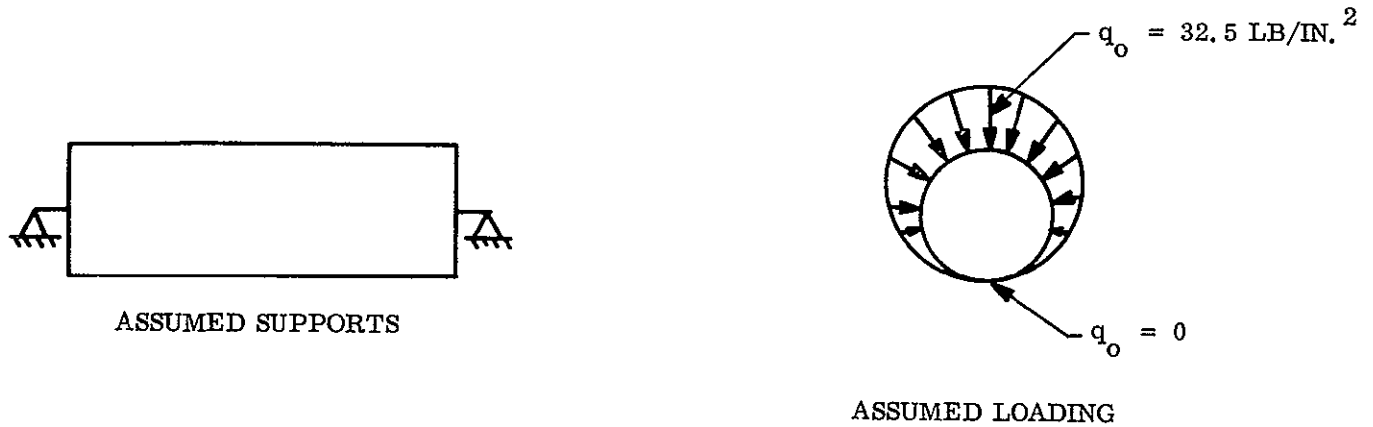
Figure 4.4-7. Support and Loading for Storage Drum Optimization Study

This loading is representative of the conditions that exist in the rollup array and therefore a minimum weight type of construction can be determined. The maximum pressure intensity (q_o) was based on the expected loads with a blanket rigidly attached to the drum. The simple support condition was selected to yield the highest membrane loads.

The results of the analysis are presented in Table 4.4-4 and, as indicated, either a monocoque or semi-monocoque type of construction is optimum for the loading conditions imposed.

4.5 MAGNETIC FIELDS ANALYSIS

An analysis of one solar array blanket was performed to evaluate the magnetic field produced by the dc currents flowing in the circuits on that blanket. The sampling point at which the field was computed is taken at one meter above the blanket geometric center as shown in Figure 4.5-1. It was assumed that the blanket is perfectly flat, that the current in all solar cell strings is the same, that the bus strips are of negligible width, and that the blanket thickness is negligible. The basis for the analysis is the Biot-Savart Law. This analysis considered the array blanket to be composed of three different types of current carrying conductor configurations as shown in Figure 4.5-2.
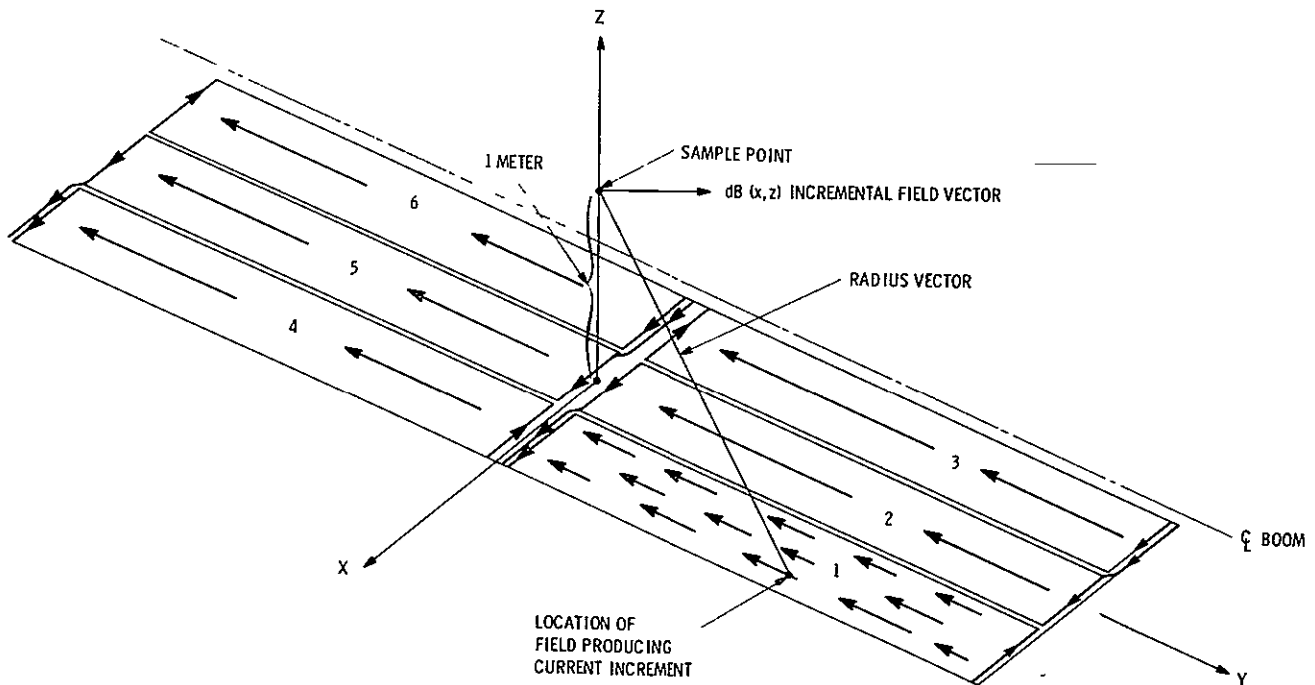
Figure 4.5-1. Arrangement of Array Current Carrying Loops on Cell
Side of Blanket
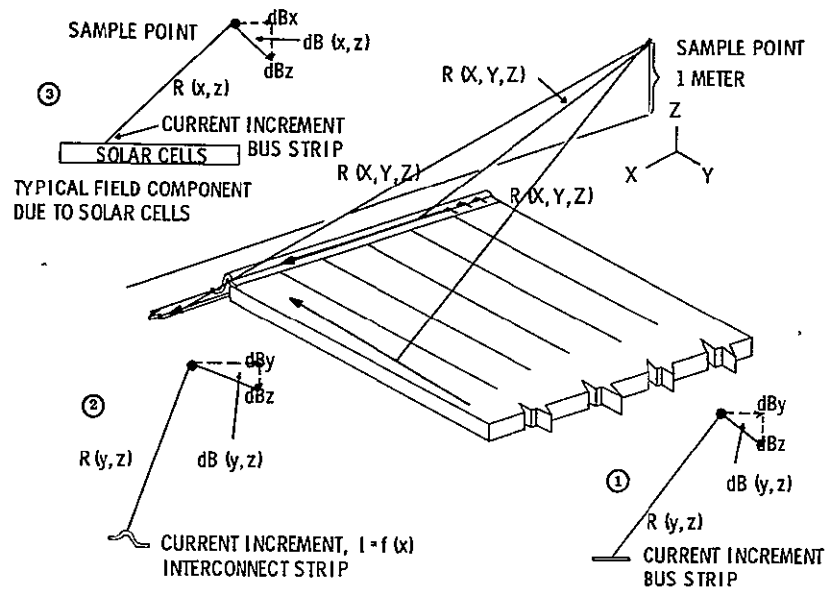
Figure 4.5-2. Pictorial Representation of Circuit Configuration

Circuit configuration No. 1 is a line conductor carrying uniform current. The magnetic field at a point P (x, y, z) can be defined with the aid of Figure 4.5-3.

From the Biot-Savart Law,

$$\Delta H = \frac{I \Delta x \sin \theta}{R^2}$$

Summing over the length of the conductor and substituting geometric relations gives the following integral.

$$H = I \int_{A_1}^{A_2} \frac{(y^2 + z^2)^{1/2}}{(x^2 + y^2 + z^2)^{3/2}} \, dx$$
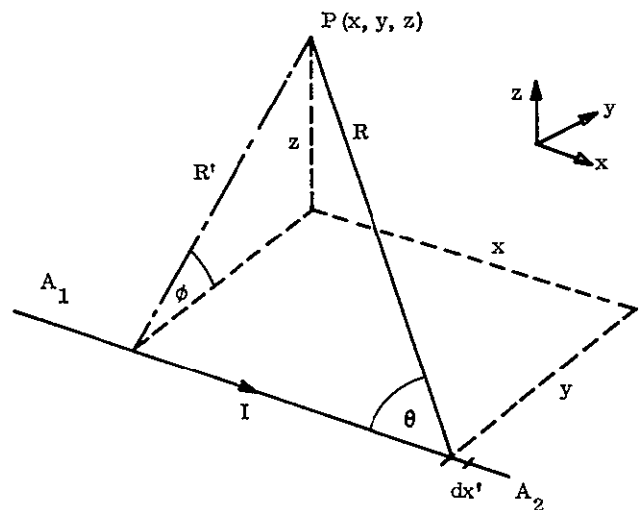
Figure 4.5-3. Line Conductor Carrying Uniform Current

Performing the integration yields:

$$H = \frac{I A_2}{\left[(y^2 + z^2)(A_2^2 + y^2 + z^2) \right]^{1/2}}$$

$$- \frac{I A_1}{\left[(y^2 + z^2)(A_1^2 + y^2 + z^2) \right]^{1/2}}$$

Circuit configuration number 2 is the line conductor in which the current varies linearly along the conductor. This case is shown pictorially in Figure 4.5-4, and the incremental field is given by:

$$dH = \frac{I (y - B_2) R' \, dy}{(B_1 - B_2) R^3}$$
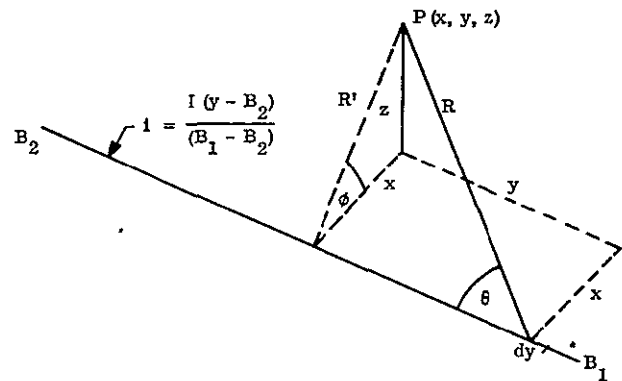
Figure 4.5-4. Line Conductor with Varying Current

Integrating this expression along the length of the conductor from B_2 to B_1 yields

$$H = \frac{I}{(B_1 - B_2)} \left\{ \left[\frac{B_2^2}{\sqrt{(x^2 + z^2)(x^2 + z^2 + B_2^2)}} - \sqrt{\frac{(x^2 + z^2)}{(x^2 + B_2^2 + z^2)}} \right] \right.$$

$$\left. - \left[\frac{B_1 B_2}{\sqrt{(x^2 + y^2)(x^2 + z^2 + B_1^2)}} - \sqrt{\frac{(x^2 + z^2)}{(x^2 + B_1^2 + z^2)}} \right] \right\}$$

Areas covered with solar cells are represented as thin sheets of current as shown in Figure 4.5-5. In this case the magnetic field increment is:

$$dH = \frac{i \, dx \, dy \, R'}{R^3}$$
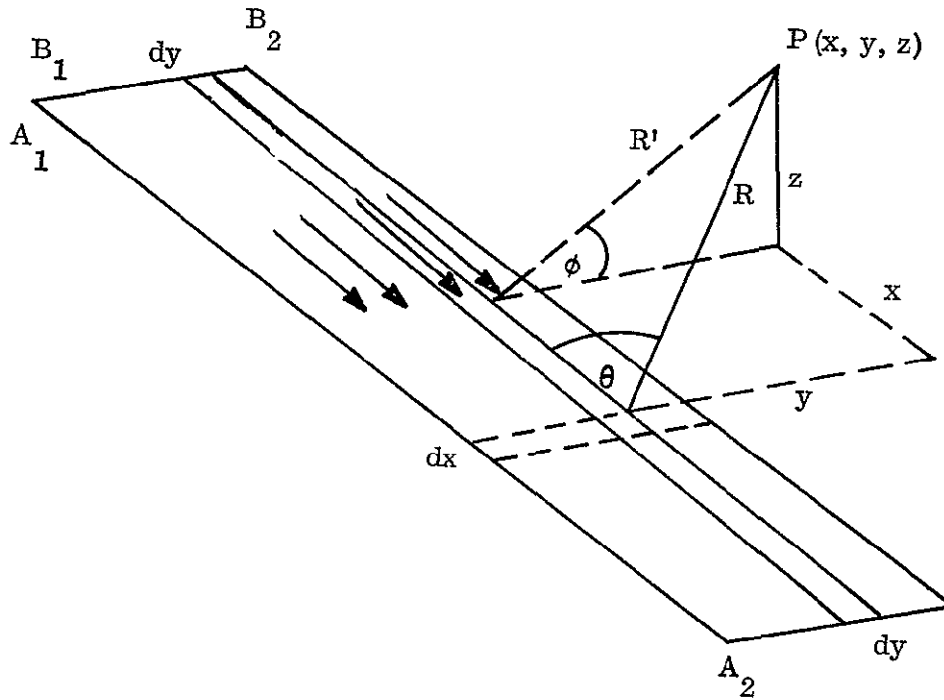
Figure 4.5-5. Sheet of Current

Integrating over the area yields

$$H = i \int_{B_1}^{B_2} \left\{ \frac{A_2}{\left[(y^2 + z^2)(A_2^2 + y^2 + z^2) \right]^{1/2}} - \frac{A_1}{\left[(y^2 + z^2)(A_1^2 + y^2 + z^2) \right]^{1/2}} \right\} dy$$

This analysis was mechanized for computer solution based on the array blanket circuit layouts shown in Figure 3.1-3. The components which contribute to the field at the sample point are summarized in Table 4.5-1. The total resultant field at the sample point is calculated as 0.83 gamma.

Table 4.5-1. Magnetic Field Components in Gamma

Circuit No.	1	2	3	4	5	6	7
Solar Cells							
x comp	-0.343	-0.393	-0.343	-0.343	-0.393	-0.343	-2.158
z comp	-0.131	0	0.131	-0.131	0	0.131	0
Interconnect							
Bus							
y comp	-0.050	-0.618	1.013	-0.196	-0.202	0.206	0.153
z comp	-0.001	0.013	-0.021	-1.000	-1.034	-1.051	-3.094
Return Bus							
y comp	-0.197	0.207	0.207	-0.103	0.105	0.105	0.324
z comp	-0.999	1.051	1.051	-1.054	1.068	1.068	2.185
Bus Conductors							
x comp	0.347	0.397	0.397	0.293	0.392	0.392	2.218
y comp	0.032	0.097	-0.063	-0.015	0.067	-0.042	+0.076
z comp	0.240	0.041	0.031	0.154	-0.034	-0.133	+0.299
TOTAL FIELD							
IN x	0.004	0.004	0.054	-0.050	-0.001	0.049	0.060
IN y	-0.215	-0.314	1.157	-0.314	-0.030	0.269	0.553
IN z	-0.891	1.105	1.192	-2.031	0.0	0.015	-0.610

4.6 RELIABILITY ANALYSIS

The reliability analysis consisted of two areas of investigation:

1. An numerical reliability prediction of the electrical components.

2. A failure mode, effect and criticality analysis of the entire system

4.6.1 RELIABILITY PREDICTION OF ELECTRICAL COMPONENTS

The components considered and investigated for this analysis were the solar cells, slip ring assembly, BI-STEM actuator motor, electrical connectors and microswitches.

Failure rates used in this analysis were selected from published data and the source of the data used is cited. In most cases, the failure rates are based on many unit hours of operation. For example, the solar cell failure rate is based on 3.4 by 10^9 part hours and the slip rings on 26 by 10^6 part hours.

The analysis indicated that the array requiring all 55176 solar cells to be operable has a reliability of 0.95 for a time period of 5880 hours (245 days). A detailed analysis of the solar cell blankets considering all the possible combinations of failures for a partial success would, of course, result in a higher reliability.

This numerical analysis presented in Table 4.6-1 should be considered as a relative comparison between different electrical components constituting the solar array.

4.6.2 FAILURE MODE, EFFECT AND CRITICALITY ANALYSIS (FMECA)

This FMECA was performed to identify possible failure modes and assess the effects of such failures on the performance of the array. The following assumptions and definitions have been applied to this analysis:

1. Structural failures such as the collapse of a support member are not being considered in this analysis.

Table 4. 6-1. Results of Numerical Analysis

Part Time	Quantity	Failure Rate (X 10^{-6})	Failure Rate Data Source	R (for 245 days)
Solar Cells	55176	0. 00014	NASA [1]	0. 956 [2]
Slip Ring Assembly	2	4. 273	FARADA [3]	0. 999 [4]
Actuator Motor	1	1. 1	MIL–HDBK 217 A	0. 999 [4]
Connectors	5	0. 13	MIL–HDBK 217 A	0. 999
Microswitches	3	0. 25	MIL–HDBK 217 A	0. 996
				0. 949 R TOTAL

1. NASA Report by Welfred M. Redler dated 1964, Office of Reliability and Quality Assurance, Washington, D. C.

2. 0. 956 represents a worst case condition where all 55176 Solar Cells are required to be operable.

3. FARADA Report June 1, 1967 page 4. 308

4. Ten complete extension/retraction cycles consuming 4. 47 hours used for this calculation.

2. It has been assumed that all input signals and power originating outside of the solar array are available at the required time and only at that time.

3. It has been assumed that necessary circuit protection and fail safe devices are present in other subsystems supplying signals and power to the solar array.

4. Part failures included in the description of a failure mode for a separate and distinct part are not listed separately unless they perform more than one function. This eliminates duplications and insures clarity and brevity.

5. Definition of Criticality:

   a. Category I: (Single Point Failure)

      One failure such that if it occurred it would cause the loss of the required subsystem output. The required output is defined herein as 2461 watts at 102 volts 1 A.U., AMO, 55°C, beginning-of-mission.

   b. Category II:

      One failure such that if a second associated failure were to occur it would cause loss of the required subsystem output.

   c. Category III:

      All failures not included in criticality categories I or II including degraded operations.

The detailed results of this analysis are shown in Appendix C. Six separate hardware items have been identified as Category I, single failure points. These six hardware items possess a total of ten separate failure modes. Two hardware items were identified as Category II failures.

It has been concluded that the single failure points identified cannot be eliminated without prohibitive weight and complexity penalities. The selected approach is to consider the failure modes during design to minimize their chances of occurring and to recognize that all category I and II identified parts require special care during storage, handling, assembly, testing and shipment. Reduction in the probability of failure of these items will be ensured through special inspection and test procedures to be specifically developed at a later date.

SECTION 5

MANUFACTURING AND PROCESS DEVELOPMENT

The major emphasis during this reporting period has been directed towards the design and fabrication of the tooling required for the array blanket fabrication. In addition, the process development activity associated with interconnection soldering has been progressing.

5.1 INTERCONNECT SOLDER PLATING

A process has been developed which utilizes a selectivity solder plated silver expanded metal interconnect. This plated interconnect is soldered to the front and rear solar cell contact through the application of heat from an infrared lamp.

Figure 5.1-1 shows an enlarged photograph of the proposed interconnect. Note the zones of solder plating on the expanded metal. This technique yields a uniform solder coating on the mesh which ensures a minimum amount of solder used to attach the interconnect to the cell. This enhances the integrity of the solder joint and the solar cell structure during temperature cycling. Figures 5.1-2 and 5.1-3 show the rear and front side connections, respectively, using this solder plating approach. The development activity is continuing in an effort to further reduce the thickness of solder which is plated on the expanded metal. The plated material is Sn60 solder over which is deposited a silver layer to obtain a composite material which has a 2 percent silver content (equivalent to Sn62 solder).

5.2 TOOLING

All tooling required for the solar array blanket fabrication has been identified and designs have been released for the items listed below:

Drawing No.	Title
TDL-2018	"X" and "Y" Indexing Table
TDL-2019	Form and Trim Die
TDL-7013	Button Forming Fixture
TDL-7011	Glassing Fixture
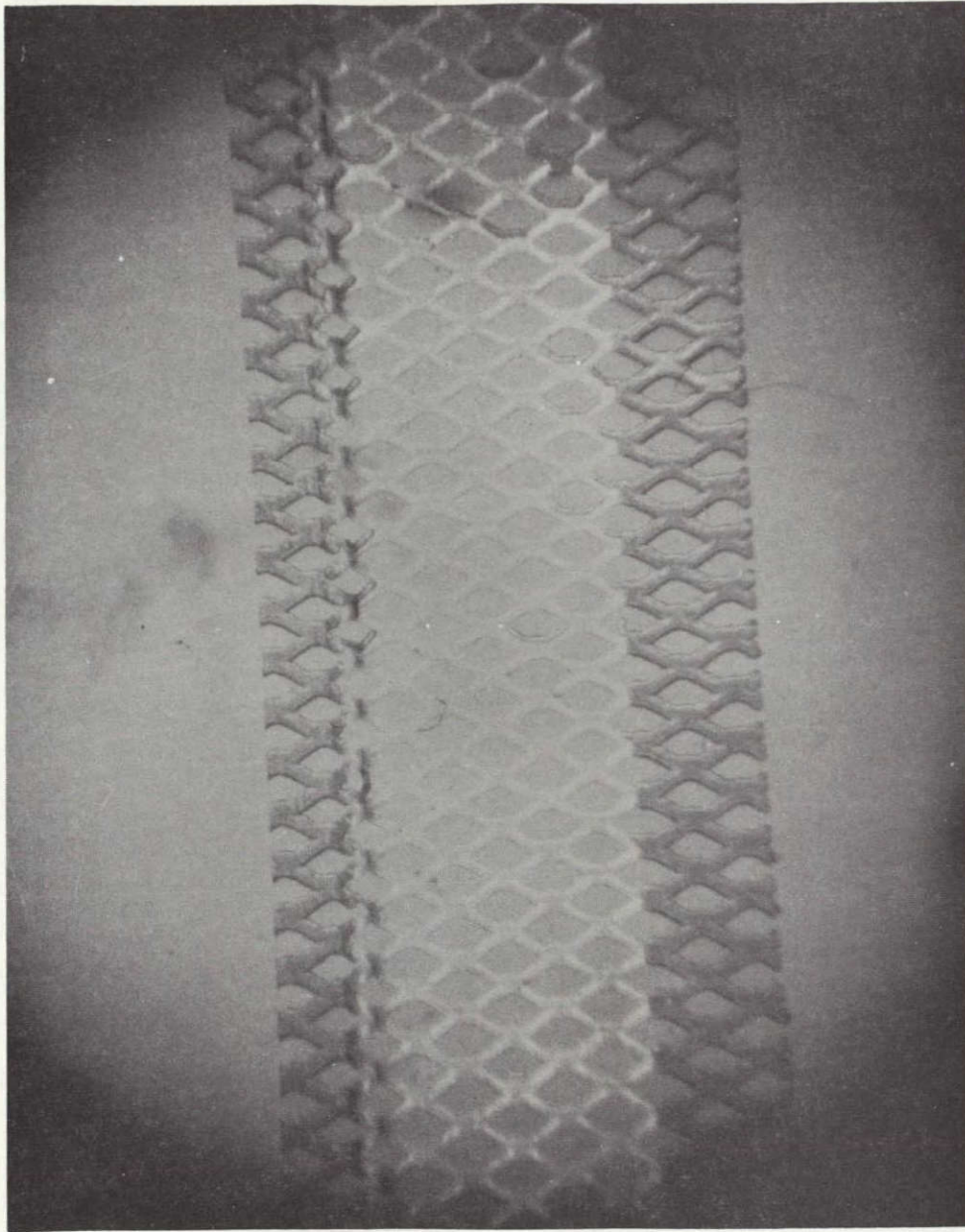
Figure 5.1-1. Selectivity Plated Ag Expanded Metal Interconnect
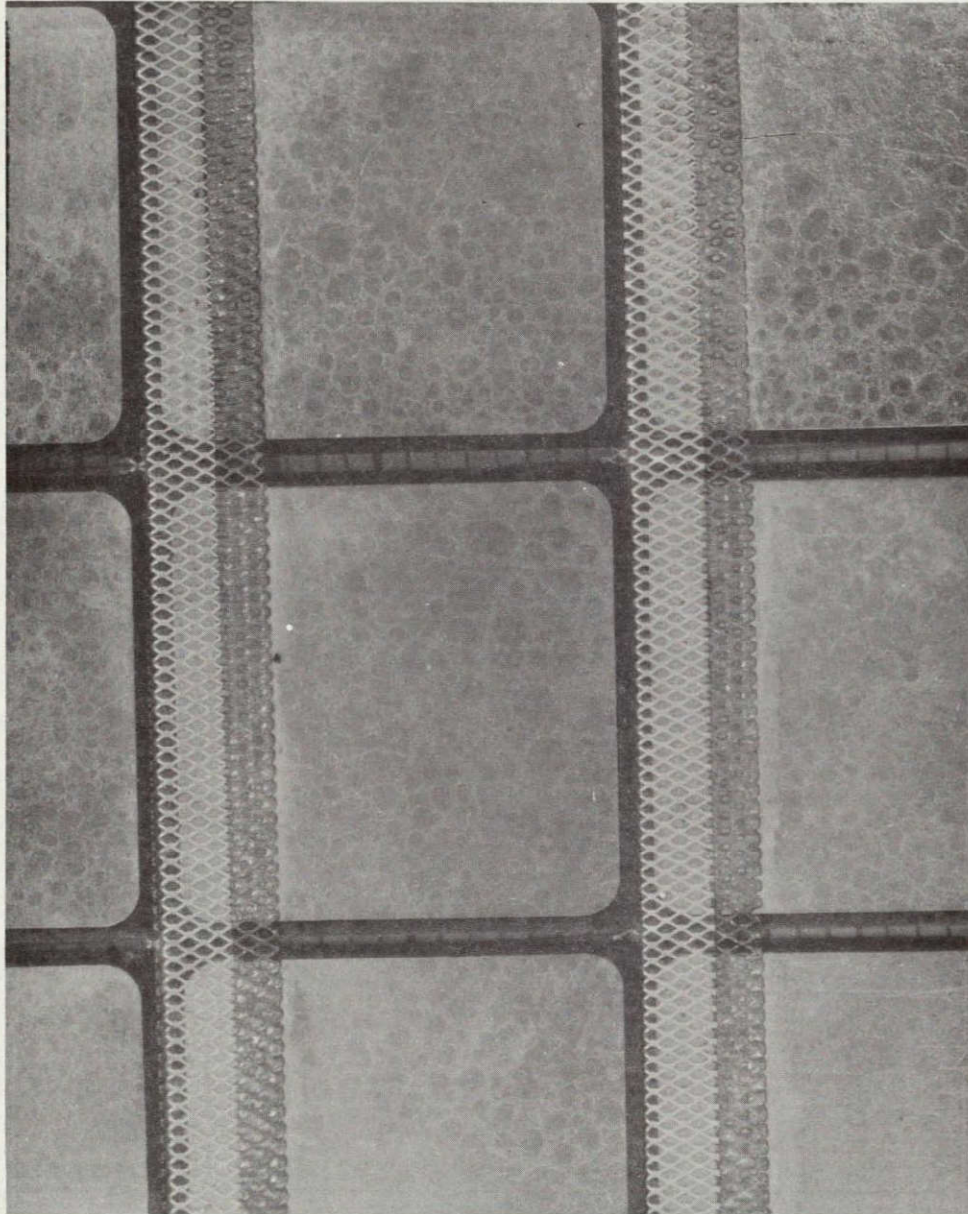
Figure 5.1-2. "P" Contact Connection Using Soldered Plated Ag Expanded Metal
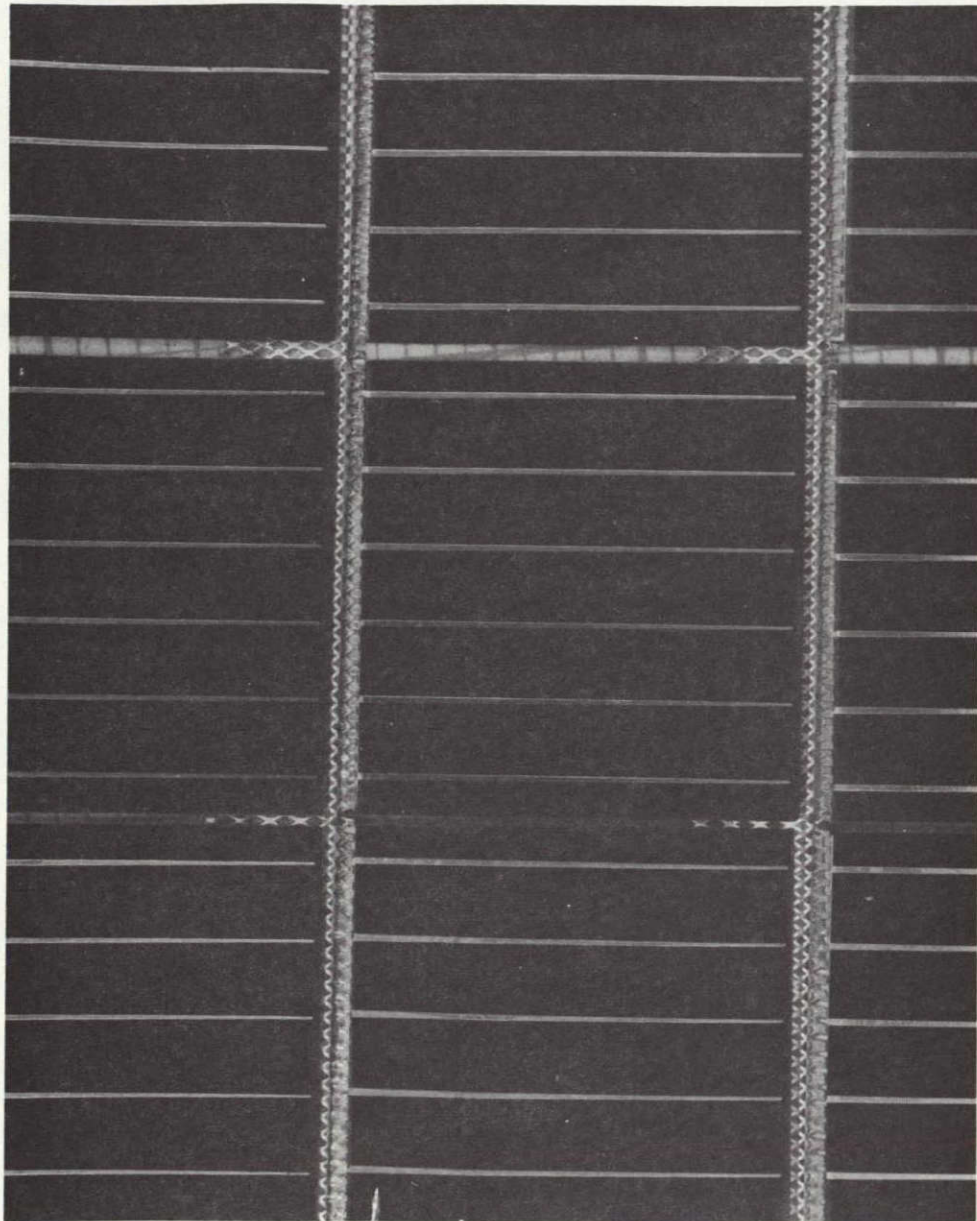
Figure 5.1-3. "N" Contact Connection Using Soldered Plated Ag Expanded Metal

TDL-7018	Soldering Fixture
TDL-7014	Curing Table
TDL-7019	Dummy Glassing Fixture
TDL-7012	Holding Fixture
TDL-7017	Roller for Kapton

The "X" and "Y" Indexing Table (TDL-2018) is used to precisely position the infrared heat lamp for the soldering of the interconnects. The Form and Trim Die (TDL-2019) is used to form and trim the solder plated Ag expanded metal interconnects. The fabrication of this tool has been completed and Figure 5.2-1 shows it in use. The Button Forming Fixture (TDL-7013) is essentially a template which controls the diameter, thickness and position of the RTV560 cushioning buttons on the rear of the array blanket substrate. The Glassing Fixture (TDL-7011) is a holding fixture for the 0.003-inch solar cell coverglass. The 380 pieces of glass required for the 19 by 20 cell module are placed in this fixture to obtain the precise spacing necessary to achieve proper mating with the solar cell module. The Soldering Fixture (TDL-7018) positions the solar cells and interconnects for the soldering process. Solar cells are held face down in the fixture and soldering of both connections in one row are accomplished simultaneously with heat from an infrared lamp source. The Curing Table (TDL-7014) is a mobile 100 by 48 inch horizontal surface which is used for curing the array blanket adhesive (SMRD-745). The area of the substrate to be bonded is placed on the horizontal surface with the remaining portions of the blanket on take-up rollers at either end of the table. Following completion of the bonding operation, the table is wheeled into an oven for the curing of the adhesive. The completed area is then rolled onto the take-up roller exposing a new area of the substrate for the bonding operation.

The Dummy Glassing Fixture (TDL-7019) is used to position the dummy glass (0.011 by 0.750 by 0.750 inch) simulated solar cells at the precise spacing required for the bonding of the dummy solar cell modules.

The Holding Fixture (TDL-7012) is a 1/16-inch-thick piece of plexiglass which is used to hold the coverglass and the dummy glass for transfer from the Glassing Fixture (TDL-7011) or the Dummy Glassing Fixture (TDL-7019) to the cell holding fixture or the substrate. The glass is held to this fixture by taping through a hole over each piece of glass. The Roller for Kapton (TDL-7017) provides an 8-inch-diameter storage drum for the array blanket during the fabrication process. Two such drums are provided with the curing table to store both the completed portion, and the basic Kapton substrate before module bonding.
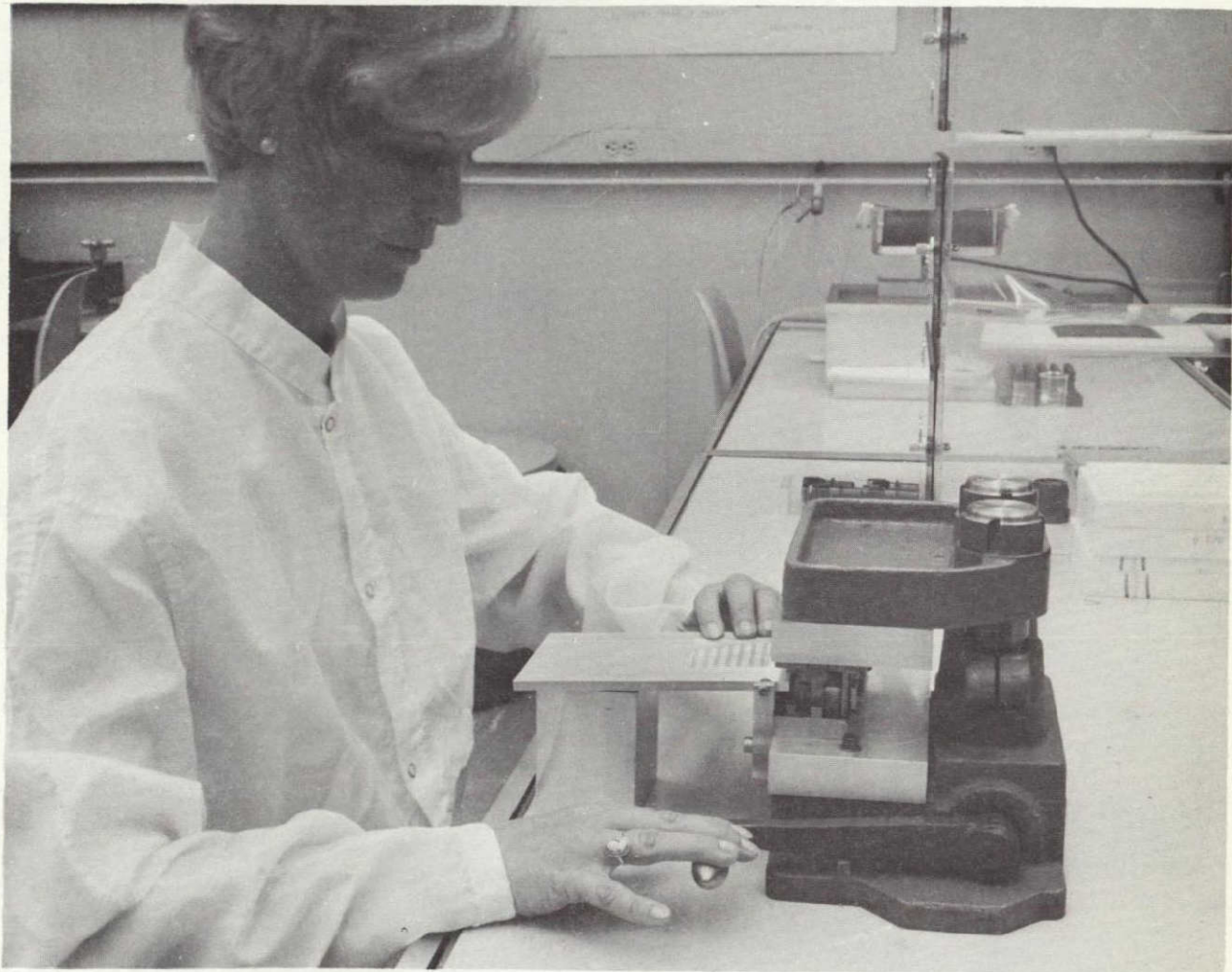
Figure 5.2-1. Interconnect Forming and Trimming Tool

6.1 DEVELOPMENT TESTS

Development tests are planned and conducted to supply information which is needed for design, analysis, or planning the program.

6.1.1 DUMMY CELL MODULE STIFFNESS EVALUATION

The prototype subsolar array which will be assembled and tested during the Phase II program will, for economic reasons, have only ten percent of its surface covered with active solar cells. The remaining area is to be covered with dummy cells. A preliminary development test was performed to determine if the physical characteristics of the proposed construction was appreciably different from that of solar cells mounted on the typical rollup array substrate of Kapton and cushioning buttons.

Two configurations of solar cell-interconnection substitute units were assembled and evaluated for degree of stiffness simulation. Both of these dummy module configurations simulate the cell by a chip of glass 0.013 inch thick by 0.75 inch square. The dummy interconnection for Configuration 1 is the same silver mesh interconnection used with solar cells, bonded to span the gap between chips with SMRD 745. For Configuration 2, the dummy interconnection is a 2 mil strip of Kapton the same width as the silver interconnection (0.26 inch). It is similarly bonded across the gap with SMRD 745.

Five cell by five cell modules were constructed of each configuration and checked for stiffness against comparable solar cell modules. The test modules included Configurations 1 and 2 and a module without simulated interconnections.

Figures 6.1-1, 6.1-2, and 6.1-3 show the deflection test set up and modules undergoing deflection testing in both the "face up" and "face down" directions. Figure 6.1-4 is a graph of the data obtained during the deflection tests. The area of most relevance is along the "0" grams load line where the units were being supported at the edges and deflected only by their
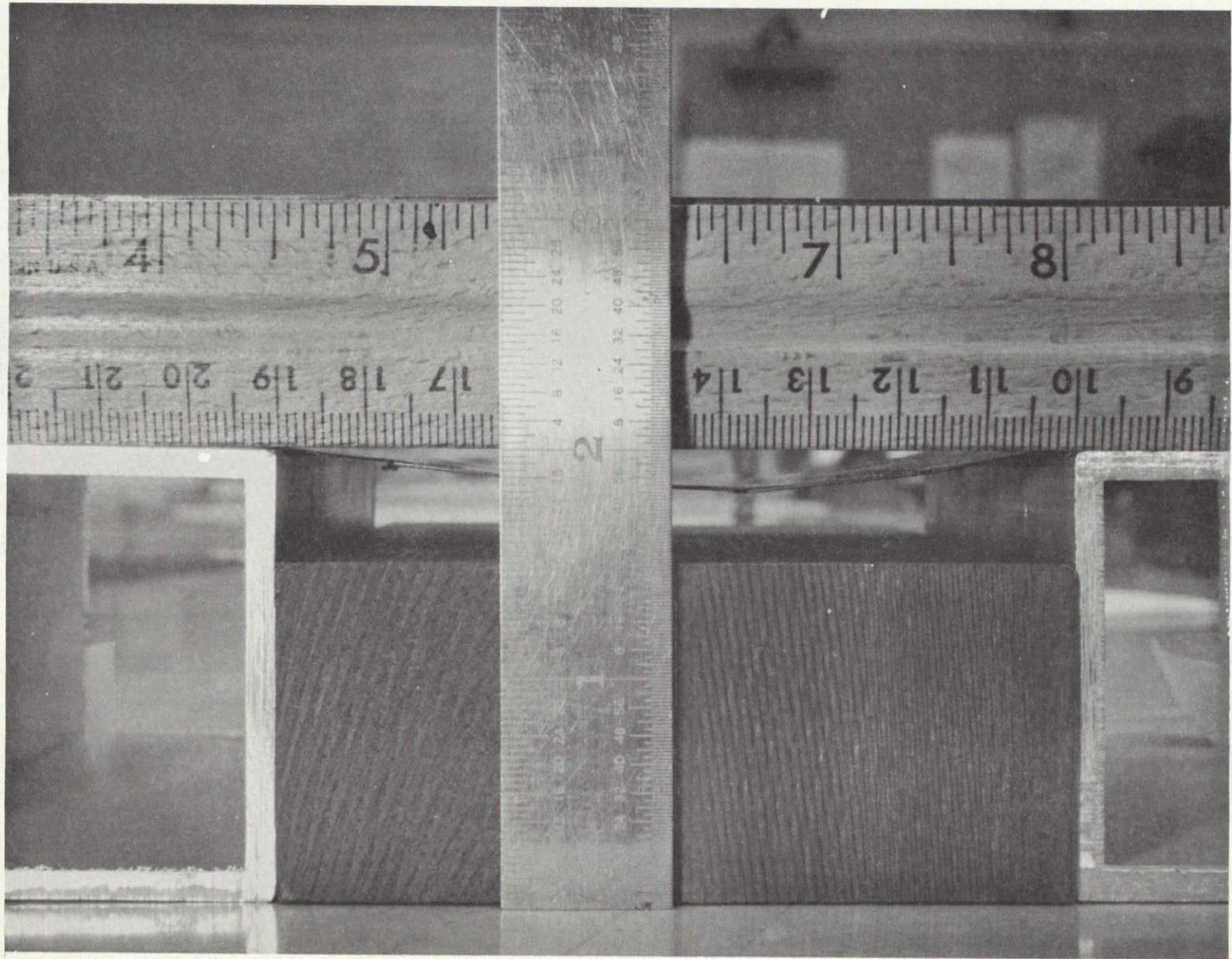
Figure 6.1-1   Solar Cell Module Deflection Test Setup
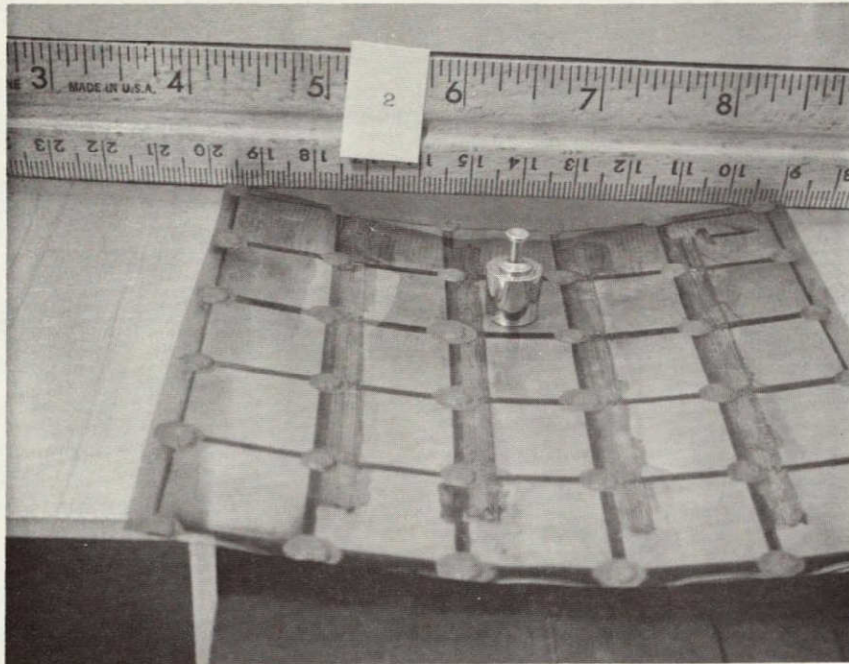
Figure 6.1-2. Face-Down Deflection Test - Active Solar Cell Module No. 1
with 5 Gram Load
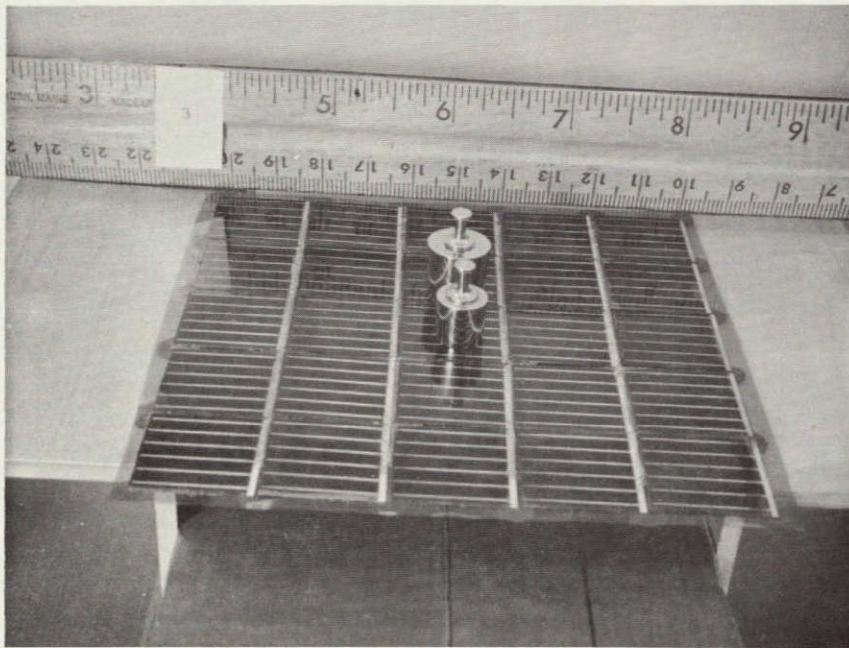
Figure 6.1-3. Face up Deflection Test - Active Solar Cell Module No. 1
with 15 Gram Load
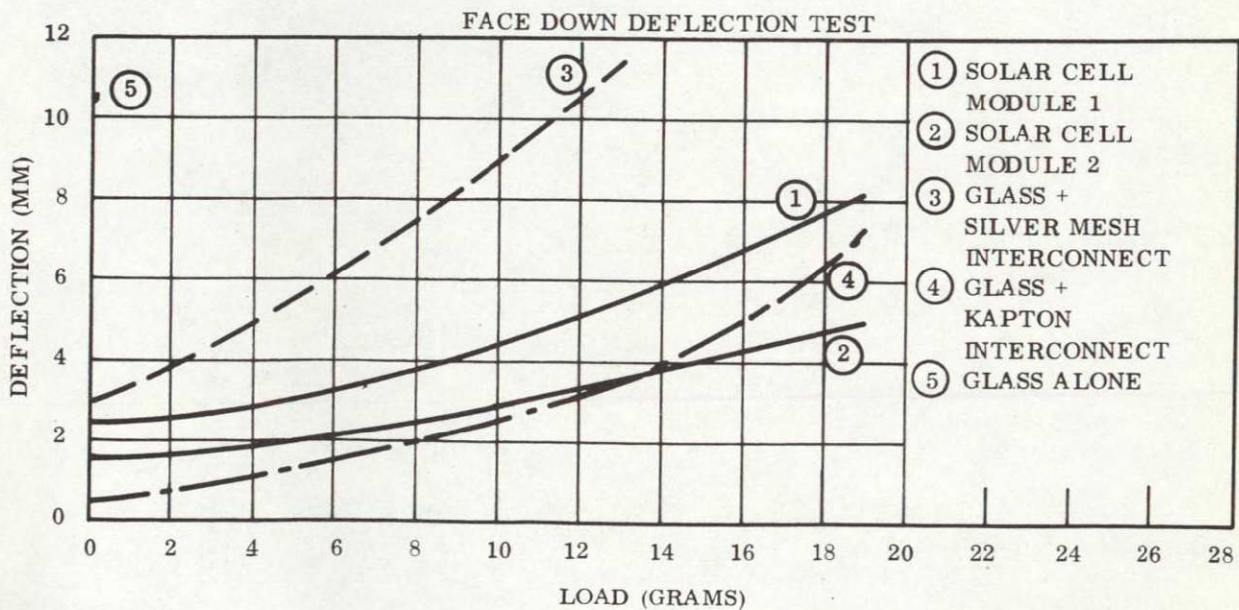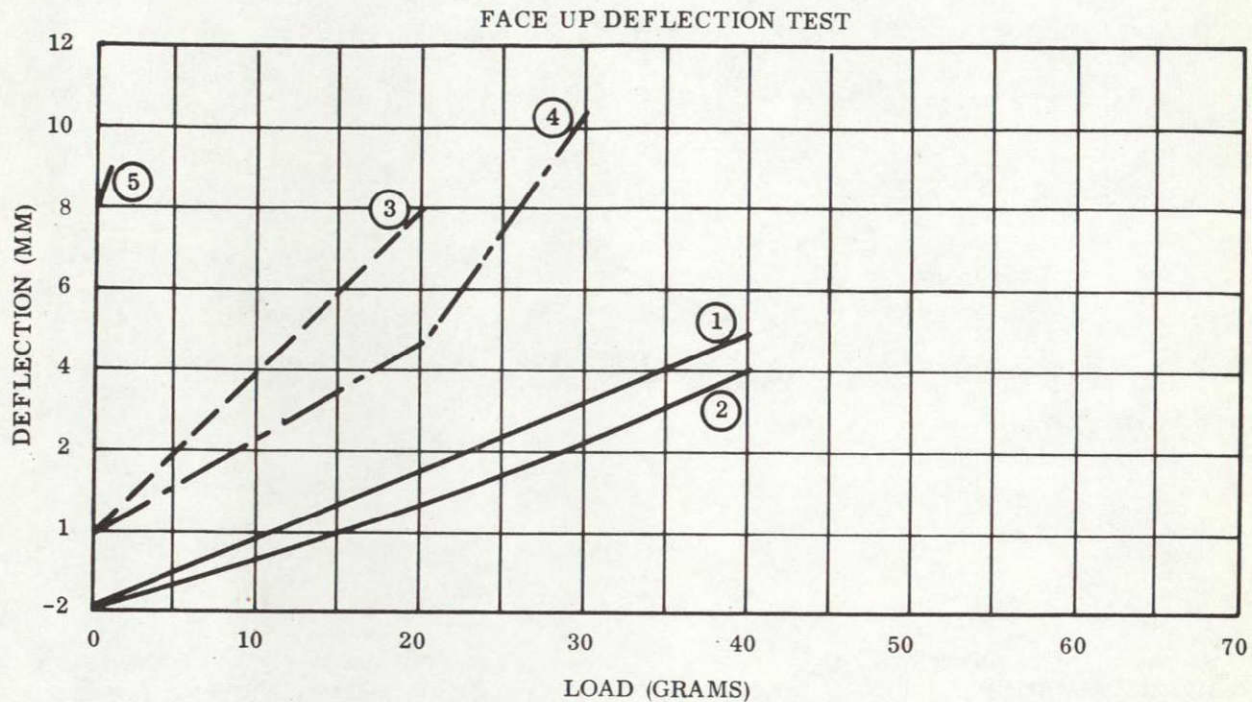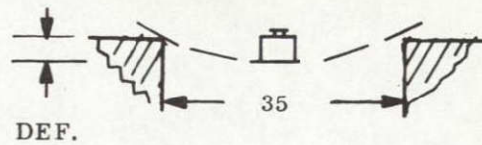
Figure 6.1-4. Load Deflection Curves

own weight. Both dummy configurations approximate the no-load stiffness of the solar cell assemblies, and the wide margin separating the group from the "glass only" module highlights the need for inclusion of a simulated interconnection.

Additional load-deflection data was obtained in the transverse direction (with the interconnections perpendicular to the supporting edges). These data are shown in Figure 6.1-5. There is an appreciable variation in the stiffness of the two solar cell modules which is probably due to a variation in the bonding process. Both types of dummy construction using interconnection simulation (silver mesh and 2 mil Kapton strips) closely correlate with solar cell module No. 1.

The Kapton strips are considered to provide the best simulation of the stiffness of the solar cell modules, and it is planned to incorporate these strips into the dummy modules on the solar cell blanket for the test unit.

6.2 SYSTEM TEST PLANNING

System test planning activities have resulted in the following technical considerations affecting the tests.

6.2.1 SHOCK AND VIBRATION TESTING

The stowed array modal and qualification vibration tests and the shock test are presently being planned for two MB-C220, 35,000 g-lb force exciters. Evaluation of these exciters shows they are adequate for stowed modal and qualification vibration testing. The use of the C-220 exciters for shock testing is marginal with regard to the time domain reproduction of the specified terminal sawtooth pulse shape. Insufficient force is available from the C-220's to provide the 250 g's peak acceleration. Also the 2 kHz frequency limitation of the exciters is marginal with respect to the 0.5 msec duration.

The alternative considered is to test to the shock spectrum equivalent of the specified shock pulse as allowed by the specification (Reference 3.). This will result in an input pulse train having a reduced peak acceleration and increased train period. The synthesized input shock train will be shaped to produce a shock spectrum identical to that associated with the specified
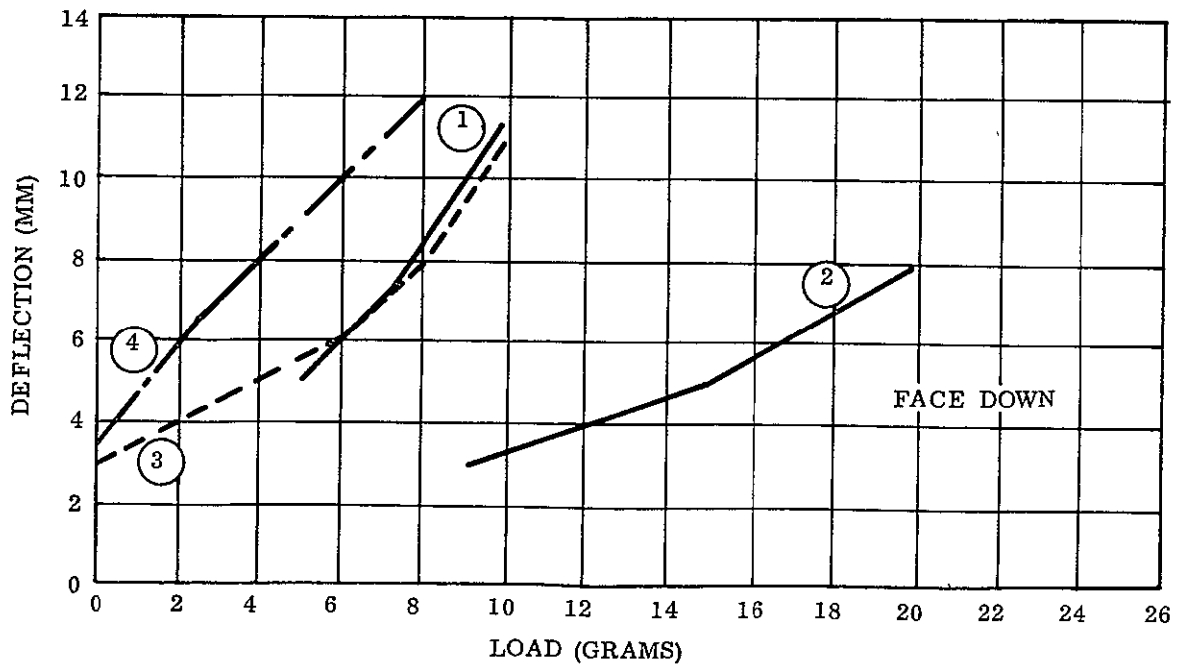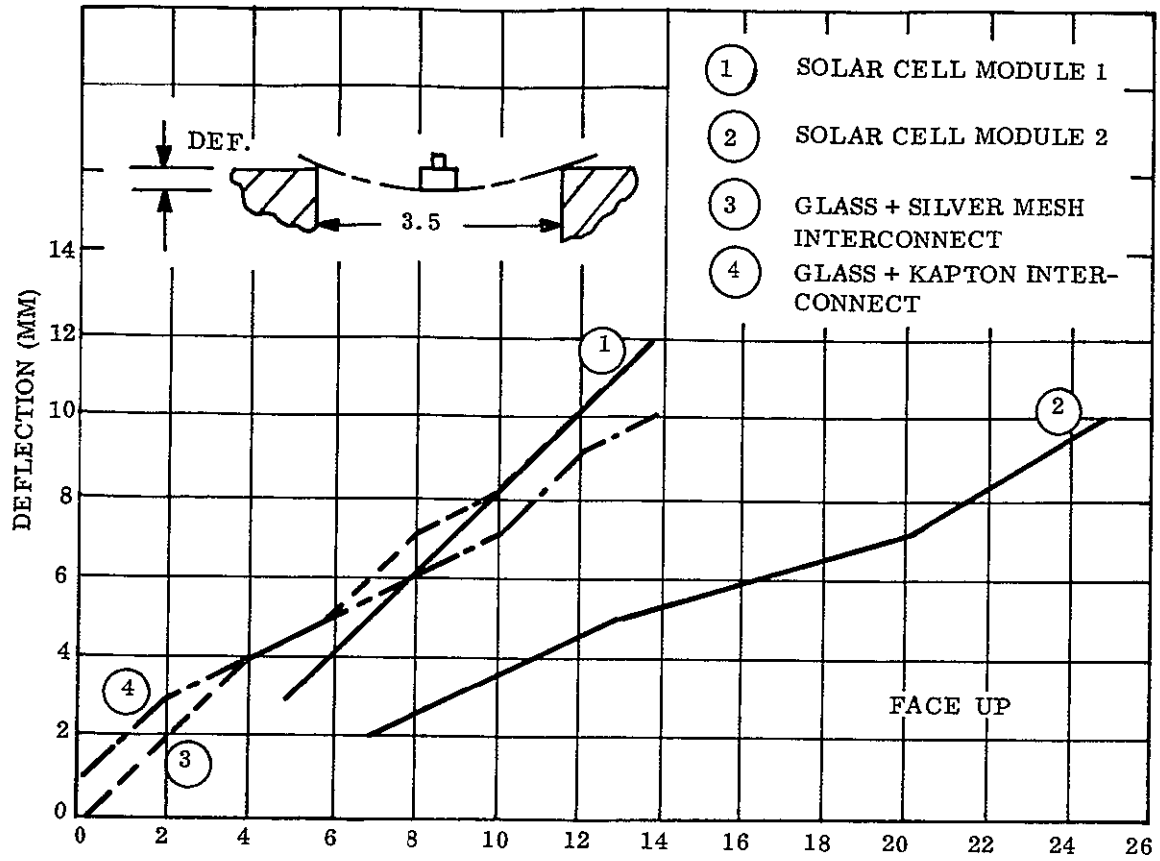
Figure 6.1-5. Load Deflection Curves – Transverse Curvature

shock spectrum identical to that associated with the specified shock pulse within the requirements of Paragraph 3.10.7.5 of Reference 3. Shock spectrum classification is a standard technique of equating the damage potential of shock pulses. If the spectrum of the synthesized shock train and that of the specified shock pulse are equal, the specimen is considered to have demonstrated survival of equivalent environmental damage potential.

6.2.2 THERMAL-VACUUM TESTING

As presently specified in Reference 3, the thermal-vacuum tests can result in excessive test time and possible damage to the test specimen. The definition of set-point temperature (i.e., the cold set-point defined by the hottest reading thermocouple and the hot set-point by the coldest reading thermocouple) can result in excessive test time because the solar array blanket wrapped on the drum forms an excellent multilayer radiant heat transfer insulation blanket. For example, during the high temperature thermal-vacuum test in the stowed configuration, it is required to force the lowest reading thermocouple to 140°C by radiant heat transfer. The time required to force a thermocouple mounted on the storage drum shell to 140°C would be extremely long (see Figure 4.2-3). In addition, the required temperature on the outermost wrap would be in excess of 140°C. A similar situation exists for the low temperature thermal-vacuum tests. Revised test requirements based on soak time periods coupled with surface temperatures are currently being studied.

SECTION 7

SUPPORT EQUIPMENT

The following items of support equipment have been identified for this project:

1. Handling Equipment

    a. Handling Fixture

    b. Dolly and Dust Cover

    c. Handling Sling

2. Test Equipment

    a. Upward Deployment

    b. Downward Deployment Aid

    c. Scanner Support Structure

    d. Modal Test Support Structure

    e. Stowed Dynamics Fixture

    f. Heat Flux Simulator

7.1 HANDLING EQUIPMENT

7.1.1 HOLDING FIXTURE

The holding fixture is used as the mounting structure for the RA250 array. As such it provides the same mechanical interface as the flight vehicle structure. The configuration for this fixture is shown in Figure 7.1-1. As may be seen from the figure, the fixture is constructed of aluminum bars and tubing. Solid bar stock is used, in places where the Rollup Array interfaces with the fixture, to provide the integrity required during the stowed vibration tests.

Figure 7.1-1. Holding Fixture

The RA250 mounts directly to the holding fixture center mounting pad. The deployable end supports are mounted to removable members at each end of the fixture. The end supports interface hole pattern is located at assembly to eliminate the necessity of close tolerance hole locations. The end supports are removable to permit attachment of deployment aid hardware. Dowel pins are used to permit accurate relocation of the end supports.

Two precision surface plates are attached to the side and end of the fixture to be used as reference surfaces for precision level indicators. The indicators are not permanently attached due to the extreme environments encountered; i.e., -130°C, $+140^{\circ}$C, high vacuum, and vibration.

7.1.2 DOLLY AND DUST COVER

The function of the dolly is to provide a mobile stable operations base for the rollup solar array during intrafacility use and to provide a convenient method of moving the unit about the facility. A dust cover will be provided to protect the array during periods of storage.

7.1.3 HANDLING SLING

The handling sling is used to lift the RA250 mounted to the holding fixture. The sling consists of a 3-inch-diameter aluminum pipe strongback with a movable hoist interface at the center and a rectangular tube spreader at each end. Longitudinal adjustment capability is provided by the movable center support, lateral adjustment capability is provided by slots in the rectangular tubes. These slots can be elongated if needed. One-quarter-inch steel cables with safety hooks provide the interface with the holding fixture at each corner.

7.2 TEST EQUIPMENT

The items identified as test equipment are the special test equipment needed to conduct the environmental tests of the RA250 in the planned facilities. Some of the tests are typical spacecraft tests and can be carried out with well-established techniques. Examples are the

stowed vibration tests. The test equipment for this type test consists of fixtures to adapt the RA250 to the facility interface. Several of the tests are unusual with the deployed vibration test being a typical example. Because the aerodynamic forces on the blanket are large relative to the other forces involved, this test will be run in a vacuum chamber. Because of the low frequencies involved displacement measurements will be made with electro-optical equipment. This equipment is part of the facility at Valley Forge; therefore, only the equipment required to support the transducers is described herein. A third category of equipment are the items needed to support the verification of RA250 performance. Some of this equipment is available at the Valley Forge facility and again only the equipment being designed will be described at this time.

7.2.1 UPWARD DEPLOYMENT AID

The upward deployment aid is used to counterbalance the weight of the solar array blankets during all upward deployment/retraction cycles. Upward deployment has been selected for health checks. A feasibility and approach trade-off study has been made and a tentative design approach selected. The present concept allows an initial upward deployment of the BI-STEM and LEM without the blankets. The forces produced by the array drum constant torque spring motor will be transmitted to the LEM through lightweight ribbons attached to the outboard ends of the LEM. This ribbon will unwrap from a sheave attached to the storage drum outboard edge guide. The displacement of the tip of the fully extended BI-STEM will be measured. The upward deployment aid will be pre-positioned to this tip location as shown in Figure 7.2-1 and the actual deployment with the array blankets installed can be accomplished with a fixed load application point.

The upward deployment aid also provides the capability to manually keep the support point directly above the boom tip and thereby provides an upward deployment of the entire system with the tip of the boom "free" to move in transverse directions.

7.2.2 DOWNWARD DEPLOYMENT AID

The array is to be deployed downward during deployed vibration and thermal vacuum testing. A sketch of the RA250 system in the vacuum chamber is shown in Figure 7.2-2.

7-6
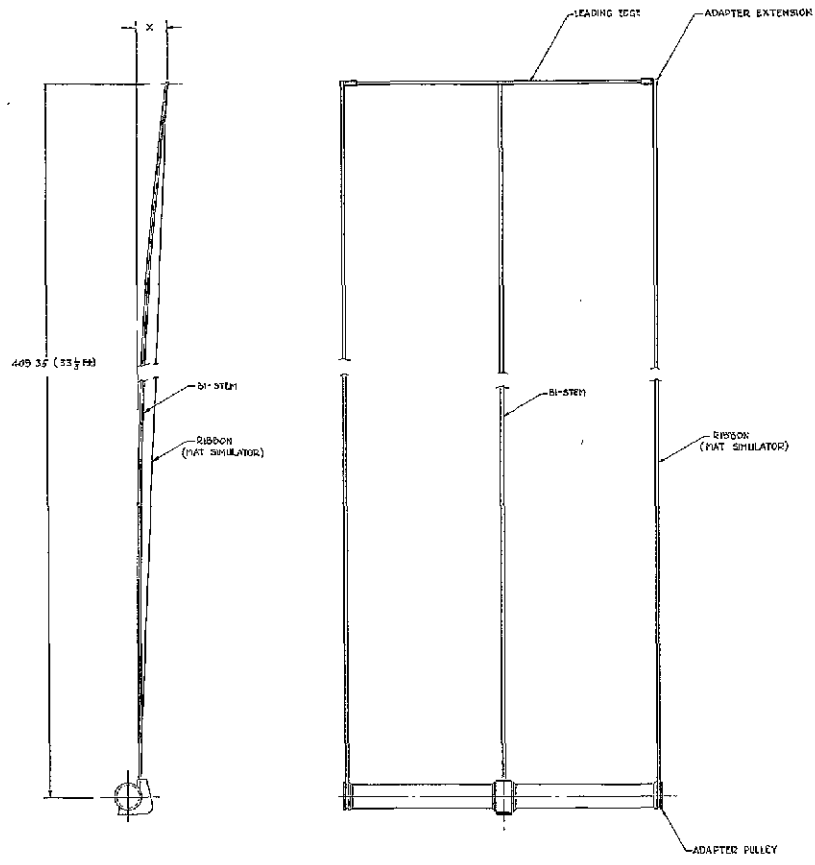
UPWARD DEPLOYMENT SIMULATION
ZERO "G" FIELD
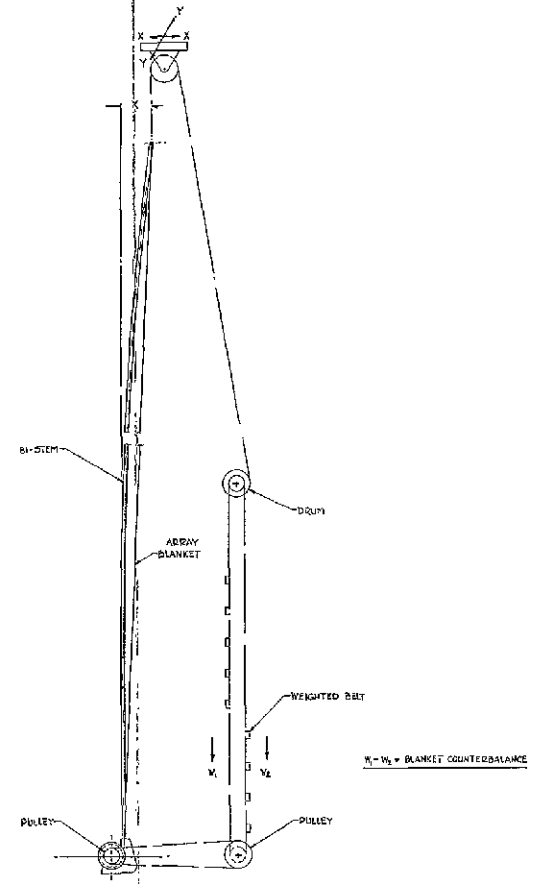
UPWARD DEPLOYMENT WITH COUNTERBALANCED
ARRAY BLANKET

Figure 7.2-1. Upward Deployment Aid Concept

17 FEET

ELEV 285 FEET

36 FEET

26 FEET
25 FEET, 6 IN

ELEV
225 FEET

ELEV
235 FEET

6 FEET 7 INCHES

ELEV
230 FEET

0
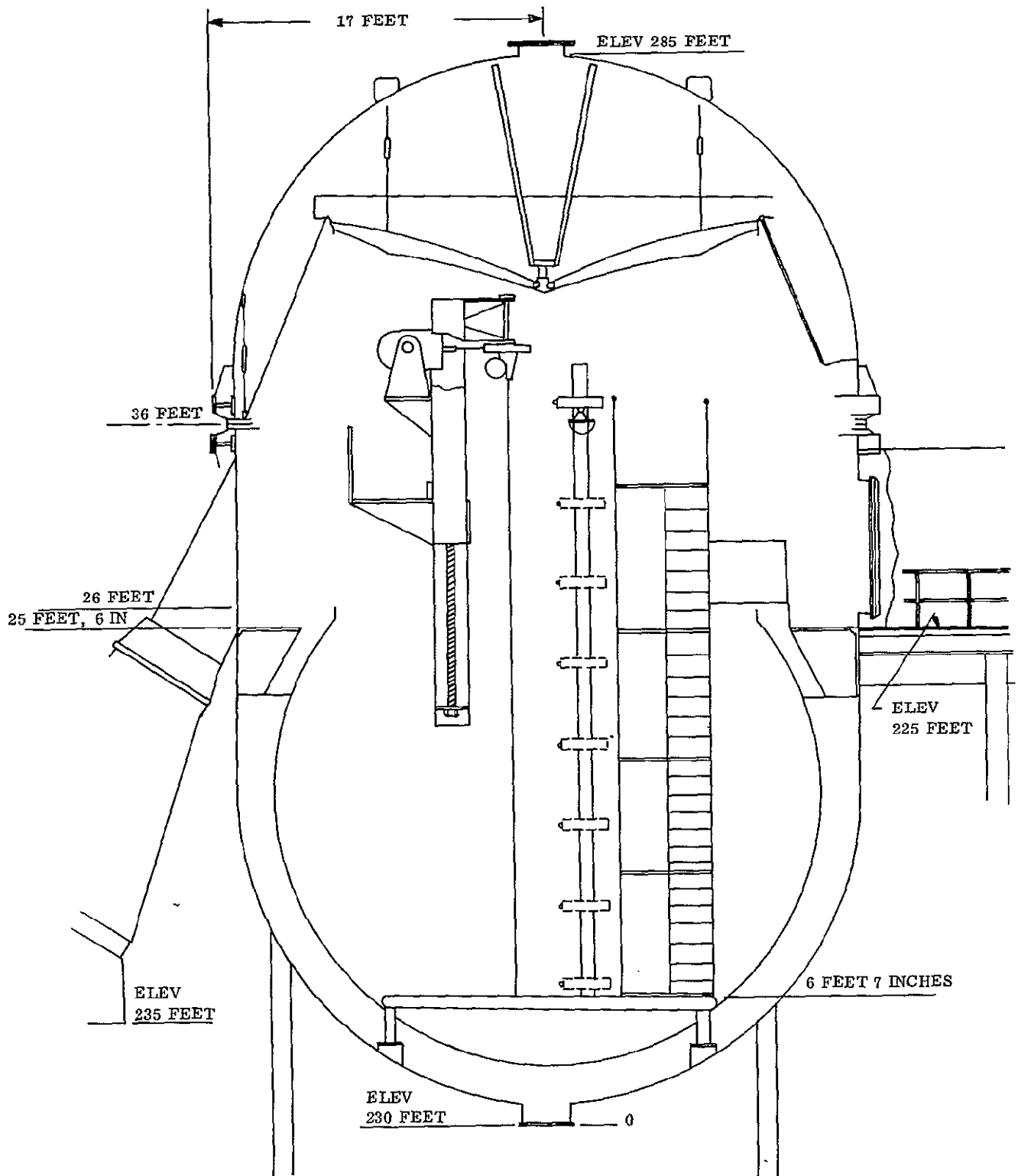
Figure 7.2-2.   RA250 Installed in Thermal-Vacuum Chambers

Several approaches to the implementation of the downward deployment aid are being investigated. The downward deployment aid becomes a part of the modal test support structure. It provides a counterbalance for the weight of the solar array blankets as they are extended.

7.2.3 SCANNER SUPPORT STRUCTURE

The scanner support structure positions the electro-optical readout heads as required to accomplish the deployed array modal vibration test. Planning completed at this time indicates that the structure will consist of two vertical beams, a horizontal carriage, and a remote drive system.

The veritical beams will be resting on the structural ring located inside (near the bottom of) the 54-foot vacuum chamber, and will be laterally supported by tension members at the catwalk level. The horizontal carriage will be a single truss-type beam which will carry the scanners and light sources in a vertical direction. The carriage will be guided by the vertical beams and driven by a chain drive. An electrical circuit will be utilized to determine and indicate the position of the carriage along the vertical beams.

Scaffolding will be located near enough to the scanner support structures to permit installation, adjustment and maintenance along the entire length of travel.

Because all of these tall structures extend into the chamber dome section they will be modular in construction to permit partial disassembly so that the chamber dome may be installed and removed.

7.2.4 MODAL TEST SUPPORT STRUCTURE

The modal test support structure provides the interface between the vacuum chamber facility and the equipment needed for the deployed modal and thermal-vacuum tests. Mounted upon the support structure will be the downward deployment aid, the low frequency exciter, and the RA250 including its holding fixture.

7.2.5 STOWED DYNAMICS FIXTURES

Planning for performance of shock and vibration testing is based on the use of a dual C-220 electrodynamic vibration capability. This system has been recently upgraded to provide 35,000 pounds force for each exciter, either vector or rms, allowing, through dual coupling, 70,000 pounds rms and 210,000 pounds (3 sigma peak).

Coupling to the stowed solar array for shock and vibration excitation in the transverse axis will be by means of a vibration fixture, essentially a simple beam design, which will be driven by the two exciters in tandem. See Figure 7.2-3a.

The lateral axis vibration and shock configuration will incorporate one shaker and hydrostatic iol bearings for supporting the array and its fixture. See Figure 7.2-3b.

7.2.6 HEAT FLUX SIMULATOR

The heat flux simulator provodes radiant heating for both the stowed and the deployed thermal tests. Banks of quartz lamps are planned as it is not intended to simulate the suns spectrum for thermal tests.
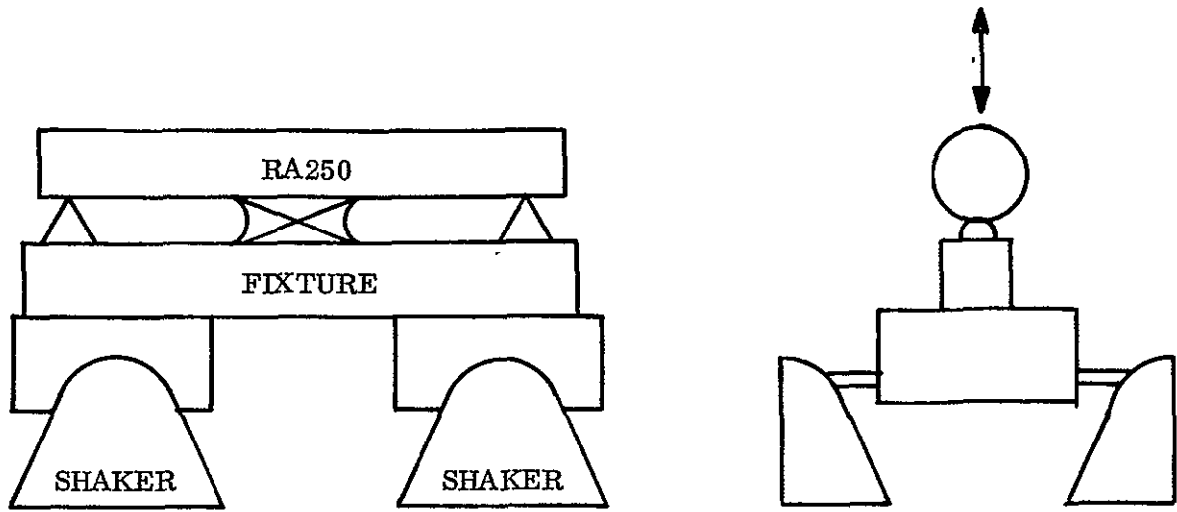
NOTE: ARRAY TURNED 90 DEGREES FOR SECOND TRANSVERSE AXIS

a. TRANSVERSE AXIS
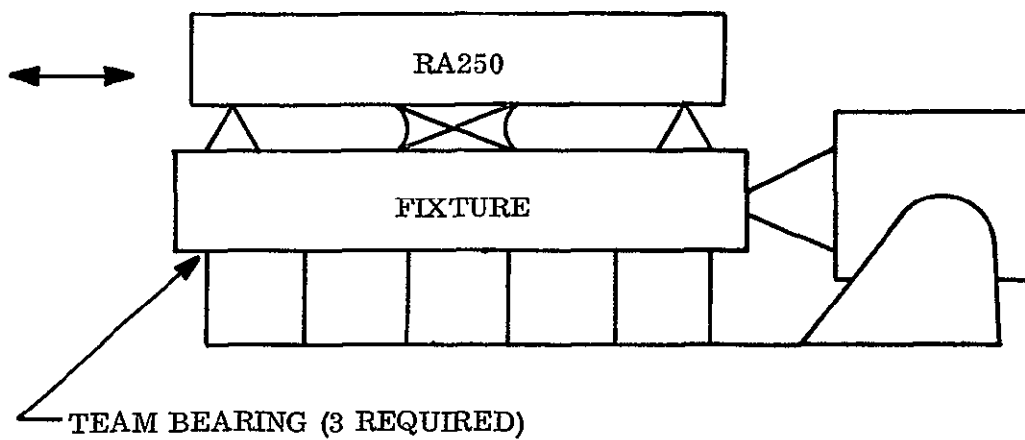
b. LONGITUDINAL AXIS

Figure 7.2-3. Stowed Vibration Fixtures

SECTION 8

CONCLUSIONS

The following conclusions have resulted from the second 3 months of effort on the design and development of the 30 watt per pound rollup subsolar array:

1. The weight goals of the program are considered achievable for the specified launch environment, although there is uncertainty as to the dynamic response characteristics of the stowed solar array blankets. Careful weight control will be required in the assembly of the solar array blanket because of the large area and large number of parts involved.

2. Modifications will be needed in the initial test concept to account for the very long thermal time constant and the large thermal gradients in the system.

SECTION 9

RECOMMENDATIONS

There are no specific recommendations at this time. Recommendations with respect to test planning, incorporation of stiffening elements in dummy solar cell modules, and modification of thermal-vacuum test plans, are being discussed with JPL. The project is in the fabrication and detailed test planning stages and additional information in these areas will be available in the next quarterly report.

SECTION 10

NEW TECHNOLOGY

No items of new technology have been reported during this report period.

SECTION 11

REFERENCES

1. Final Report, Feasibility Study - 30 Watts per Pound Rollup Solar Array, GE-SSO Report No. 68SD4301, June 21, 1968.

2. Quarterly Report No. 1, Rollup Subsolar Array, GE-SSO Report No. 69SD4282, June 12, 1969.

3. JPL Specification No. SS501407 Rev. D "Rollup Solar Cell Array, 30 Watts per Pound, Detail Specification for."

4. Deployable Large Area Solar Cell Array Testing, Ryen Report No. 20869-4, 15 August 1958, JPL Contract No. 951107.

5. Archer, J. S., "Consistent Mass Matrix for Distributed Mass Systems," Third Conference on Electronic Computation, Boulder, Colorado, June 19-21, 1963. Published in the Journal of the Structural Division, Proceedings of the American Society of Civil Engineers, Vol. 89 No. ST4, August 1963, Part 1.

6. Martin, Harold C., "On the Derivation of Stiffness Matrices for the Analysis of Large Deflection and Stability Problems," Matrix Methods in Structural Mechanics, AF FDL-TR-66-80 November 1966.

7. Bogner, F. K., Fox, R. L., Schmit, L. A. Jr., "Generation of Inter-Element-Compatible Stiffness and Mass Matrices by the Use of Interpolation Formulas," Matrix Methods in Structural Mechanics, AF FDL-TR-66-80, November, 1966.

APPENDIX A

MODAL ANALYSIS OF

ROLLUP SOLAR ARRAY

Modal Analysis of Roll Up Solar Array

Introduction

The roll up solar array consists of two rectangular blanket-like subpanels, each stretched between a drum at one end and an elastic bar at the other. The elastic bar is supported in the center by a tubular boom which is, in turn, supported at the other end with the drums. The drums are spring loaded such that the tension on the panels is essentially constant even during vibrations.

Since the subpanels are likely to be the most influential in determining the nature of the lowest system modes, due to their large mass and high flexibility, this subsystem was investigated first. The principle of minimum potential energy and Hamilton's principle were applied to determine the natural boundary conditions and the Rayliegh-, Ritz technique used to evaluate the modes.

Basic Equations

The coordinates x, y. and z were chosen in the direction of the length of the subpanel, in the direction of the width and in the transverse direction (See Figure 1). The corresponding displacements are u, v, and w. The displacements and forces are divided into two parts, the equilibrium state (superscript 0) and the perturbed or vibration state (superscript 1). The non-linear strain displacement relationships are given by:

$$\epsilon_x = \frac{\partial u^0}{\partial x} + \frac{\partial u^1}{\partial x} + \frac{1}{2} \left(\frac{\partial w^1}{\partial x} \right)^2$$

$$\epsilon_y = \frac{\partial v^0}{\partial y} + \frac{\partial v^1}{\partial y} + \frac{1}{2}\left(\frac{\partial w^1}{\partial y}\right)^2$$

$$\gamma_{xy} = \frac{\partial u^0}{\partial y} + \frac{\partial v^0}{\partial x} + \frac{\partial u^1}{\partial y} + \frac{\partial v^1}{\partial x} + \left(\frac{\partial w^1}{\partial x}\right)\left(\frac{\partial w^1}{\partial y}\right) \qquad (1)$$

The force-strain relationship is assumed to be linear and of the following form:

$$N_x = E^*\left[(\epsilon_x^0 + \epsilon_x^1) + \nu^*(\epsilon_y^0 + \epsilon_y^1)\right]$$

$$N_y = E^*\left[(\epsilon_y^0 + \epsilon_y^1) + \nu^*(\epsilon_x^0 + \epsilon_x^1)\right] \qquad (2)$$

$$N_{xy} = \frac{E^*}{2}(1 - \nu^*)\left[\gamma_{xy}^0 + \gamma_{xy}^1\right]$$

Substituting the parts of equations (1) and (2) which apply to the equilibrium position into the principle of minimum potential energy yields the following expression:

$$-E^*\iint\left\{\left[\frac{\partial^2 u^0}{\partial x^2}\,\delta u^0 + \nu^*\left(\frac{\partial v^0}{\partial x \partial y}\,\delta u^0 + \frac{\partial^2 u^0}{\partial x \partial y}\,\delta v^0\right)\right.\right.$$

$$+ \frac{\partial^2 v^0}{\partial y^2}\,\delta v^0\right] + \frac{(1-\nu^*)}{2}\left[\frac{\partial^2 u^0}{\partial y^2}\,\delta u^0 + \frac{\partial^2 v^0}{\partial x \partial y}\,\delta u^0\right.$$

$$\left.\left. + \frac{\partial^2 u^0}{\partial x \partial y}\,\delta v^0 + \frac{\partial^2 v^0}{\partial x^2}\,\delta v^0\right] + p\,\delta u^0\right\}\,dxdy$$

$$+ \iint \left\{ E^* \left[\frac{\partial u^0}{\partial x} \delta u^0 + \nu^* \frac{\partial v^0}{\partial y} \delta u^0 + \frac{(1 + \nu^*)}{2} \left[\frac{\partial u^0}{\partial y} \delta v^0 + \frac{\partial v^0}{\partial x} \delta v^0 \right] \right] \right.$$

$$\left. - N_x^0 \delta u^0 - N_{xy}^0 \delta v^0 \right\} dy \left.\right|_{x=a}^{x=a} + \int \left\{ E^* \left[\nu^* \frac{\partial u^0}{\partial x} \delta v^0 \right.\right.$$

$$\left. + \frac{\partial v^0}{\partial y} \delta v^0 + \frac{(1-\nu^*)}{2} \left[\frac{\partial u^0}{\partial y} \delta u^0 + \frac{\partial v^0}{\partial x} \delta u^0 \right] \right]$$

$$\left. - N_y^0 \delta v^0 - N_{xy}^0 \delta u^0 \right\} dx \left.\right|_{y=-b}^{y=b} = 0 \quad . \tag{3}$$

Thus the following natural boundary conditions must be satisfied:

on $x = \pm a$

$$\frac{\partial u^0}{\partial x} + \nu^* \frac{\partial v^0}{\partial y} = \frac{N_x^0}{E^*} \quad \text{or} \quad \delta(u^0) = 0$$

$$\frac{\partial u^0}{\partial y} + \frac{\partial v^0}{\partial x} = \frac{2N_{xy}^0}{(1-\nu^*)E^*} \quad \text{or} \quad \delta(v^0) = 0 \tag{4}$$

on $y = \pm b$

$$\nu^* \frac{\partial u^0}{\partial x} + \frac{\partial v^0}{\partial y} = \frac{N_y^0}{E^*} \quad \text{or} \quad \delta(v^0) = 0 \quad .$$

$$\frac{\partial u^0}{\partial y} + \frac{\partial v^0}{\partial x} = \frac{2N_{xy}^0}{(1-\nu^*)E^*} \quad \text{or} \quad \delta(u^0) = 0 \tag{5}$$

In a similar fashion; Hamilton's principle yields for the perturbed state:

$$\int_{t_0}^{t_1} \left\{ -E^* \iiint \left\{ \left[\frac{\partial^2 u^1}{\partial x^2} + \frac{\partial w^1}{\partial x} \frac{\partial^2 w^1}{\partial x^2} \right] \delta u^1 + \left[\frac{\partial^2 u^1}{\partial x^2} \frac{\partial w^1}{\partial x} + \frac{\partial u^1}{\partial x} \frac{\partial^2 w^1}{\partial x^2} \right. \right. \right.$$

$$+ \frac{3}{2} \left(\frac{\partial w^1}{\partial x} \right)^2 \left(\frac{\partial^2 w^1}{\partial x^2} \right) \bigg] \delta w^1 + \nu^* \left[\frac{\partial^2 u^1}{\partial x \partial y} + \frac{\partial w^1}{\partial x} \frac{\partial^2 w^1}{\partial x \partial y} \right] \delta v^1$$

$$+ \nu^* \left[\frac{\partial^2 u^1}{\partial x \partial y} \frac{\partial w^1}{\partial y} + \frac{\partial u^1}{\partial x} \frac{\partial^2 w^1}{\partial y^2} + \frac{1}{2} \left(\frac{\partial w^1}{\partial x} \right)^2 \frac{\partial^2 w^1}{\partial y^2} + \frac{\partial w^1}{\partial x} \frac{\partial w^1}{\partial y} \frac{\partial^2 w^1}{\partial x \partial y} \right.$$

$$\Bigg] \delta w^1 + \nu^* \left[\frac{\partial^2 v^1}{\partial x \partial y} + \frac{\partial w^1}{\partial y} \frac{\partial^2 w^1}{\partial x \partial y} \right] \delta u^1 + \nu^* \left[\frac{\partial^2 w^1}{\partial x^2} \frac{\partial v^1}{\partial y} \right.$$

$$+ \frac{\partial w^1}{\partial x} \frac{\partial v^2}{\partial x \partial y} + \frac{1}{2} \frac{\partial^2 w^1}{\partial x^2} \left(\frac{\partial w^1}{\partial y} \right)^2 + \frac{\partial w^1}{\partial x} \frac{\partial w^1}{\partial y} \frac{\partial^2 w^1}{\partial x \partial y} \right] \delta w^1$$

$$+ \left[\frac{\partial^2 v^1}{\partial y^2} + \frac{\partial^2 w^1}{\partial y^2} \left(\frac{\partial w^1}{\partial y} \right)^2 \right] \delta v^1 + \left[\frac{\partial^2 v^1}{\partial y^2} \frac{\partial w^1}{\partial y} + \frac{\partial v^1}{\partial y} \frac{\partial^2 w^1}{\partial y^2} \right.$$

$$+ \frac{3}{2} \left(\frac{\partial w^1}{\partial y} \right)^2 \frac{\partial^2 w^1}{\partial y^2} \bigg] \delta w^1 + \left[\frac{\partial^2 u^0}{\partial x^2} \right] \delta u^1 + \left[\frac{\partial^2 u^0}{\partial x^2} \frac{\partial w^1}{\partial x} + \frac{\partial u^0}{\partial x} \frac{\partial^2 w^1}{\partial x^2} \right] \delta w^1$$

$$+ \nu^* \left[\frac{\partial^2 u^0}{\partial x \partial y} \right] \delta v^1 + \nu^* \left[\frac{\partial^2 u^0}{\partial x \partial y} \frac{\partial w^1}{\partial y} + \frac{\partial u^0}{\partial x} \frac{\partial^2 w^1}{\partial y^2} \right] \delta w^1 + \left[\frac{\partial^2 v^0}{\partial y^2} \right] \delta v^1$$

$$+ \left[\frac{\partial^2 v^0}{\partial y^2} \frac{\partial w^1}{\partial y} + \frac{\partial v^0}{\partial y} \frac{\partial^2 w^1}{\partial y^2} \right] \delta w^1 + \nu^* \left[\frac{\partial^2 v^0}{\partial x \partial y} \right] \delta u^1 + \nu^* \left[\frac{\partial^2 v^0}{\partial x \partial y} \frac{\partial w}{\partial x} \right.$$

$$+ \frac{\partial v^0}{\partial y} \frac{\partial^2 w^1}{\partial x^2} \bigg] \delta w^1 + \frac{(1 - \nu^*)}{2} \left[\frac{\partial^2 u^0}{\partial y^2} + \frac{\partial^2 v^0}{\partial x \partial y} \right] \delta u^1$$

A-4

$$+ \frac{(1-\nu^*)}{2}\left[\frac{\partial^2 u^0}{\partial x \partial y} + \frac{\partial^2 v^o}{dx^2}\right]\delta v^1 + \frac{(1-\nu^*)}{2}\left[\frac{\partial^2 u^0}{\partial x \partial y} \quad \frac{\partial w^1}{\partial y}\right.$$

$$+ \frac{\partial u^0}{\partial y} \quad \frac{\partial^2 w^1}{\partial x \partial y} + \frac{\partial^2 v^0}{\partial x^2} \quad \frac{\partial w^1}{\partial y} + \frac{\partial v^0}{\partial x} \quad \frac{\partial^2 w^1}{\partial x \partial y} + \frac{\partial^2 u^0}{\partial y^2} \quad \frac{\partial w^1}{\partial x}$$

$$+ \frac{\partial u^0}{\partial y} \quad \frac{\partial^2 w^1}{\partial x \partial y} + \frac{\partial^2 v^0}{\partial x \partial y} \quad \frac{\partial w^1}{\partial y} + \frac{\partial v^0}{\partial x} \quad \frac{\partial^2 w^1}{\partial x \partial y}\Big]\delta w^1$$

$$+ \frac{(1-\nu^*)}{2}\left[\frac{\partial^2 u^1}{\partial y^2} + \frac{\partial^2 v^1}{\partial x \partial y} + \frac{\partial^2 w^1}{\partial x \partial y} \quad \frac{\partial w^1}{\partial y} + \frac{\partial w^1}{\partial x} \quad \frac{\partial^2 w^1}{\partial y^2}\right]\delta u^1$$

$$+ \frac{(1-\nu^*)}{2}\left[\frac{\partial^2 u^1}{\partial x \partial y} + \frac{\partial^2 v^1}{\partial x^2} + \frac{\partial^2 w^1}{\partial x^2} \quad \frac{\partial w^1}{\partial y} + \frac{\partial w^1}{\partial x} \quad \frac{\partial^2 w^1}{\partial x \partial y}\right]\delta v^1$$

$$+ \frac{(1-\nu^*)}{2}\left[\frac{\partial^2 u^1}{\partial x \partial y} \quad \frac{\partial w^1}{\partial y} + \frac{\partial u^1}{\partial y} \quad \frac{\partial^2 w^1}{\partial x \partial y} + \frac{\partial^2 v^1}{\partial x^2} \quad \frac{\partial w^1}{\partial y} + \frac{\partial v^1}{\partial x} \quad \frac{\partial w^1}{\partial x \partial y}\right.$$

$$+ \frac{\partial^2 w^1}{\partial x^2}\left(\frac{\partial w^1}{\partial y}\right)^2 + 2\frac{\partial w^1}{\partial x} \quad \frac{\partial w^1}{\partial y} \quad \frac{\partial^2 w^1}{\partial x \partial y} + \frac{\partial^2 u^1}{\partial y^2} \quad \frac{\partial w^1}{\partial x} + \frac{\partial u^1}{\partial y} \quad \frac{\partial^2 w^1}{\partial x \partial y}$$

$$+ \frac{\partial^2 v^1}{\partial x \partial y} \quad \frac{\partial w^1}{\partial x} + \frac{\partial v^1}{\partial x} \quad \frac{\partial^2 w^1}{\partial x \partial y} + 2\frac{\partial w^1}{\partial x} \quad \frac{\partial w^1}{\partial y} \quad \frac{\partial^2 w^1}{\partial x \partial y} + \left(\frac{\partial w^1}{\partial x}\right)^2 \frac{\partial^2 w^1}{\partial y^2}\Big]\delta w^1$$

$$+ p\,\delta u^1\Big\}dxdy + \rho^*\iint\left[\frac{\partial^2 u^1}{\partial t^2}\,\delta u^1 + \frac{\partial^2 v^1}{\partial t^2}\,\delta v^1 + \frac{\partial^2 w^1}{\partial t^2}\,\delta w^1\right]\partial x \partial y$$

$$+\iint E^*\left\{\left[\frac{\partial u^1}{\partial x} + \frac{1}{2}\left(\frac{\partial w^1}{\partial x}\right)^2\right]\delta u^1 + \left[\frac{\partial u^1}{\partial x} \frac{\partial w^1}{\partial x} + \frac{1}{2}\left(\frac{\partial w^1}{\partial x}\right)^3\right]\delta w^1\right.$$

$$+ \nu^*\left[\frac{\partial v^1}{\partial y} + \frac{1}{2}\left(\frac{\partial w^1}{\partial y}\right)^2\right]\delta u^1 + \nu^*\left[\frac{\partial v^1}{\partial y} \frac{\partial w^1}{\partial x} + \frac{1}{2} \frac{\partial w^1}{\partial x}\left(\frac{\partial w^1}{\partial y}\right)^2\right]$$

$$\cdot \delta w^1 + \left(\frac{\partial u^0}{\partial x}\right)\delta u^1 + \left[\frac{\partial u^0}{\partial x} \quad \frac{\partial w^1}{\partial x}\right]\delta w^1 + \nu^*\left(\frac{\partial v^0}{\partial y}\right)\delta u^1$$

$$+ \nu^* \left[\frac{\partial v^0}{\partial y} \; \frac{\partial w^1}{\partial x} \right] \delta w^1 \; + \; \frac{(1 - \nu^*)}{2} \left[\frac{\partial u^0}{\partial y} + \frac{\partial v^0}{\partial x} \right] \delta v^1$$

$$+ \frac{(1 - \nu^*)}{2} \left[\frac{\partial u^0}{\partial y} + \frac{\partial v^0}{\partial x} \right] \left(\frac{\partial w^1}{\partial y} \right) \delta w^1 \; + \; \frac{(1 - \nu^*)}{2} \left[\frac{\partial u^1}{\partial y} + \frac{\partial v^1}{\partial x} \right.$$

$$\left. + \left(\frac{\partial w^1}{\partial x} \right) \left(\frac{\partial v^1}{\partial y} \right) \right] \delta v^1 \; + \left[\frac{\partial u^1}{\partial y} \; \frac{\partial w^1}{\partial y} \; + \; \frac{\partial v^1}{\partial x} \; \frac{\partial w^1}{\partial y} + \frac{\partial w^1}{\partial x} \left(\frac{\partial w^1}{\partial y} \right)^2 \right]$$

$$\cdot \, \delta w^1 \Bigg\} - \; (N_x^0 + N_x^1) \; (\delta u^1 + \delta w^1 \, \frac{\partial w^1}{\partial x})$$

$$-(N_{xy}^0 + N_{xy}^1) \, (\delta v^1 + \delta w^1 \; \frac{\partial w^1}{\partial y}) \Bigg] \; dy \; \Bigg|_{x=-a}^{x=a} \quad \cdot$$

$$+ \int \left[E^* \Bigg\{ \nu^* \left[\frac{\partial u^1}{\partial x} \; + \; \frac{1}{2} \left(\frac{\partial w^1}{\partial x} \right)^2 \right] \delta v^1 + \nu^* \left[\frac{\partial u^1}{\partial x} \; \frac{\partial w^1}{\partial y} \; + \; \frac{1}{2} \left(\frac{\partial w^1}{\partial x} \right)^2 \; \frac{\partial w^1}{\partial y} \right] \right.$$

$$\cdot \, \delta w^1 \; + \left[\frac{\partial v^1}{\partial y} + \frac{1}{2} \left(\frac{\partial w^1}{\partial y} \right)^2 \right] \delta v^1 \; + \left[\frac{\partial v^1}{\partial y} \; \frac{\partial w^1}{\partial y} + \frac{1}{2} \left(\frac{\partial w^1}{\partial y} \right)^3 \right] \delta w^1$$

$$+ \nu^* \frac{\partial u^0}{\partial x} \; \delta v^1 + \nu^* \left[\frac{\partial u^0}{\partial x} \; \frac{\partial w^1}{\partial y} \right] \delta w^1 \; + \; \frac{(1 - \nu^*)}{2} \left[\frac{\partial u^0}{\partial y} \; + \; \frac{\partial v^0}{\partial x} \right] \delta u^1$$

$$+ \frac{(1 - \nu^*)}{2} \left[\frac{\partial u^0}{\partial y} \; \frac{\partial w^1}{\partial x} + \frac{\partial v^0}{\partial x} \; \frac{\partial w^1}{\partial x} \right] \delta w^1 \; + \; \frac{(1 - \nu^*)}{2} \left[\frac{\partial u^1}{\partial y} + \frac{\partial v^1}{\partial x} \right.$$

$$+ \frac{\partial w^1}{\partial x} \; \frac{\partial w^1}{\partial y} \Bigg] \delta u^1 \; + \; \frac{(1 - \nu^*)}{2} \left[\frac{\partial u^1}{\partial y} \; \frac{\partial w^1}{\partial x} + \frac{\partial v^1}{\partial x} \; \frac{\partial w^1}{\partial x} + \left(\frac{\partial w^1}{\partial x} \right)^2 \; \frac{\partial w^1}{\partial y} \right]$$

$$\cdot \, \delta w^1 \Bigg\} - \; (N_y^0 + N_y^1) \; (\delta v^1 + \delta w^1)$$

$$-(N_{xy}^0 + N_{xy}^0)(\delta u^1 + \delta w^1) \quad dx \right] \; \Bigg|_{y=-b}^{y=b} \Bigg\} dt = 0 \qquad (6)$$

Using the results of equations (3), (4), and (5), the following natural boundary conditions can be derived:

on $x = \pm a$

$$\left[\frac{\partial u^1}{\partial x} + \frac{1}{2}\left(\frac{\partial w^1}{\partial x}\right)^2\right] + \nu^*\left[\frac{\partial v^1}{\partial y} + \frac{1}{2}\left(\frac{\partial w^1}{\partial y}\right)^2\right] = \frac{N_x^1}{E^*}$$

or $\delta(u^1) = 0$

$$\left[\frac{\partial u^1}{\partial y} + \frac{\partial v^1}{\partial x} + \frac{\partial w^1}{\partial x}\frac{\partial w^1}{\partial y}\right] = \frac{2N_{xy}^1}{(1-\nu^*)E_\nu} \tag{7}$$

or $\delta(v^1) = 0$

on $y = \pm b$

$$\nu^*\left[\frac{\partial u^1}{\partial x} + \frac{1}{2}\left(\frac{\partial w^1}{\partial x}\right)^2\right] + \left[\frac{\partial v^1}{\partial y} + \frac{1}{2}\left(\frac{\partial w^1}{\partial y}\right)^2\right] = \frac{N_y^1}{E^*}$$

or $\delta(v^1) = 0$

$$\left[\frac{\partial u^1}{\partial y} + \frac{\partial v^1}{\partial x} + \left(\frac{\partial w^1}{\partial x}\right)\left(\frac{\partial w^1}{\partial y}\right)\right] = \frac{2N_{xy}^1}{(1-\nu^*)E^*} \tag{8}$$

or $\delta(u^1) = 0$

The third boundary condition on both boundaries is automatically satisfied if both membrance forces are specified, since only two forces are possible. If both forces are not specified then w^1 must be given. w^1 must be such as to eliminate rigid body motions. A brief discussion of these boundary conditions is given by Novozhilov[1]. These expressions can also be found by reducing the expressions obtained for sandwich plates by Yu [2] in the manner described by Goldenveizer [3]. The same results are obtained.

Due to the difficulty of determining the exact force distribution at the ends attached to the bar and the length of the subpanels it is felt that the Rayleigh-Ritz method will yield the best results (Yu [4]). For the equilibrium state, assume the following displacements:

$$u^0 = \sum_{i=1}^{P} a_i^0 \, u_i^0 \, (x, y)$$

$$v^0 = \sum_{i=1}^{Q} b_i^0 \, v_i^0 (x, y) \tag{9}$$

where $u_i^0 (x, y)$ and $v_i^0 (x, y)$ are functions which satisfy the appropriate boundary conditions. a_i^0 and b_i^0 are constant coefficients to be determined.

Substituting equations (9) into the expression for potential energy yields:

$$U = \frac{1}{2} E^* \left[\sum_{i}^{P} \sum_{i}^{P} a_i^0 a_j^0 I_{ij}^1 + \sum_{i}^{P} \sum_{i}^{Q} 2 a_i^0 b_j^0 I_{ij}^2 \right.$$

$$\left. + \sum_{i}^{Q} \sum_{j}^{Q} b_i^0 b_j^0 I_{ij}^3 \right] - 2 b \cdot W^* \sum_{i}^{P} a_i^0 I_i^4 \quad ; \tag{10}$$

where W^* is the weight of the panels per unit area when suspended vertically (zero under zero gravity), and;

$$I_{ij}^1 = \iint \left[\frac{\partial u_i^0}{\partial x} \frac{\partial u_j^0}{\partial x} + \frac{(1-\nu^*)}{2} \frac{\partial u_i^0}{\partial y} \frac{\partial u_j^0}{\partial y} \right] dx \, dy \quad ,$$

$$I_{ij}^2 = \iint \left[\nu^* \frac{\partial u_i^0}{\partial x} \frac{\partial v_j^0}{\partial y} + \frac{(1 - \nu^*)}{2} \frac{\partial u_i^0}{\partial y} \frac{\partial v_j^0}{\partial x} \right] dx \, dy \, ,$$

$$I_{ij}^3 = \iint \left[\frac{(1 - \nu^*)}{2} \frac{\partial v_i^0}{\partial x} \frac{\partial v_j^0}{\partial x} + \frac{\partial v_i^0}{\partial y} \frac{\partial v_j^0}{\partial y} \right] dx\,dy \qquad (11)$$

$$I_i^4 = \iint \left[(a - x)\, u_i^0 \right] dx\,dy \quad .$$

Minimimizing the energy expression with respect to the coefficients yields the following expressions for a_i^0 and b_i^0:

for m = 1, P

$$a_m^0 I_{mm}^1 + \sum_i^P (1 - \delta_{mi}) a_i^0 I_{im}^1 + \sum_i^Q b_i^0 I_{mi}^2 = \frac{2bW^*}{E^*} I_m^4 \qquad (12)$$

for m = 1, Q

$$b_m^0 I_{mm}^3 + \sum_i^Q (1 - \delta_{mi}) b_i^0 I_{im}^3 + \sum_i^P a_i^0 I_m^2 = 0$$

where δ_{ij} is the kronecker delta

(δ_{ij} = 0 if i ≠ j and δ_{ij} = 1 if i = j). If the functions u_i^0 and v_i^0 are chosen as orthogonal functions, equations (12) can be further simplified.

For the perturbed or vibration state, assume the following displacement functions:

$$u^1 = \sum_{i=1}^R a_i^1 u^1(x, y)\, e^{i\omega t}$$

$$v^1 = \sum_{i=1}^S b_i^1 v^1(x, y) e^{i\omega t} \qquad (13)$$

$$w^1 = \sum_{i=1}^T c_i^1 w^1(x, y) e^{i\omega t}$$

Substituting equation (13) into the usual expression for the Hamiltonian,

and integrating over $2\tau/\omega$ (where $0 < \tau \le \pi$) yields:

$$H = \int_0^{2\tau/\omega} L\,dt = \left[U_m^0 + A^0\right]\frac{2\tau}{\omega} + \frac{1}{2}E^*\Biggl\{\left[\sum_i^R \sum_j^R a_i^1 a_j^1 J_{ij}^1\right.$$

$$+ \sum_i^R \sum_j^S 2a_i^1 b_j^1 J_{ij}^2 + \sum_i^S \sum_j^S b_i^1 b_j^1 J_{ij}^3\biggr](e^{4\tau i}-1)\,\frac{1}{2i\omega}$$

$$+\left[\sum_i^R \sum_j^T \sum_k^T a_i^1 c_j^1 c_k^1 J_{ijk}^5 + \sum_i^S \sum_j^T \sum_k^T b_i^1 c_j^1 c_k^1 J_{ijk}^6\right]$$

$$\cdot(e^{6\tau i}-1)(\frac{1}{3i\omega}) + \left[\sum_i^T \sum_j^T \sum_k^T \sum_\ell^T c_i^1 c_j^1 c_k^1 c_\ell^1 J_{ijk\ell}^7\right]$$

$$\cdot(e^{8\tau i}-1)(\frac{1}{4i\omega}) + \left[\sum_i^T \sum_j^T \sum_k^R (1-\nu^*)c_i^1 c_j^1 a_k^1 J_{ijk}^8\right.$$

$$+\sum_i^T \sum_j^T \sum_k^S (1-\nu^*)c_i^1 c_j^1 b_k^1 J_{ijk}^9\right](e^{6\tau i}-1)\,(\frac{1}{3i\omega})$$

$$+\left[\sum_i^T \sum_j^T \sum_k^T \sum_\ell^T \frac{(1-\nu^*)}{2}c_i^1 c_j^1 c_k^1 c_\ell^1 J_{ijk\ell}^{10}\right](e^{8\tau i}-1)\,(\frac{1}{4i\omega})$$

$$+\left[\sum_i^R 2a_i^1 K_i^1\right](e^{2\tau i}-1)\,(\frac{1}{i\omega}) + \left[\sum_i^T \sum_j^T 2c_i^i c_j^i K_{ij}^5\right]$$

$$(e^{4\tau i}-1)\,(\frac{1}{2i\omega}) + \left[\sum_i^S 2b_i^1 K_i^2\right](e^{2\tau i}-1)\,(\frac{1}{i\omega})$$

$$+\left[\sum_i^T \sum_j^T 2c_i^1 c_j^1 K_{ij}^6\right](e^{4\tau i}-1)\,(\frac{1}{2i\omega})$$

$$+\left[\sum_i^R a_i^1 K_i^3 + \sum_i^S b_i^1 K_i^4\right](e^{2\tau i}-1)\left(\frac{1}{i\omega}\right)$$

$$\left. +\left[\sum_i^T \sum_j^T c_i^1 c_j^1 K_{ij}^7\right](e^{4\tau i}-1)\left(\frac{1}{2i\omega}\right)'\right\}$$

$$+\left[\sum_i^T \sum_i^T a_i^1 a_j^1 K_{ij}^8 + \sum_i^S \sum_j^S b_i^1 b_j^1 K_{ij}^9\right.$$

$$\left. + \sum_i^T \sum_j^T c_i^1 c_j^1 K_{ij}^{10}\right](e^{4\tau i}-1)\left(\frac{\rho^*\omega}{2i}\right)$$

$$-2bW^*\left[\sum_i^R a_i^1 J_i^4\right](e^{2\tau i}-1)\left(\frac{1}{i\omega}\right) \qquad ; \qquad (14)$$

where the following integrals have been defined:

$$J_{ij}^1 = \int\int\left[\frac{\partial u_i^1}{\partial x}\frac{\partial u_j^1}{\partial x} + \frac{(1-\nu^*)}{2}\frac{\partial u_i^1}{\partial y}\frac{\partial u_j^1}{\partial y}\right]dxdy$$

$$J_{ij}^2 = \int\int\left[\nu^*\frac{\partial u_i^1}{\partial x}\frac{\partial v_j^1}{\partial y} + \frac{(1-\nu^*)}{2}\frac{\partial u_i^1}{\partial y}\frac{\partial v_j^1}{\partial x}\right]dxdy$$

$$J_{ij}^3 = \int\int\left[\frac{\partial v_i^1}{\partial y}\frac{\partial v_j^1}{\partial y} + \frac{(1-\nu^*)}{2}\frac{\partial v_i^1}{\partial x}\frac{\partial v_j^1}{\partial x}\right]dxdy$$

$$J_i^4 = \int\int\left[(a-x)u_i^1\right]dxdy$$

$$J_{ijk}^5 = \int\int\left[\frac{\partial u_i^1}{\partial x}\left(\frac{\partial w_j^1}{\partial x}\frac{\partial w_k^1}{\partial x} + \nu^*\frac{\partial w_j^1}{\partial y}\frac{\partial w_k^1}{\partial y}\right)\right]dxdy$$

$$J_{ijk}^6 = \iint \left[\frac{\partial v_i^1}{\partial y} \left(\frac{\partial w_j^1}{\partial y} \frac{\partial w_k^1}{\partial y} + \nu^* \frac{\partial w_j^1}{\partial x} \frac{\partial w_k^1}{\partial x} \right) \right] dxdy \qquad (15)$$

$$J_{ijk\ell}^7 = \iint \left[\frac{\partial w_i^1}{\partial x} \frac{\partial w_j^1}{\partial x} \frac{\partial w_k^1}{\partial x} \frac{\partial w_\ell^1}{\partial x} + 2\nu^* \frac{\partial w_i^1}{\partial x} \frac{\partial w_j^1}{\partial x} \frac{\partial w_k^1}{\partial y} \frac{\partial w_\ell^1}{\partial y} \right.$$
$$\left. + \frac{\partial w_i^1}{\partial y} \frac{\partial w_j^1}{\partial y} \frac{\partial w_k^1}{\partial y} \frac{\partial w_\ell^1}{\partial y} \right] dxdy$$

$$J_{ijk}^8 = \iint \left[\frac{\partial w_i^1}{\partial x} \frac{\partial w_j^1}{\partial y} \frac{\partial u_k^1}{\partial y} \right] dxdy$$

$$J_{ijk}^9 = \iint \left[\frac{\partial w_i^1}{\partial x} \frac{\partial w_j^1}{\partial y} \frac{\partial v_k^1}{\partial y} \right] dxdy$$

$$J_{ijk\ell}^{10} = \iint \left[\frac{\partial w_i^1}{\partial x} \frac{\partial w_j^1}{\partial y} \frac{\partial w_k^1}{\partial x} \frac{\partial w_\ell^1}{\partial y} \right] dxdy$$

and;

$$K_i^1 = \iint \left[\left(\frac{\partial u^0}{\partial x} + \nu \frac{\partial v^0}{\partial y} \right) \frac{\partial u_i^1}{\partial x} \right] dxdy$$

$$K_i^2 = \iint \left[\left(\nu^* \frac{\partial u^0}{\partial x} + \frac{\partial v^0}{\partial y} \right) \frac{\partial v_i^1}{\partial y} \right] dxdy$$

$$K_i^3 = \iint \left[(1 - \nu^*) \left(\frac{\partial u^0}{\partial y} + \frac{\partial v^0}{\partial x} \right) \frac{\partial u_i^1}{\partial y} \right] dxdy$$

$$K_i^4 = \iint \left[(1 - \nu^*) \left(\frac{\partial u^0}{\partial y} + \frac{\partial v^0}{\partial x} \right) \frac{\partial v_i^1}{\partial y} \right] dxdy$$

$$K_{ij}^5 = \iint \left[\left(\frac{\partial u^0}{\partial x} + \nu^* \frac{\partial v^0}{\partial y} \right) \frac{\partial w_i^1}{\partial x} \frac{\partial w_j^1}{\partial x} \right] dxdy \qquad (16)$$

$$K_{ij}^6 = \iint \left[\left(\nu^* \ \frac{\partial u^0}{\partial x} + \frac{\partial v^0}{\partial y} \right) \ \frac{\partial w_i^1}{\partial y} \ \frac{\partial w_j^1}{\partial y} \right] dxdy \tag{16}$$

$$K_{ij}^7 = \iint \left[(1 - \nu^*) \left(\frac{\partial u^0}{\partial y} + \frac{\partial v^0}{\partial x} \right) \ \frac{\partial w_i^1}{\partial x} \ \frac{\partial w_j^1}{\partial y} \right] dxdy$$

$$K_{ij}^8 = \iint \left[u_i^1 \ u_j^1 \right] \ dxdy$$

$$K_{ij}^9 = \iint \left[v_i^1 \ v_j^1 \right] \ dxdy$$

$$K_{ij}^{10} = \iint \left[w_i^1 \ w_j^1 \right] \ dxdy$$

According to Hamilton's principle, the integral of equation (14) must be an extremum. Applying the Rayleigh-Ritz method yields the following equations. For $m = 1, R$:

$$\frac{1}{2} E^* \left\{ \left[2a_m^1 J_{mm}^1 + \sum_i^R (1-\delta_{mi}) a_i^1 (J_{mi}^1 + J_{im}^1) + \sum_j^S 2b_j^1 J_{mj}^2 \right] \right.$$

$$\left. (e^{4\tau i}-1) \left(\frac{1}{2i_\omega} \right) + \left[\sum_j^T \sum_k^T c_j^1 c_k^1 \ J_{mjk}^5 \right. \right.$$

$$\left. + \sum_i^T \sum_j^T (1 - \nu^*) c_i^1 c_j^1 J_{ijm}^8 \right] \left(e^{6\tau i}-1 \right) \left(\frac{1}{3i_\omega} \right)$$

$$\left. + \left[2K_m^1 + K_m^3 \right] (e^{2\tau i}-1) \left(\frac{1}{i_\omega} \right) \right\} + \left[2a_m^1 K_{mm}^8 \right.$$

$$\left. + \sum_j^R (1 - \delta_{mj}) a_j^1 (K_{mj}^8 + K_{jm}^8) \right] \left(e^{4\tau i}-1 \right) \left(\frac{\rho^* \omega}{2i} \right)$$

$$- \left[2 bW^* J_m^4 \right] \left(e^{2\tau i}-1 \right) \left(\frac{1}{i_\omega} \right) = 0 \tag{17}$$

A-13

For m = 1, S

$$-\frac{1}{2} E^* \left\{ \left[\sum_i^R 2a_i^1 J_{im}^2 + 2b_m^1 J_{mm}^3 + \sum_i^S (1-\delta_{im}) b_i^1 (J_{im}^3 + J_{mi}^3) \right] \right.$$

$$\cdot (e^{4\tau i}-1)(\frac{1}{2i_\omega}) + \left[\sum_i^T \sum_j^T c_j^1 c_k^1 J_{mjk}^6 \right.$$

$$+ \sum_i^T \sum_j^T (1 - \nu^*) c_i^1 c_j^1 J_{ijm}^9 \left] (e^{6\tau i}-1)(\frac{1}{3i_\omega}) \right.$$

$$+ \left[2K_m^2 + K_m^4 \right] (e^{2\tau i}-1)(\frac{1}{i_\omega}) \right\} + \left[2b_m^1 \dot{K}_{mm}^9 \right.$$

$$\left. + \sum_i^S (1 - \delta_{im}) b_i^1 (K_{im}^9 + K_{mi}^9) \right] (e^{4\tau i}-1) \left(\frac{\rho^*_\omega}{2i} \right) = 0 \qquad (18)$$

For m = 1, T

$$\frac{1}{2} E^* \left\{ \left[\sum_i^R 2a_i^1 c_m^1 J_{imm}^5 + \sum_i^R \sum_j^T a_i^1 (1 - \delta_{jm}) c_j^1 (J_{ijm}^5 + J_{imj}^5) \right. \right.$$

$$+ \sum_i^S 2b_i^1 c_m^1 J_{imm}^5 + \sum_i^S \sum_j^T b_i^1 (1 - \delta_{jm}) c_j^1 (J_{ijm}^6 + J_{imj}^6)$$

$$+ \sum_i^R 2 (1 - \nu^*) a_i^1 c_m^1 J_{mmk}^8 + \sum_i^R \sum_j^T (1 - \nu^*) a_i^1 (1 - \delta_{jm}) c_j^1 (J_{jmi}^8 + J_{mji}^8)$$

$$+ \sum_i^S 2(1 - \nu^*) b_i^1 c_m^1 J_{mmi}^9 + \sum_i^S \sum_j^T (1 - \nu^*) b_i^1 (1 - \delta_{jm}) c_j^1 (J_{jmi}^9 + J_{mji}^9) \right]$$

$$(e^{6\tau i}-1)(\frac{1}{3i_\omega}) + \left[4(c_m^1)^3 (J_{mmmm}^7 + \frac{(1-\nu^*)}{2} J_{mmmm}^{10}) \right.$$

$$+\sum_{i}^{T} 3\,(c_m^1)(1 - \delta_{im})\,c_i^1\,(J_{immm}^{7} + \circ\circ\circ + \frac{(1-\nu^*)}{2}J_{immm}^{10} + \circ\circ\circ)$$

$$+\sum_{i}^{T}\sum_{j}^{T} 2\,(c_m^1)\,(1 - \delta_{im})\,(1 - \delta_{jm})\,(c_i^1 c_j^1)(J_{ijmm}^{7} + \circ\circ\circ$$

$$+\frac{(1-\nu^*)}{2}\,J_{ijmm}^{10}{}_{\circ\circ\circ}\,) + \sum_{i}^{T}\sum_{j}^{T}\sum_{k}^{T}(1 - \delta_{im})\,(1 - \delta_{jm})\,(1 - \delta_{km})$$

$$\left.(J_{ijkm}^{7} + \circ\circ\circ + \frac{(1-\nu^*)}{2}\,J_{ijkm}^{10}{}_{\circ\circ})\right]\,(e^{8\tau i}-1)\,(\frac{1}{4i_\omega})$$

$$+\left[4c_m^1(K_{mm}^{5} + K_{mm}^{6}\right.$$

$$+\frac{1}{4}\,K_{mm}^{7}) + \sum_{i=1}^{T} 2(1 - \delta_{im})c_i^1\,(K_{im}^{5} + K_{mi}^{5} + K_{im}^{6} + K_{mi}^{6}$$

$$\left.+\frac{1}{4}\,K_{im}^{7} + \frac{1}{4}K_{mi}^{7})\right](e^{4\tau i}-1)(\frac{1}{2i_\omega})\,\Bigg\}$$

$$+\left[2c_m^1 K_{mm}^{10} + \sum_{i=1}^{T}(1 - \delta_{im})c_i^1\,(K_{im}^{10} + \dot{K}_{mi}^{10})\right]\left(\frac{\rho_\omega^*}{2i}\right)$$

$$\cdot(e^{4\tau i}-1) = 0 \tag{19}$$

The notation $(\circ\circ\circ)$ indicates all permutations of the four indices.

Equations(17) - (19) can be linearized to yield the following equations:

For m = 1, R

$$\left[a_m^1 J_{mm}^1 + \sum_{i}^{R}(1 - \delta_{mi})a_i^1 J_{im}^1 + \sum_{i}^{S} b_i^1 J_{mj}^2\right]\frac{(e^{4\tau i}-1)}{2}$$

$$+ \left[K_m^1 + \frac{1}{2} K_m^3 \right] (e^{2\tau i} - 1) - \frac{2bW^*}{E^*} J_m^4 (e^{2\tau i} - 1)$$

$$+ \frac{\rho^* \omega^2}{E^*} \left[a_m^1 K_{mm}^8 + \sum_i^R (1 - \delta_{mi}) a_i^1 K_{im}^8 \right] (e^{4\tau i} - 1)$$

$$= 0 \qquad\qquad ;$$

For $m = 1, S$

$$\left[b_m^1 J_{mm}^3 + \sum_i^S (1 - \delta_{im}) b_i^1 J_{im}^3 + \sum_i^R a_i^1 J_{im}^2 \right] \frac{(e^{4\tau i} - 1)}{2}$$

$$+ \left[K_m^2 + \frac{1}{2} K_m^4 \right] (e^{2\tau i} - 1) + \frac{\rho^* \omega^2}{E^*} \left[b_m^1 K_{mm}^9 \right.$$

$$\left. + \sum_i^S (1 - \delta_{im}) b_i^1 K_{im}^9 \right] (e^{4\tau i} - 1) = 0 \quad ; \qquad\qquad (20)$$

For $m = 1, T$

$$\left[2 c_m^1 (K_{mm}^5 + K_{mm}^6 + \frac{1}{4} K_{mm}^7 + \sum_i^N (1 - \delta_{im}) c_i^1 (2 K_{im}^1) \right.$$

$$\left. + 2 K_{im}^6 + \frac{1}{4} (K_{im}^7 + K_{mi}^7) \right] \frac{(e^{4\tau i} - 1)}{2}$$

$$+ \frac{\rho^* \omega^2}{E^*} \left[c_m^1 K_{mm}^{10} + \sum_{i=1}^N (1 - \delta_{im}) c_i^1 K_{im}^{10} \right] (e^{4\tau i} - 1) = 0 \quad .$$

Again these expressions can be simplified by the careful choice of

orthogonal functions to represent the displacements.

A-16

Coordinate Functions

The coordinate functions to be used in equations (9) and (13) must satisfy the boundary conditions described by equations (4) and (5) for the equilibrium state and equations (7) and (8) for the perturbed state. Under the conditions described for the solar panel, the following boundary conditions were chosen for the equilibrium state:

on $x = \pm a$;

$$v^0 = 0 \quad ,$$

$$\frac{\partial u^0}{\partial x} + \nu^* \frac{\partial v^0}{\partial y} = \frac{N_x^0}{E^*} \quad , \tag{21}$$

on $y = \pm b$;

$$\nu^* \frac{\partial u^0}{\partial x} + \frac{\partial v^0}{\partial y} = 0 \quad ,$$

$$\frac{\partial u^0}{\partial y} + \frac{\partial v^0}{\partial x} = 0 \quad . \tag{22}$$

Because of the difficulty of finding functions whose zeroth and first order derivatives are both zero on a given boundary, it is very difficult to select functions which are orthogonal. Thus, it was decided to compromise and use the method of Lagrange multipliers to satisfy the remaining boundary conditions. On this basis, the following functions were selected for the equilibrium solution:

$$u^0 = a_0^0 x + \sum_{i=1}^{P} a_i^0 \left[x \cos \frac{(2i-1)\pi y}{2b} \right]$$

$$v^0 = \sum_{i=1}^{Q} b_i^0 \left[y \cos \frac{(2i-1)\pi x}{2a} \right] \tag{23}$$

with the following auxilliary conditions:

$$\sum_{i=1}^{P} \frac{-4ba_i^0(-1)^i}{(2i-1)\pi} - \int_{y=-b}^{y=b} \frac{N_x^0}{E^*} \, dy = 0$$

$$\sum_{i=1}^{Q} \frac{-4ab_i^0(-1)^i}{(2i-1)\pi} = 0 \tag{24}$$

The method of Lagrange multipliers is a technique for solving a set of equations resulting from a minimization process. Define a new function:

$$F = f + \ell_1 g_1 + \cdots \cdots \ell_n g_n \tag{25}$$

where f is the original function to be minimized, g_n are the auxiliary functions, and ℓ_n are the arbitrary multipliers. The function F is then minimized with respect to the original coefficients and the ℓ's, thus resulting in sufficient equations to solve for the coefficients and the multipliers.

For the equilibrium state, the following matrix equation can be written

$$\left[A^0 \right] \begin{bmatrix} a_0^0 \\ a_i^0 \\ \vdots \\ b_i^0 \\ \vdots \\ \ell_1 \\ \ell_2 \end{bmatrix} = \left[B^0 \right] \tag{26}$$

where A^0 and B^0 are matrices in terms of integrals of the coordinate functions. These can be partioned into a more convenient form.

$$A_{11}^0 = E^* I_{00}^1$$

$$A_{12}^0 = E^* I_{0i}^1$$

$$A_{13}^0 = E^* I_{0i}^2$$

$$A_{14}^0 = 0 \tag{27}$$

$$A_{15}^0 = 0$$

$$A_{22}^0 = E^* I_{ii}^1$$

$$A_{23}^0 = E^* I_{ij}^2$$

$$A_{24}^0 = \frac{-4b(-1)^i}{(2i-1)\pi} \tag{28}$$

$$A_{25}^0 = 0$$

$$A_{33}^0 = E^* I_{jj}^3$$

$$A_{34}^0 = 0 \tag{29}$$

$$A_{35}^0 = \frac{-4a(-1)^i}{(2j-1)\pi}$$

$$A_{44}^0 = 0$$

$$A_{45}^0 = 0 \tag{30}$$

$$A_{55}^0 = 0 \tag{31}$$

$$B_1^0 = 2bW*I_0^4$$

$$B_2^0 = 2bW*I_i^4$$

$$B_3^0 = 0 \tag{32}$$

$$B_4^0 = \frac{2bN_x^0}{E*}$$

$$B_5^0 = 0$$

Repeated indices in the above sub-matrices indicate that only the diagonal terms are non-zero. Note that A^0 is a symmetric matrix.

The following boundary conditions were chosen for the perturbed state, on $x = \pm a$;

$$v^1 = 0$$

$$\int_{y=b}^{y=-b} \left\{ \left[\frac{\partial u^1}{\partial x} + \frac{1}{2}\left(\frac{\partial w^1}{\partial x}\right)^2 \right] + \nu* \left[\frac{\partial v^1}{\partial y} + \frac{1}{2}\overline{\left(\frac{\partial w^1}{\partial y}\right)}^2 - \frac{N_x^1}{E*} \right] \right\} \, dy = 0 , \tag{33}$$

on $y = \pm b$;

$$\int_{x=-a}^{x=a} \left\{ \left[\frac{\partial v^1}{\partial y} + \frac{1}{2}\left(\frac{\partial w^1}{\partial y}\right)^2 \right] + \nu* \left[\frac{\partial u^1}{\partial x} + \frac{1}{2}\left(\frac{\partial w^1}{\partial x}\right)^2 \right] \right\} \, dx = 0$$

$$\int_{x=-a}^{x=a} \left\{ \left[\frac{\partial u^1}{\partial y} + \frac{\partial v^1}{\partial x} + \left(\frac{\partial w^1}{\partial x}\right)\left(\frac{\partial w^1}{\partial y}\right) \right] \right\} \, dx = 0 \tag{34}$$

A-20

Again, in order to simplify somewhat the subsequent calculations, the following coordinate functions were selected for the perturbed state:

$$u^1 = \sum_{i=1}^{R} a_i^1 \ x \cos \frac{(2i-1)\pi y}{2b} \ e^{i\omega t}$$

$$v^1 = \sum_{i=1}^{S} b_i^1 \ y \cos \frac{(2i-1)\pi x}{2a} \ e^{i\omega t} \tag{35}$$

$$w^1 = \sum_{i=1}^{T} c_i^1 \ \sin \frac{(2i-1)\pi x}{2a} \ \sin \frac{(2i-1)\pi y}{2b} \ e^{i\omega t}$$

with the following auxilliary conditions;

$$\sum_{i=1}^{R} \frac{-4ba_i^1 (-1)^i}{(2i-1)\pi} - \int_{y=-b}^{y=b} \frac{N_x^1}{E*} \ dy = 0 \ ,$$

$$\sum_{i=1}^{S} \frac{-4ab_i^1(-1)^i}{(2i-1)\pi} = 0 \tag{36}$$

$$\sum_{i=1}^{T} c_i^1 = 0$$

Note that this last relationship implies that w^1 is zero for the four corners.

The following matrix equation can now be written:

$$\begin{bmatrix} A^1 \end{bmatrix} \begin{bmatrix} a_i^1 \\ \vdots \\ b_i^1 \\ \vdots \\ c_i^1 \\ \vdots \\ \ell_1 \\ \ell_2 \\ \ell_3 \end{bmatrix} = \begin{bmatrix} B^1 \end{bmatrix} . \tag{37}$$

A^1 is a function of the perturbed coordinate functions, the natural frequencies and the equilibrium position. It can also be conveniently partioned into the following sub-matrices:

$$A^1_{11} = E^* \left(\frac{e^{4\tau i} - 1}{2} \right) \left[J^1_{ii} + 2 \frac{\rho^*}{E^*} \omega^2 K^8_{ii} - \right]$$

$$A^1_{12} = E^* \left(\frac{e^{4\tau i} - 1}{2} \right) J^2_{ij}$$

$$A^1_{13} = 0 \tag{38}$$

$$A^1_{14} = \frac{-4b(-1)^i}{(2i-1)\pi}$$

$$A^1_{15} = 0$$

$$A^1_{16} = 0 \quad .$$

$$A^1_{22} = E^* \left(\frac{e^{4\tau i} - 1}{2} \right) \left[J^3_{ii} + 2 \frac{\rho^*}{E^*} \omega^2 K^9_{ii} \right]$$

$$A^1_{23} = 0$$

$$A^1_{24} = 0 \tag{39}$$

'

$$A^1_{25} = \frac{-4a(-1)^i}{(2i-1)\pi}$$

$$A^1_{26} = 0$$

$$A^1_{33} = E^* \left(\frac{e^{4\tau i} - 1}{2} \right) \left[2(K^5_{ii} + K^6_{ii}) + 2 \frac{\rho^*}{E^*} \omega^2 K^{10}_{ii} \right]$$

$$A_{33}^1 = E* \left(\frac{e^{4\tau^i}-1}{2} \right) \left[2K_{ij}^1 \right] \qquad\qquad i \neq j$$

$$A_{34}^1 = 0 \tag{40}$$

$$A_{35}^1 = 0$$

$$A_{36}^1 = \delta_{ij}$$

$$B_1^1 = (e^{2\tau^i}-1) \left[2bW*J_i^4 - E* (K_i^1 + \frac{1}{2} K_i^3) \right]$$

$$B_2^1 = (e^{2\tau^i}-1) \left[-E* (K_i^2 + \frac{1}{2} K_m^4) \right]$$

$$B_3^1 = 0 \tag{41}$$

$$B_4^1 = \frac{2bN_x^1}{E*}$$

$$B_5^1 = 0$$

$$B_6^1 = 0$$

A^1 is a symmetric matrix. Those sub-matrices not shown are zero.

The values of the non-zero integrals from equations (14), (15) and (16) are as follows:

$$I_{00}^1 = 4ab$$

$$I_{0i}^1 = I_{i0}^1 = \frac{8ab}{(2i-1)\pi}$$

$$I_{ii}^1 = J_{ii}^1 = 2ab\left[1 + \frac{(1-\nu^*)}{24}(2i-1)^2 \pi^2 \left(\frac{a}{b}\right)^2\right]$$

$$I_{0i}^2 = \frac{8ab\nu^*}{(2i-1)_\pi} \tag{42}$$

$$I_{ij}^2 = J_{ij}^2 = \frac{16\,a\,b\,\nu^*}{(2i-1)(2j-1)_\pi 2} + \frac{(1-\nu^*)}{2}\left[\frac{(2i-1)(2j-1)_\pi^2}{ab}\right]$$

$$I_{ii}^3 = J_{ii}^3 = \frac{(1-\nu^*)}{2}\left[\frac{(2i-1)_\pi}{2a}\right]^2 \left(\frac{2ab^3}{3}\right) + 2\,ab$$

$$I_0^4 = \frac{-4a^3b}{3}$$

$$I_i^4 = J_i^4 = \frac{-8a^3b}{3(2i-1)_\pi}$$

and;

$$K_i^1 = a_0^0\left[\frac{8ab}{(2i-1)_\pi}\right] + a_i^0(2\,ab) + \nu^* \sum_{k=1}^Q \frac{16ab(b_k^0)}{\pi^2(2k-1)(2i-1)}$$

$$K_i^2 = a_0^0\left[\frac{8ab\nu^*}{(2i-1)_\pi}\right] + b_i^0(2ab) + \nu^* \sum_{k=1}^P \frac{16ab(a_k^0)}{\pi^2(2k-1)(2i-1)}$$

$$K_i^3 = (1-\nu^*)\left[a_i^0\left[\frac{(2i-1)_\pi}{2b}\right]^2 \left(\frac{2ba^3}{3}\right)\right] + \sum_{k=1}^Q \frac{16ab(b_k^0)}{\pi^2(2k-1)(2i-1)}$$

$$K_i^4 = (1-\nu^*)\left[b_i^0\left[\frac{(2i-1)_\pi}{2a}\right]^2 \frac{2ab^3}{3}\right] + \sum_{k=1}^P \frac{16ab(a_k^0)}{\pi^2(2k-1)(2i-1)} \tag{43}$$

$$K_{ii}^5 = \frac{b_\pi}{a}(2i-1)^2\left[\frac{a_0^0\pi}{4} - \frac{\nu^* b_i^0}{2(2i-1)} + \frac{\nu^* b}{2a}\sum_{k=1}^Q \frac{b_k^0}{(2k-1)}\right]$$

A-24

$$K_{ii}^6 = \frac{a\pi}{b} (2i-1)^2 \left[\frac{\nu^* a_0^0 \pi}{4} - \frac{b_i^0}{2(2i-1)} + \frac{a}{2b} \sum_{k=1}^{Q} \frac{b_k^0}{(2k-1)} \right]$$

$$K_{ii}^8 = \frac{2a^3 b}{3}$$

$$K_{ii}^9 = \frac{2b^3 a}{3}$$

$$K_{ii}^{10} = ab$$

The term $(e^{n_T i} - 1)$ can be written in terms of trigonometric functions as follows:

$$(e^{n_T i} - 1) = (\cos n_T - 1) + i \sin n_T \tag{44}$$

The real part of equation (44) is used.

Solution

First the equilibrium state is determined. The A^0 matrix is established from equations (27)-(31) and equations (42). The B^0 matrix is established from equations (32) and (42). The coefficients can be determined by solving the matrix equation (26). The displacements are given by equations (23). Once the a^0 and b^0 coefficients are known, the A^1 matrix is found from equations (38) to (40) and equations (42) and (43). The B^1 matrix is determined from equation (41) and equations (42) and (43).

The natural frequencies are those values of ω which causes the determinate of A^1 to be zero. Thus, if sufficient terms are taken in the displacement series, all the desired natural frequencies can be determined. The

corresponding natural modes are determined to within a constant

by substituting each natural frequency into the matrix equation (37)

and solving for a_i^1, b_i^1, and c_i^1 in terms of a_1^1, b_1^1 and c_1^1. Equations

(35) then give the modal shapes (with undetermined amplitudes).

The time increment τ is an arbitrary quantity to be chosen

as a parameter. It should be noted, however, that the matrix A^1

becomes singular when τ is a multiple of $\left(\dfrac{\pi}{4}\right)$. Thus τ should be

chosen smaller than this number.

Conclusions

Matrix equations for the computation of the natural freq-

uencies and modal shapes have been derived for the solar panel. The

displacements have been broken into the static deformation, due to the

imposed load, and the perturbed deformation, or vibration about the

equilibrium position.

Coordinate functions were assumed which partially satisfied

the boundary conditions. The method of Lagrange multipliers was used

to satisfy the remaining boundary conditions.

The choice of coordinate functions was somewhat abritrary.

A more complicated function would be required to adequately describe

the condition of zero vertical displacement at the drum end and non-zero

displacement (equal to the motion of the boom and end piece) at the

other end. Such a function was not felt to be necessary at this time.

References

1. Novozhilov, V. V.; Then Shell Theory; P. Noordhoff Ltd.; 1964.

2. Yu, Y. Y.; "Nonlinear Flexural Vibrations of Sandwich Plates"; The Journal of the Acostical Society of America, Vol. 34, No. 9, Part 1, Sept. 1962; pp. 1176-1183.

3. Goldenveizer, A. L.; Theory of Elastic Thin Shells; Pergamon Press; 1961, pp. 110-121.

4. Yu, Y. Y.; private communication.

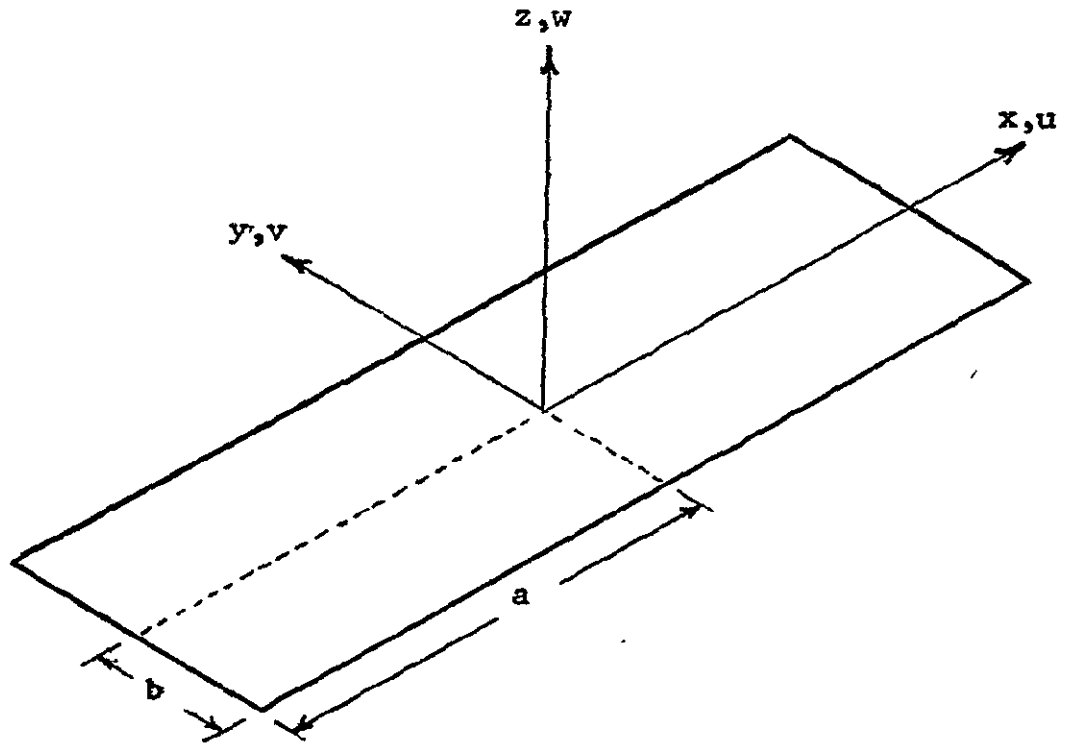5. Fung, Y. C.; Foundation of Solid Mechanics; Prentice-Hall, Inc. 1965.

Figure 1.   COORDINATE SYSTEM OF SOLAR PANEL

APPENDIX B

STRESS ANALYSIS DATA SHEET
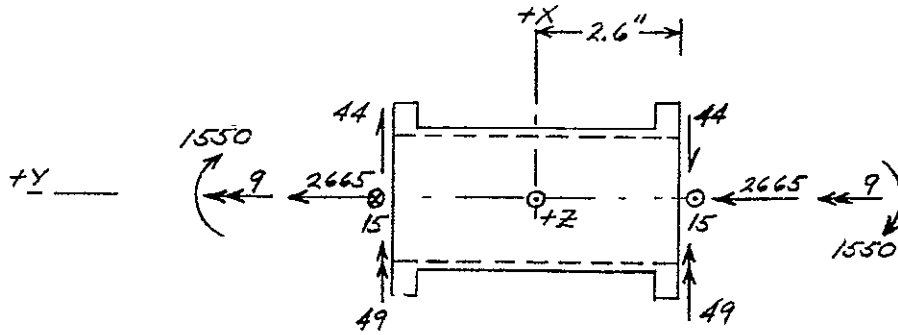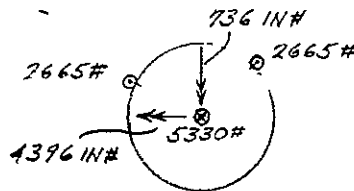
CENTER SUPPORT

"Y" DIRECTION LOADING

FIG. 1

SUPPORT TUBE APPLIED ULT. LOADING

THE AXIAL LOAD IS REACTED BY SHEAR FLOWS IN THE SIDE
PANELS. THE INDUCED MOMENTS ARE REACTED BY THE SP ...
PINS CONNECTING THE SUPPORT TUBE & SUPPORT BRACKET

"Z" AXIS COVER PLATE

$t = .063"$

―COVER PLATE TO SUPPORT
TUBE ATTACHMENTS

9-BA 5's CRITICAL IN BEARING
IN COVER PLATE

$$\frac{e}{D} = \frac{.25}{.15625} = 1.6$$

MAT'L HK31A-H24 MAG.

MIL-M-26075

$F_{SU} = 23,000$ PSI

$F_{BPU} = 49,000$ PSI $\quad e/D = 1.5$

$F_{BRU} = 57,000$ PSI $\quad e/D = 2.0$

$E = 6.5 \times 10^6$ PSI

CENTER SUPPORT

—"Z" AXIS COVER PLATE

ALLOWABLE SHEAR PER RIVET = 556 #

ALLOWABLE BRG. PER RIVET = .063 × .15625 × 50,600 = 498 #

TOTAL ALLOWABLE SHEAR LOAD = 9 × 498 = 4482

$$M.S = \frac{4482}{2665} - 1 = +.68 \text{ ULT. BRG.}$$

— SHEAR STRESS IN NET SECTION
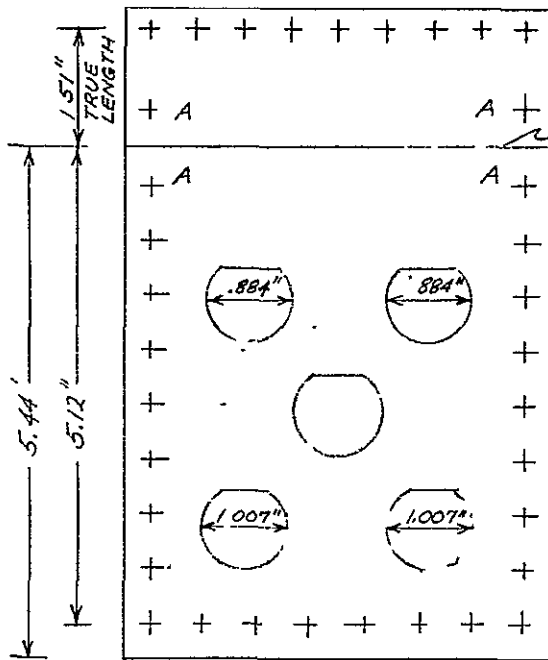
BEND LINE

MIN. NET SHEAR SECT
$$= .063 (4.5 - 2 × 1.007) = .1566 \text{ IN}^2$$

$$f_s = \frac{2665}{.1566} = 17,016 \text{ PSI}$$

$$M.S. = \frac{23000}{17016} - 1 = +.35 \text{ ULT.}$$

CENTER SUPPORT

- "Z" AXIS COVER PLATE
  - PANEL SHEAR BUCKLING

$$f_{SCR} = \frac{KE}{1-\mu^2}\left(\frac{t}{b}\right)^2 \quad REF. \ 2$$

$a = 5.12''$

$b = 4.0$

$a/b = 1.28$

$K = 6.58 \quad ALL \ EDGES \ SIMPLY \ SUPPORTED$

$f_{SCR} = 11,248 \ PSI$

$$f_s = \frac{2665}{.063 \times 4.0} = 10575 \ PSI$$

$$M.S = \frac{11248}{10575} - 1 = +.06 \quad SHEAR \ BUCKLING$$

THIS MARGIN IS CONSERVATIVE INASMUCH AS EDGES ARE SEMI-CLAMPED RATHER THAN SIMPLY SUPPORTED AND CONNECTORS WILL TEND TO STIFFEN PLATE

- COVER PLATE TO CENTER SUPPORT BRACKET ATTACHMENTS

NET SHEAR LOAD ON LONGER EDGES $= 2665 \times \frac{6.63}{4.0} = 4417 \ \#$

ALLOWABLE SHEAR LOAD FOR 10 BK5'S $= 4980 \#$

$$M.S. = \frac{4980}{4417} - 1 = .13 \quad ULT \ BEARING$$

NET SHEAR ON SHORT EDGE $= 2665 \#$

ALLOWABLE SHEAR LOAD FOR 6 BK5'S $= 3367 \# \quad e/b > 2.0$

$$M.S = \frac{3367}{2665} - 1 = .26 \quad ULT \ BEARING$$

CENTER SUPPORT.

"Y" DIRECTION LOADING

+"Z" AXIS COVER PLATE
$t = .063"$

MAT'L HK31A-H24 MAG.
MIL-M-26075

$F_{SU} = 23,000$ PSI

$F_{BRU} = 49,000$ PSI $e/D = 1.5$

$F_{BRU} = 57,000$ PSI $e/D = 2.0$

$E = 6.5 \times 10^6$ PSI

$V = 2665\#$ ULT. SHEAR LOAD
APPLIED BY SUPPORT TUBE

1.62"

BEND LINE

39"

4.84"

.64"

.8"

TRUE LENGTH

40"
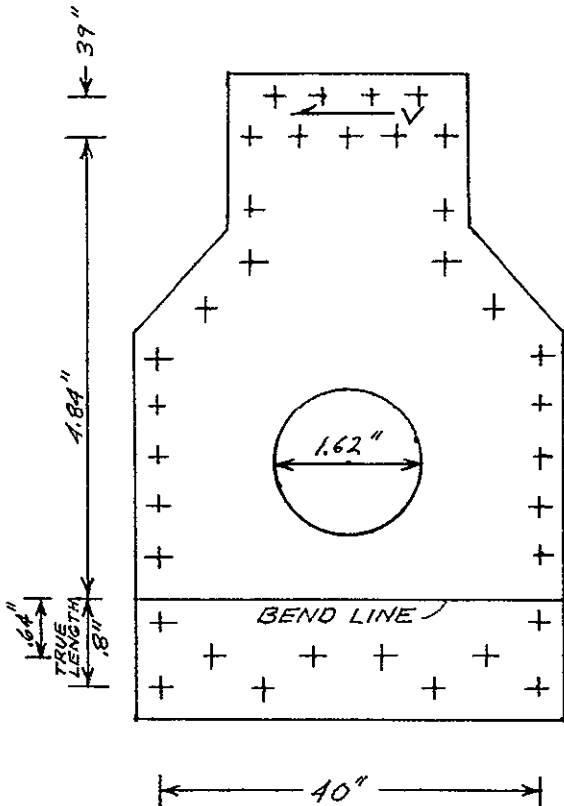
- COVER PLATE TO SUPPORT TUBE ATTACHMENTS

ALLOWABLE SHEAR LOAD FOR 6-BK5's = 2988 $e/D = 1.6$

ALLOWABLE SHEAR LOAD FOR 3-BK5's = 1683 $e/D > 2$

TOTAL = 4671

$$M.S. = \frac{4671}{2665} - 1 = +.75 \text{ ULT. BEARING.}$$

CENTER SUPPORT

+ "Z" AXIS COVER PLATE

AVERAGE SHEAR FLOW IN REMAINDER OF ATTACHMENTS

$$= \frac{2665}{4} = 666 \text{ PPI ULT.}$$

TOTAL SHEAR IN LONG EDGE OF PANEL

$$= 666 \left[\frac{.8 + .64}{2} + 2.53 + 1.31 + \frac{1}{2} \times .39 + 1.41 \right] = 4106 \text{ \# ULT.}$$

ALLOWABLE SHEAR LOAD FOR 10 BK5'S = 4980 $e/_D = 1.6$

$$M.S. = \frac{4980}{4106} - 1 = +.21 \text{ BRG. ULT.}$$

TOTAL SHEAR IN 4" PANEL EDGE = 2665#

ALLOWABLE SHEAR LOAD FOR 6 BK5'S = 3367 $e/_D > 2.0$

$$M.S. = \frac{3367}{2665} - 1 = +.26 \text{ BRG. ULT.}$$

CENTER SUPPORT TUBE

WALL & FLANGE CRITICAL FOR LOADING IN "Y" DIRECTION
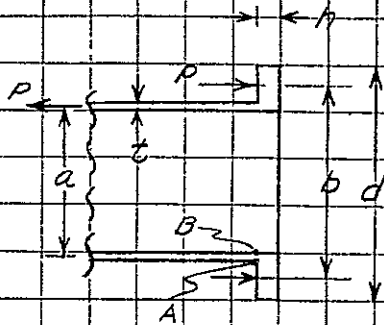
$h = .25''$ MAT'L ~ ZK 60A-T5 MAG.

$d = 4''$ QQ-M-31

$b = 3.5''$ $F_{TU} = 45,000$ PSI

$t = .1''$ $F_{TY} = 34,200$ PSI

$a = 2.78''$ $F_{CY} = 22,200$ PSI

$P = 2664 \# ULT.$

NOTE ~ 1550 IN# MOMENT (REF. FIG.1)
WERE CONSERVATIVELY NEGLECTED BE-
CAUSE FLANGE IS BACKED UP BY SUPPORT
BRACKET IN AREAS CRITICAL FOR THIS
TYPE LOADING.

$$V_0 = \frac{-2T_2(h + .5377f)P}{1.86 ft + T_1[h^2(2 + .116\,T_1 \frac{f}{t}) + 1.6103\,fh + .866\,f^2]}$$

$$M_0 = \frac{(h^2 T_1 + 1.86\,ft)V_0 + hT_2 P}{1.5\,T_1 h - 3.464\,t}$$

WHERE $f = \sqrt{a t}$, $T_1 = \frac{t^3(3a^2 + 5d^2)}{h^3(d^3 - a^3)}$, $T_2 = \frac{3.58\,t^3}{h^3(d^2 - a^2)}\left[\frac{d^2}{3}\,LN\frac{b}{a} + .1(b^2 - a^2)\right]$ REF. 2

$f = .5273$

$T_1 = .7984$

$T_2 = .04655$

$V_0 = -226.60763$ #/IN

$M_0 = +53.85313$ IN#/IN

<u>CENTER SUPPORT TUBE</u>

<u>WALL BENDING STRESS</u>

$$f_{bW} = \frac{6 M_0}{b^2} = 32,310 \text{ PSI} \quad TENS. \text{ AT "A"}$$

DIRECT STRESS IN WALL

$$f_{tW} = \frac{P}{\pi a t} = 3050 \text{ PSI} \quad TENS.$$

MAX TENSION AT "A" = 35,360 PSI ULT.

$$M.S. = \frac{45,000}{35,360} - 1 = +.27 \quad ULT.$$

$$M.S. = \frac{1.25 \times 34,000}{35,360} - 1 = +.20 \quad YIELD$$

MAX COMPRESSION AT "B" = 23,400 PSI LIMIT

$$M.S. = \frac{22000}{23400} - 1 = -.06 \quad YIELD$$

NOTE: WALL THICKNESS WAS INCREASED TO .110"

$$f_A \approx 21,400 - 2,200 = 19,200 \text{ PSI} \quad COMP. \text{ LIMIT}$$

$$M.S = \frac{22000}{19200} - 1 = +.15 \quad YIELD$$

RADIAL BENDING STRESS IN FLANGE

$$f_{bF} = \frac{6}{h^2} \left(M_0 - \tfrac{1}{2} V_0 h \right) = 7890 \text{ PSI} \quad ULT.$$

TANGENTIAL BENDING STRESS IN FLANGE

$$f_{bFT} = f_{bF} + \frac{.8}{h^2 (d^2 - a^2)} \left[d^2 \left(-.15 M_0 + 7.5 h V_0 + 1.492 P \, LN \frac{b}{a} \right) + .4475 P \left(b^2 - a^2 \right) \right]$$

$$= 8375 \text{ PSI}$$

CENTER SUPPORT TUBE

RADIAL & TANGENTIAL DIRECT STRESSES ARE NEGLIGIBLE

M.S. HIGH FOR BIAXIAL STRESS CONDITION IN FLANGE.

DRUM SUPPORT SHAFT

WALL & FLANGE CRITICAL FOR LOADING IN "Y" DIRECTION

ANALYSIS IS SIMILAR TO THAT PERFORMED FOR CENTER
SUPPORT TUBE

$h = .3"$ MAT'L ~ ZK60A-T5 MAG. QQ-M-31

$d = 4"$ $F_{TU} = 45,000 \, PSI$

$b = 3.5"$ $F_{TY} = 34,000 \, PSI$

$t = .1275"$ $F_{CY} = 22,000 \, PSI$

$a = 2.748"$

$P = 2664 + \dfrac{2 \times 1550}{3.5} = 3550 \, \# \, ULT.$

$f = .592$

$T_1 = .93238$

$T_2 = .01152$

$V_0 = -56.21182 \, \#/IN$

$M_0 = 15.41437 \, IN\#/IN$

WALL BENDING STRESS $f_{bw} = \pm 5690 \, PSI$

WALL DIRECT STRESS $f_{tw} = \pm 3225 \, PSI$

$M.S. = \dfrac{45,000}{8915} - 1 = HIGH$

M.S. HIGH FOR FLANGE BY INSPECTION

CENTER SUPPORT

"Y" DIRECTION LOADING ~ $f_y = 133$ CPS

REACTIONS AT BASE
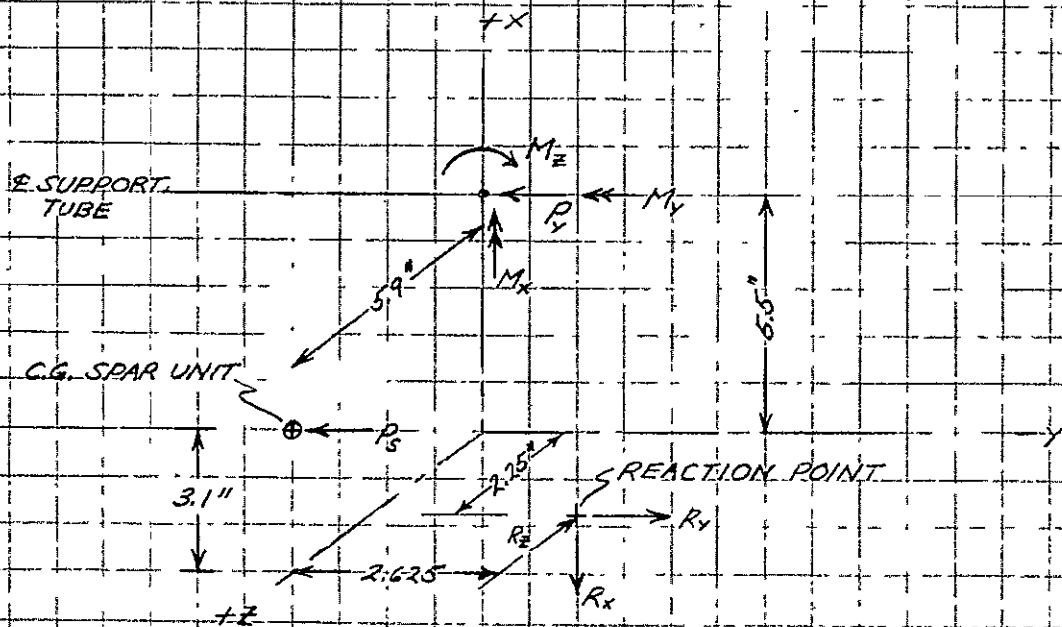
FIG. 2

P_s = DYNAMIC RESPONSE OF SPAR UNIT FOR 133 CPS MODE = 303#

LOADS APPLIED AT CENTER OF SUPPORT TUBE FOR 133 CPS MODE
(REF. FIG. 1)

$P_y = 2 \times 2665 = 5330$#
$M_x = 2 \times 49 - 2 \times 15 \times 2.6 = 20$ IN#
$M_y = 2 \times 9 = 18$ IN#
$M_z = 2 \times 1550 + 2 \times 44 \times 2.6 = 3329$ IN#

NEGLECT M_x & M_y

BY			
CK.		
DATE		REV.	

GENERAL ● ELECTRIC

PAGE

MODEL *RA-250*

REPORT

CENTER SUPPORT

REACTIONS AT BASE

$$R_x = \frac{1}{4 \times 2.625}\left[5.5 P_y + 3.1 P_3 - M_z\right] = 2564 \,\#$$

SHEAR REACTION FOR $M_{XS} = 5.9 P_3$

$$R_{YZS} = \frac{5.9 P_S}{.4 \sqrt{2.625^2 + 2.25^2}} = 129 \,\#$$

$$R_{YS} = R_{YZS} \times \frac{2.25}{3.457} = 84 \,\#$$

$$R_{ZS} = R_{YZS} \times \frac{2.625}{3.457} = 98 \,\#$$

$$R_Y = R_{YS} + \frac{5330 + 303}{4} = 1492 \,\#$$

$$R_Z = R_{ZS} = 98 \,\#$$

NET RESULTANT SHEAR REACTION = 1495 \,\#

<u>CENTER SUPPORT</u>

MAX. RESPONSE OF SPAR UNIT

REACTIONS AT BASE

THE MAX. RESPONSE OF SPAR UNIT OCCURS AT 200 CPS.
AT THIS FREQUENCY THE RESPONSE LOADS OF THE G.E.
STRUCTURE WILL BE LOW & HAVE THEREFORE BEEN NEGLECTED
IN DETERMINING BASE REACTIONS.

$$P_S = 1.25 \times 3 \times W \sqrt{\frac{\pi}{2} \times G f_n Q} \qquad 3.6 \ ULT. \ RESPONSE \ LOAD$$

WHERE

$W = 12 \ LB.$
$Q = 12$ DATA SUPPLIED BY SPAR
$f_n = 200 \ CPS$
$G = 1.7 \ g^2/CPS$

$P_S = 3602 \# \ ULT.$

LOAD DIRECTION / REACTION	"X" AXIS	"Y" AXIS	"Z" AXIS
R_x	3262	1063	1241
R_y		1901	
R_z		1167	901
RESULTANT SHEAR		2230	

<u>CENTER SUPPORT</u>

<u>BASE ATTACHMENTS</u>

FOUR $\frac{1}{4}''$ 125,000 PSI H.T. BOLTS WILL BE ADEQUATE

ALLOW. TENSION = 4080 # PER BOLT

ALLOW. SHEAR = 3680 # PER BOLT

FOR SPAR UNIT MAX. RESPONSE

$$M.S. = \frac{4080}{3262} - 1 = +.25 \text{ TENS.}$$

FOR "Y" DIRECTION LOADING USING THE INTERACTION FORMULA (REF. 1)

$$\frac{X^3}{a^3} + \frac{Y^2}{b^2} = 1$$

WHERE X = 1495 #

a = 3680 #

Y = 2564 #

b = 4080 #

M.S. = +.42 INTERACTION SHEAR & TENSION

CENTER SUPPORT

BASE PAD ANALSIS - MAX. RESPONSE OF SPAR UNIT
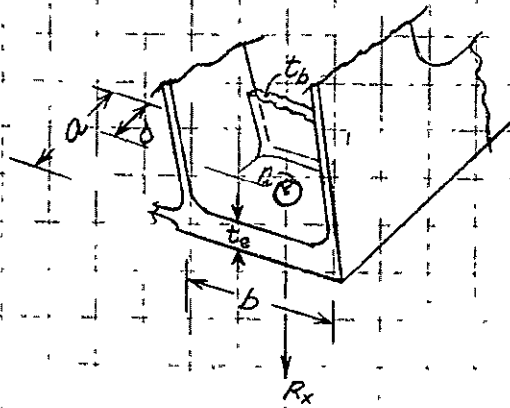
MAT'L ~ ZK 60A - T5 MAG.

QQ-M-31

$F_{TU} = 45,000$ PSI

$F_{TY} = 34,000$ PSI

$F_{CY} = 22,000$ PSI

$a = .91$ "

$d = .41$ "

$b = 1.25$ "

$t_b = .04$ "

$t_e = .25$ "

$r_o = .140$ "

BENDING STRESS IN PAD

$$f_b = \frac{R_x (2d - t_b) K_3}{t_e^2 a} \qquad (REF. 3)$$

$$= \frac{3262 (.82 - .04).74}{.25^2 \times .91} = 33105 \text{ PSI ULT.}$$

$$M.S. = \frac{45000}{33105} - 1 = +.36 \text{ ULT (CONSERVATIVE BECAUSE}$$

PLASTIC BENDING EEFECTS ARE IGNORED)

CENTER SUPPORT

MAX. SPAR UNIT RESPONSE

REACTIONS AT SPAR-G.E. INTERFACE
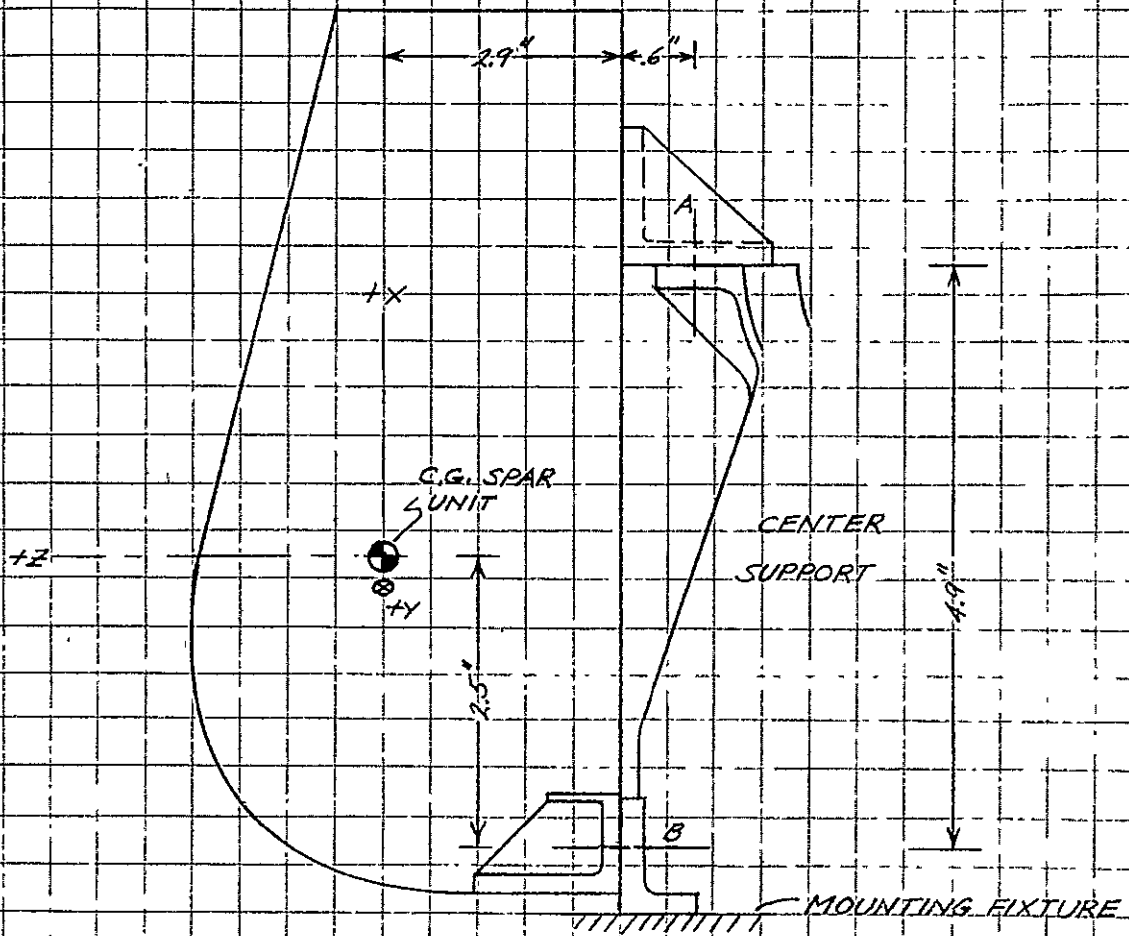
MAX. RESPONSE LOAD AT C.G. SPAR UNIT = 3602# ULT.

<u>CENTER SUPPORT</u>

REACTIONS AT SPAR-G.E. INTERFACE

+ "X" AXIS LOADING

ASSUME ALL SHEAR TAKEN BY BOLTS "B" BECAUSE OF STIFFER
LOAD PATH TO RIGID MOUNTING FIXTURE

$$V_B = \frac{3602}{2} = 1801 \# \text{ EACH BOLT}$$

$$P_B = \frac{2.9 \times 3602}{2 \times 4.9} = 1066 \# \text{ EACH BOLT}$$

$$V_A = 1066 \# \text{ EACH BOLT}$$

"Z" AXIS LOADING

$$P_B = \frac{2.4 \times 3602}{2 \times 4.9} = 882 \# \text{ EACH BOLT}$$

$$V_A = 919 \# \text{ EACH BOLT}$$

"Y" AXIS LOADING

ASSUME SHEAR IS DISTRIBUTED ACCORDING TO ELEMENTARY
THEORY TO ONE BOLT "B" AND TO ONE BOLT "A". THE SHEAR
STIFFNESS OF THE SPAR UNIT IS NOT SUFFICIENT TO DEVEL-
OPE A SIGNIFICANT M_z WHICH WOULD BE RESISTED BY A
COUPLE IN BOLTS "B"

$$V_{AY} = \frac{2.5 \times 3602}{4.9} = 1838 \# \text{ EACH BOLT}$$

$$V_B = 1764 \# \text{ EACH BOLT}$$

CENTER SUPPORT

REACTIONS AT SPAR—G.E. INTERFACE

"Y" AXIS LOADING

$$V_{A\overline{z}} = \frac{1838 \times 3.5}{3.36} = 1911 \text{ \# EACH BOLT}$$

$V_A = 2651$ # RESULTANT

$$P_B = \frac{2.9 \times 1764}{5.875} = 871 \text{ \# EACH BOLT}$$

FOUR $\frac{1}{4}$ " 150,000 PSI H.T. BOLTS ARE ADEQUATE

ALLOW. TENSION = 5328 # PER BOLT
ALLOW. SHEAR = 4415 # PER BOLT

FOR "Y" AXIS LOADING

$$M.S. = \frac{4415}{2651} - 1 = +.67 \text{ ULT. SHEAR}$$

FOR "X" AXIS LOADING USING THE INTERACTION FORMULA

$$\frac{X^3}{a^3} + \frac{Y^2}{b^2} = 1$$

WHERE $X = 1801$ #

$a = 4415$ #

$Y = 1066$ #

$b = 5328$ #

$M.S. = +1.22$ INTERACTION SHEAR & TENSION

CENTER SUPPORT

MAX SPAR UNIT RESPONSE

LOWER SPAR UNIT ATTACHMENT FITTINGS – "X" AXIS LOADING
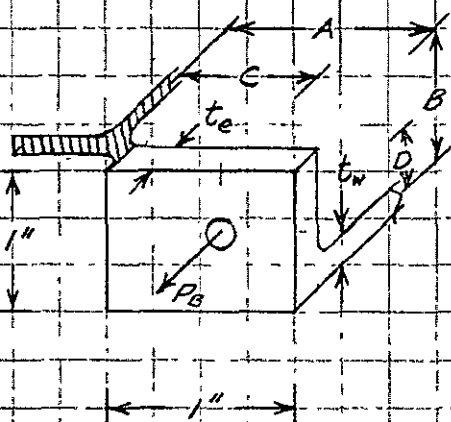
$MAT'L \sim ZK\,60A-T5\,MAG.$

$QQ-M-31$

$F_{TU} = 45,000\,PSI$

$F_{TY} = 34,000\,PSI$

$F_{CY} = 22,000\,PSI$

$F_{BRU} \approx 57,000\,PSI$ $e/D = 1.5$

$A = 1.07"$

$B = .875"$

$C = .698"$

$D = .475"$

$t_e = .190"$

$t_w = .25"$

TO CONVERT ANGLE FITTING TO EQUIVALENT BATHTUB FITTING FOR STANDARD ANALYSIS, THE FOLLOWING PROCEDURE IS EMPLOYED (REF. 3)
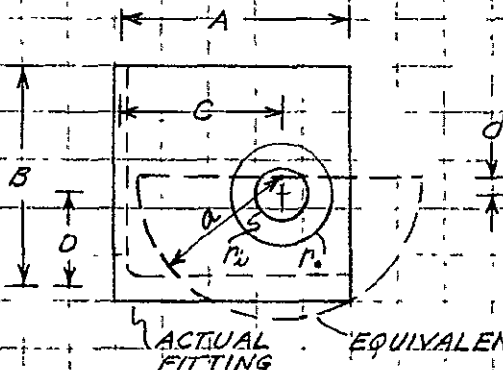
$r_b = .139$ (BOLT HOLE RADIUS)

$r_o = .219$ (BOLT HEAD RADIUS)

ACTUAL FITTING   EQUIVALENT FITTING

$$a = \frac{A+B}{\pi} = .619"$$

$$d = a - \left(\frac{C+D}{2}\right) = .033"$$

CENTER SUPPORT

LOWER SPAR UNIT ATTACHMENT FITTINGS

PAD BENDING STRESS

$$f_b = \frac{P_a}{t_e^2} K_1 K_2$$

WHERE

$P_B = 1066\# \ ULT$

$K_1 = 3.06 \quad (REF. \ 3)$

$K_2 = .345$

$f_b = 31,174 \ PSI. \ ULT$

$M.S. = \dfrac{45000}{31,174} - 1 = +.44 \ ULT.$ (CONSERVATIVE BECAUSE PLASTIC BENDING EFFECTS ARE IGNORED)

PAD BEARING STRESS — "X" AXIS LOADING

$$f_{brg} = \frac{1801}{.190 \times .25} = 37916 \ PSI \ ULT.$$

$$M.S = \frac{57000}{37916} - 1 = +.50 \ ULT. \ BRG.$$

<u>CENTER SUPPORT</u>

MAX SPAR UNIT RESPONSE

UPPER SPAR UNIT ATTACHMENT FITTINGS — "X" AXIS LOADING

FITTING LOADS (WHICH CAUSE PAD BENDING) COULD RESULT ONLY FROM + "X" AXIS LOADING WITH A VERY LOOSE FIT FOR BOLTS "B". THE LOAD PER BOLT TAKEN FOR ANALYTICAL PURPOSES ASSUMES 70% OF THE TOTAL "SHEAR" REACTION IN BOLTS "A" AND MUST BE CONSIDERED TO BE CONSERVATIVE. THE ANALYSIS IS SIMILAR TO THAT FOR THE LOWER ATTACHMENT FITTINGS.
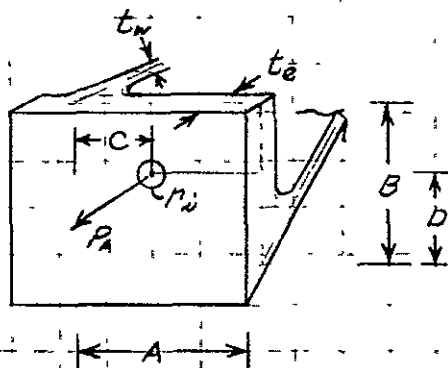
MAT'L ~ ZK60A-T5
QQ-M-31.

$A = .905$"
$B = 1.18$"
$C = .485$"
$D = .81$"
$t_e = .19$"
$t_w = .13$"
$r_w = .139$"
$r_o = .219$"

CONVERTING ANGLE FITTING TO EQUIVALENT BATHTUB FITTING (AS BEFORE)

$$a = \frac{A+B}{\pi} = .664$$

$$d = a - \frac{C+D}{2} = .016$$

CENTER SUPPORT

UPPER SPAR UNIT ATTACHMENT FITTINGS

PAD BENDING

$$f_b = \frac{P_A}{t_e^2} K_1 K_2$$

WHERE

$P_A = .7 \times 1801 = 1261 \#$ ULT.

$K_1 = 3.33$

$K_2 = .465$

$f_b = 54,076$ PSI APPARENT STRESS

ALLOWABLE APPARENT BENDING STRESS $(K_p = 1.5) = 60,000$ PSI

$$M.S = \frac{60000}{54076} - 1 = +.11 \text{ ULT.}$$ (PLASTIC BENDING EFFECTS
CONSIDERED BUT STILL CONSERVATIVE
BECAUSE OF APPLIED LOADING.)

PAD BEARING STRESS —"Y" AXIS LOADING

$$f_{bng} = \frac{2651}{.190 \times .25} = 55,811 \text{ PSI ULT.}$$

$$M.S. = \frac{57,000}{55,811} - 1 = +.02 \text{ ULT. BRG.}$$

GUIDE FLANGE

−202° F. SOAK CONDITION
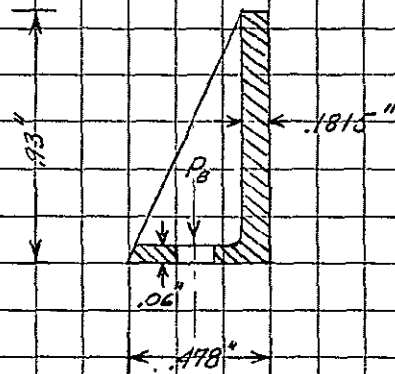
$MAT'l \sim TEXTOLITE - GR\ 11682$

$MIL-P-18177\ GEB$

$F_B = 50,000\ PSI\ MIN\ (REF.5)$

.1815"

.93"

P_B

.06"

.478"

SECT THRU BOLT HOLE

FROM COMPUTER ANALYSIS

$P_B = 92.22\#$

$f_b < 1000\ PSI\ IN\ GROSS\ SECTION$

M.S. = HIGH FOR SECTION BENDING STRESSES

SHEAR TEAR-OUT AT EDGE OF BOLT HEAD HOLE

.375"

EFFECTIVE

$EFFECTIVE\ SHEAR\ AREA = \frac{\pi}{2} \times 375 \times .06 = .0353\ IN^2$

$f_s = \frac{92.22}{.0353} = 2609\ PSI$

M.S. = HIGH FOR SHEAR TEAR-OUT

GUIDE FLANGE

$-202°F$ SOAK CONDITION

BENDING UNDER BOLT HEAD
    CONDITION IS ANALOGOUS TO FIXED CIRCULAR PLATE LOADED
    AT INNER EDGE
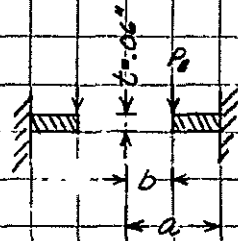
$$\frac{a}{b} = \frac{.1875}{.1} = 1.875$$

$$f_b = \frac{\beta P_B}{t^2} \quad \text{WHERE} \quad \beta = .4 \quad (\text{REF. 3})$$

$$f_b = 10,246 \; PSI$$

M.S. = HIGH FOR BENDING UNDER BOLT HEAD

MOVEABLE ARM

+ "Y" DIRECTION LOADING

LOAD-REACTION FREE BODY (ULT.)
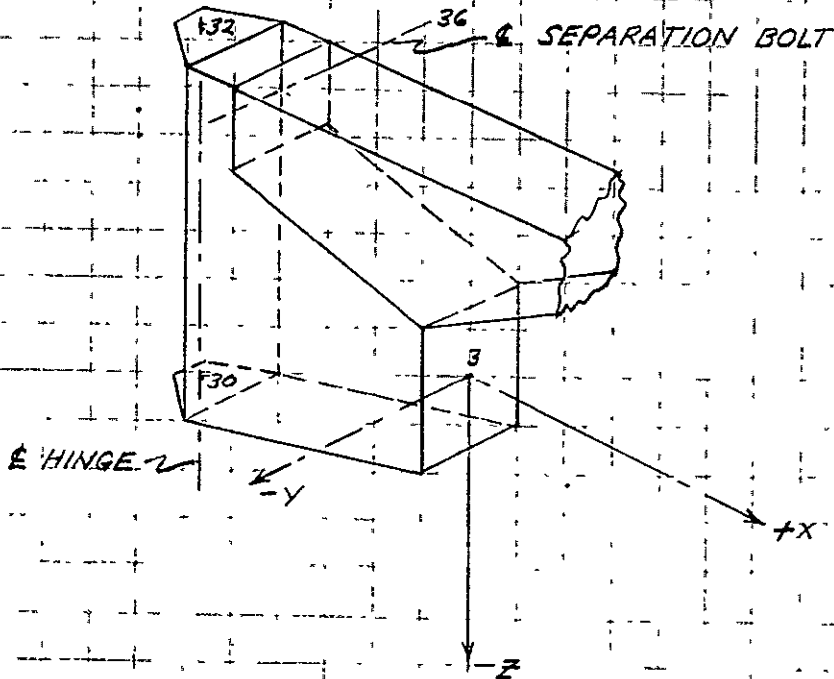
JOINT	X (#)	Y (#)	Z (#)	M_X (IN#)	M_Y (IN#)	M_Z (IN#)
3	+ 44.76	+ 680.94	− 14.84	− 774.45	− 8.60	− 612.55
36	− 44.48	− 3050.83	− 308.08	+ 21.58	− 6.00	+ 9.80
32	− 4.55	+ 2385.89	+ 322.89	~	~	~
30	+ 4.85	− 16.16	~	~	~	~

HINGE BRACKET

"Y" DIRECTION LOADING

LUG ANALYSIS (JOINT 32) (REF.4)
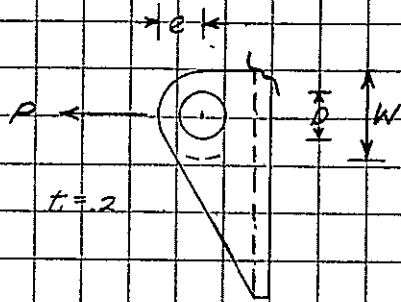
$MAT'L \sim ZK60A-T5\ MAG$

$QQ-M-31$

$F_{TU} = 45,000\ PSI$

$F_{TY} = 36,000\ PSI$

$F_{SU} = 22,000\ PSI$

$W = .76\ ''$

$D = .38\ ''$

$e = .38\ ''$

$t = .2\ ''$

$P = 1193\#\ ULT.\ EACH\ LUG.$

TENSION IN NET SECTION

$$P_U = K_T A_T F_{TU}$$

$WHERE\ A_T = .38 \times .2 = .076\ IN^2$

$K_T = .59\ FOR\ W/D = 2$

$$P_U = 2018\#$$

$M.S. = +.69\ ULT.\ TENSION$

HINGE BRACKET

"Y" DIRECTION LOADING

LUG ANALYSIS

SHEAR-OUT BEARING

$$P_{BRU} = K_{BRU} A_{BR} F_{TU}$$

WHERE $A_{BR} = .076 \, IN^2$

$K_{BRU} = .85$ FOR $e/_D = 1$ $D/_t = 1.9$

$$P_{BRU} = 2907 \#$$

$M.S. = 1.44$ ULT. SHEAR-OUT BEARING

SHEAR TEAR-OUT

$$P_U = F_{SU} A_S$$

$$= 22,000 \times .38 \times .2 = 1672$$

$M.S. = +.40$ ULT. SHEAR TEAR-OUT

HINGE PIN ~ .378" DIA.   MAT'L ~ 6AL-4V TITANIUM

MIL-T-9047

$F_{SU} = 80,000 \, PSI$

ALLOWABLE DOUBLE DOUBLE SHEAR LOAD = 17,955 #

$M.S. = HIGH$ IN SHEAR

HINGE BRACKET

"Y" DIRECTION LOADING

BOLT FITTING ANALYSIS

MAT'L ~ ZK60A-T5 MAG
QQ-M-31
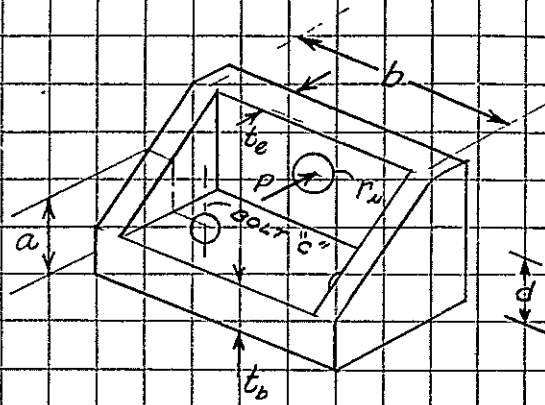
$a = .63"$
$b = 2.395"$
$d = .875"$
$t_e = .250"$
$t_b = .250"$
$r_u = .315"$ *
$P = 3051\# \ ULT.$

PAD BENDING

$$f_b = \frac{P(2d - t_b)K_3}{t_e^2 a} \qquad WHERE \quad K_3 = .365 \quad (REF. 3.)$$

$$= 42423 \ PSI \ APPARENT \ STRESS$$

ALLOWABLE APPARENT BENDING STRESS $(K_b = 1.5) = 60,000 \ PSI$

$$M.S = \frac{60000}{42423} - 1 = +.41 \ ULT.$$

* ASSUMED BOLT HOLE RADIUS WHICH CONSIDERS STIFFENING
EFFECT OF BOLT CATCHER DEVICE

FORM 1-8136 B (9-58)

B-26

HINGE BRACKET

"Y" DIRECTION LOADING

REACTIONS IN BOLTS "C"
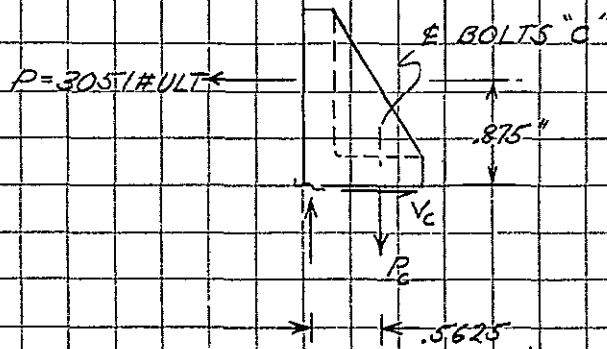
$V_C = 1526 \#$ EACH BOLT

$P_C = \dfrac{1}{2} \; \dfrac{.875 \times 3051}{.5625} = 2373 \#$ EACH BOLT

$\frac{1}{4}"$ 125,000 PSI H.T. BOLTS ARE ADEQUATE

SEPARATION BOLT

"Y" DIRECTION LOADING

BOLT FREE BODY (ULT.)
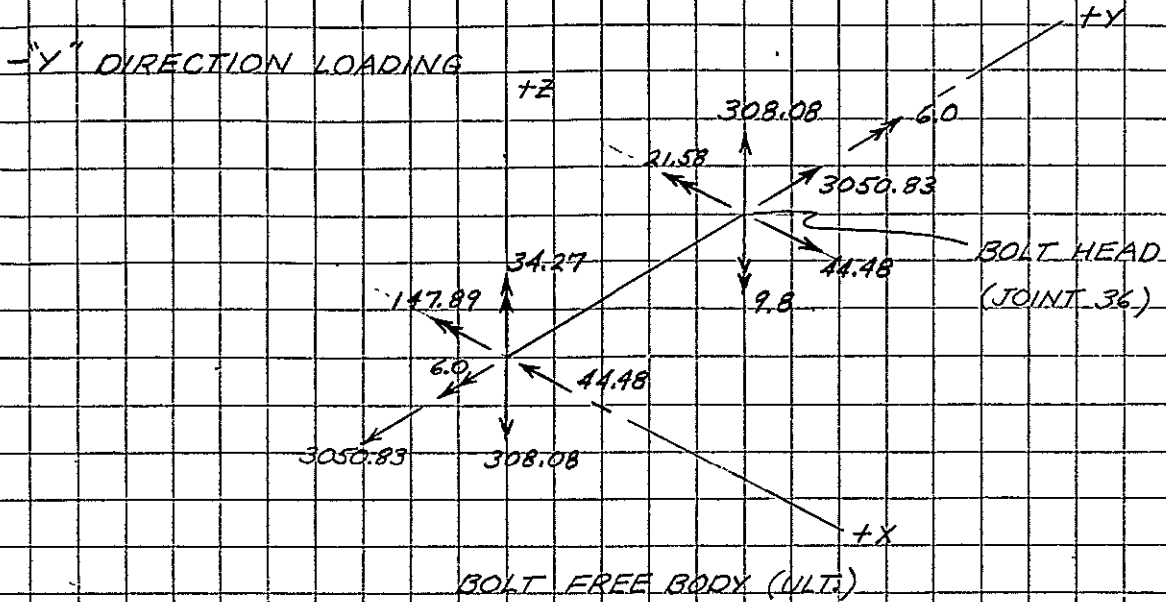
ALLOWABLE LOADS FOR $\frac{3}{8}''$ 6AL-4V TITANIUM BOLT

TENSION ~ 14,000 #

SHEAR ~ 10,500 #

BENDING ~

ULT. BENDING MOMENT $= F_B \frac{I}{C}$

THE MODULUS OF RUPTURE F_B IS DETERMINED FROM

THE EXPRESSION $F_b = f_m + f_b (K-1)$ (REF. 4) WHERE

$f_m = 160,000$ PSI

$f_b = 140,000$ PSI

$K = 1.7$ CIRCULAR SECTION SHAPE FACTOR

$F_b = 258,000$ PSI

$M_B = 258,000 \times .003336 = 861$ IN # (IN THREADS)

SEPARATION BOLT

—"Y" DIRECTION LOADING

MAX RESULTANT MOMENT = 152 IN #

MAX RESULTANT SHEAR = 311 #

$$M.S. = \frac{1}{\sqrt{(R_a + R_b)^2 + R_s^2}} - 1 \quad (REF. 4) \quad WHERE \qquad R_a = \frac{3051}{14000}$$

$$R_b = \frac{152}{861}$$

$$= +1.53 \ ULT. \ INTERACTION$$

$$R_s = \frac{311}{10500}$$

DRUM SHELL

"Y" DIRECTION LOADING

DRUM SHELL TO INBOARD END CAP ATTACHMENTS

END CAP
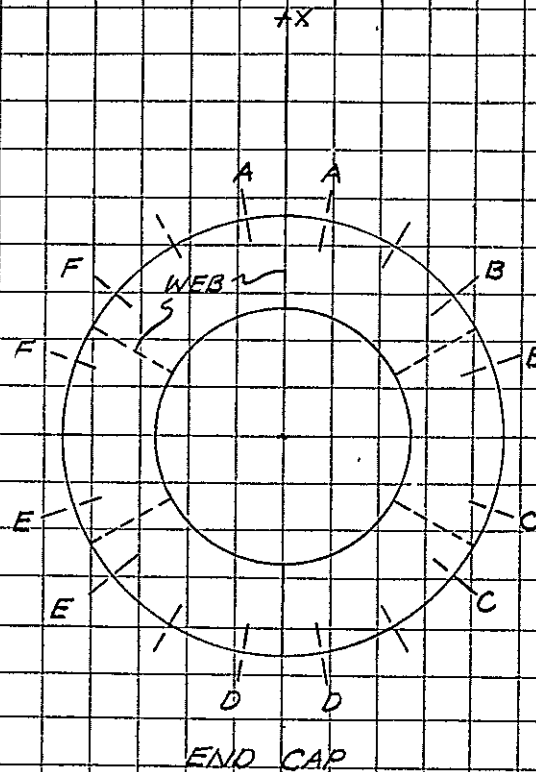
CONSERVATIVELY ASSUME THAT ALL LOAD IS TRANSFERRED
IN BOLTS IMMEDIATELY ADJACENT TO WEBS

BOLT	LOAD PER BOLT (LBS)
A	78
B	108
C	171
D	205
E	176
F	112

SHEAR LOAD/BOLT ~ "Y" DIRECTION

DRUM SHELL

DRUM SHELL TO INBOARD END CAP ATTACHMENTS

ATTACHMENTS ~ NAS-1142 BRAZIER BOLT

ALLOWABLE SHEAR IN BOLT = 1922#
ALLOWABLE BRG. IN .020" BERYLLIUM SHEET
$= .164 \times .02 \times 100,000 = 328 \#$ *(REF. 5)*
ALLOWABLE BRG. IN .060 ZK60A-T5 MAG. END CAP
$= .164 \times .06 \times 57,000 = 561 \#$ $e/D = 1.64$

$$M.S. = \frac{328}{205} - 1 = +.60 \text{ ULT. BRG. IN BE. SHEET}$$

DRUM SHELL

"Y" DIRECTION LOADING

COMPRESSION BUCKLING

THE MAXIMUM LENGTHWISE AVERAGE COMPRESSIVE STRESS IN THE SHELL IS 2202 PSI ULT.

ALLOWABLE BUCKLING STRESS

$$f_{CR} = \frac{K_c \pi^2 E}{12(1-\mu^2)} \left[\frac{t}{L}\right]^2 \quad (REF. 4)$$

WHERE K_c IS A FUNCTION OF $Z = \frac{L^2}{rt}(1-\mu^2)^{\frac{1}{2}}$ AND

$E = 44 \times 10^6$ PSI (REF. 5)
$t = .02''$
$r = 3.99''$
$L = 46.56''$
$\mu = .3$

$K_c = 5000, \quad Z = 25,917$

$f_{CR} = 36,686$ PSI

M.S. = HIGH COMPRESSIVE BUCKLING

DRUM SHELL

ANTI-SYMMETRICAL "Z" DIRECTION LOADING

BUCKLING DUE TO BENDING MOMENT

THE MAX. COMPRESSIVE STRESS DUE TO BENDING
IS 22,307 PSI ULT. AT MID-SPAN

ALLOWABLE BUCKLING STRESS

$$\frac{f_{CR}}{E} = 6 \times 10^{-4} \quad (REF.\ 4) \quad FOR \quad \frac{L}{r} = 11.67, \quad \frac{r}{t} = 200$$

$$f_{CR} = 26400 \ PSI$$

$$M.S. = \frac{26400}{22307} - 1 = +.18 \quad BUCKLING$$

BUCKLING DUE TO SHEAR

MAX. SHEAR STRESS IS 3472 PSI ULT NEAR END OF DRUM SHELL

ALLOWABLE BUCKLING STRESS

$$f_{SCR} = \frac{1.25 K_t \pi^2 E}{12(1-\nu^2)} \left(\frac{t}{L}\right)^2 \quad (REF.\ 4)$$

WHERE K_t IS A FUNTION OF $Z = \frac{L^2}{rt}(1-\nu^2)^{\frac{1}{2}}$

$$K_t = 960, \quad Z = 25917$$

$$f_{SCR} = 8805 \ PSI$$

$$M.S. = \frac{8805}{3472} - 1 = +.54 \quad SHEAR \ BUCKLING$$

INBOARD END CAP

ANTI-SYMMETRICAL "Z" DIRECTION LOADING

CRITICAL STRESS CONDITION OCCURS IN OUTER CAP AT JUNCTURE WITH RADIAL WEB. SECTION PROPERTIES ARE CONSERVATIVELY TAKEN AT WEAKEST LOCATION IN OUTER CAP

MAT'L ~ ZK60A-T5
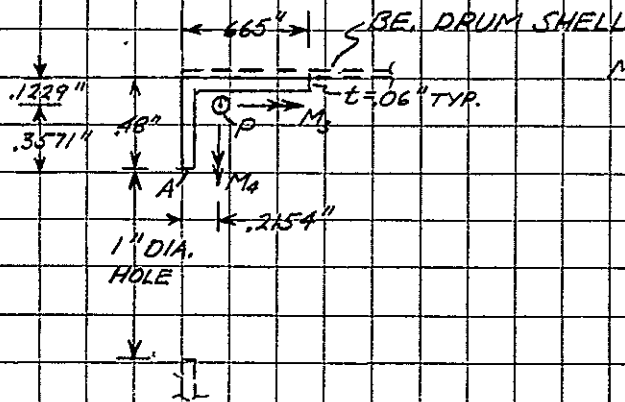
QQ-M-31

$F_{TU} = 45,000$ PSI

$F_{TY} = 34,000$ PSI

$F_{CY} = 22,000$ PSI

$A = .0651$ IN^2

$I_3 = .001271$ IN^4

$I_4 = .007814$ IN^4

$P = 264.62$ # ULT.

$M_3 = 110.14$ IN# ULT.

$M_4 = 2.30$ IN# ULT.

MAX. COMPRESSIVE STRESS AT PT. "A"

$$f_c = \frac{.3571\,M_3}{I_3} + \frac{.2154\,M_4}{I_4} - \frac{P}{A} = 30945 + 63 - 4065 = 26943 \text{ PSI ULT.}$$

$$f_c = \frac{26943}{1.25} = 21554 \text{ PSI LIMIT}$$

$$M.S. = \frac{22000}{21554} - 1 = +.02 \text{ YIELD CONSERVATIVE}$$

MINIMUM MARGINS OF SAFETY

ITEM		LOAD CONDITION	MODE OF FAILURE	MARGIN OF SAFETY
CENTER SUPPORT —	− Z AXIS COVER PLATE	"Y" AXIS	SHEAR BUCKLING	+.06
	− Z COVER PLATE, ATTACHMENTS		BEARING	+.13
	+ Z COVER PLATE, ATTACHMENTS		BEARING	+.21
	− SUPPORT TUBE BASE		WALL BENDING	+.15 YLD.
	− ATTACHMENTS	SPAR UNIT RESPONSE	TENSION	+.25
	− BASE ATTACHMENT FITTING		BENDING	+.36
	− SPAR UNIT ATTACHMENTS		SHEAR	+.67
	− SPAR ATTACHMENT FITTINGS		BENDING	+.11
	− SPAR ATTACHMENT FITTINGS		BEARING	+.02
MOVABLE ARM — HINGE BRACKET LUG		"Y" AXIS	SHEAR TEAR-OUT	+.40
	− SEP. BOLT FITTING		BENDING	+.41
	− SEPARATION BOLT		INTERACTION BEND & TENS.	+1.53
DRUM SHELL — END CAP ATTACHMENTS			BEARING	+.60
DRUM SHELL —		ANTI-SYM. "Z" DIRECT.	BUCKLING	+.18
INBOARD END CAP — OUTER FLANGE		ANTI-SYM. "Z" DIRECT.	BENDING	+.02 YLD.

REFERENCES

1). MIL-HDBK-5A, FEB. 8, 1966

2). FORMULAS FOR STRESS & STRAIN (FOURTH EDITION), R.J. ROARK

3) G.E. STRUCTURAL DESIGN DATA

4) ANALYSIS & DESIGN OF FLIGHT VEHICLE STRUCTURES, E.F. BRUHN

5) VENDOR MATERIALS PROPERTY DATA

Program.   30W/# Rollup Solar Array   Prepared by: G. Borie

System:

Subsystem: Date: 18 June 69

Module:

PART DESCRIPTION·		STORAGE DRUM
QUANTITY:		2 per array
Assumed Failure:	#1	Fails to rotate (both)
	#2	Fails to rotate (one only)
	#3	
	#4	
	#5	Main Shaft
Cause:	#1	Failed (seized) Main Shaft Bearing (pairs)
	#2	Failed Negator take-up spool bearings
	#3	
	#4	
	#5	
Effect on	#1	Solar Array Cannot be deployed fully
Components	#2	
	#3	
	#4	
	#5	
Present Compensating		
Provisions	#1	
	#2	
	#3	
	#4	
	#5	
Remarks and Recommendations:		Lubrication and bearing selection and test prove compatibility of bearing/lubricant and environment there by increasing the reliability.
Criticality		I

Program: 30W/# Rollup Solar Array

Prepared by: G. Borie

System: _____

Subsystem: _____

Module: _____

PART DESCRIPTION:	BI-STEM SOLAR PANEL ACTUATOR
QUANTITY:	1 per array

Assumed Failure:		
	#1	Boom fails to extend
	#2	Boom fails to retract
	#3	Premature extension
	#4	Boom retracts fully in orbit
	#5	Length not stable, boom erected

Cause:		
	#1	Motor electrical failure, bearing failure, extend SW fails open, retractor partial retract SW fail closed. Motor SW fails open (s1 or S3)
	#2	Motor is shorted or open, binding bearings, extend SW fails closed retract or partial retract SW fail open, motor switch (S1 or S3) fails open.
	#3	Extend SW fails closed
	#4	Full retract switch fails closed
	#5	Motor/spool gear failure

Effect on Components		
	#1	Solar array cannot be deployed
	#2	Solar array cannot be stowed
	#3	Possible BI-STEM Motor damage and or structural damage to boom
	#4	Damage to solar array
	#5	Damage to solar array

Present Compensating Provisions		
	#1	
	#2	
	#3	
	#4	
	#5	

Remarks and Recommendations:	Full retract SW should be disabled prior to launch

Criticality	I

Program: 30W/# Rollup Solar Array

Prepared by: G. Borie

System: _____

Date: 18 June 69

Subsystem: _____

Module: _____

PART DESCRIPTION:		SOLAR ARRAY BLANKET
QUANTITY:		2 per array
Assumed Failure:	#1	Physical damage
	#2	Chemical/structural change or damage
	#3	Loss of attachment to storage drum or leading edge
	#4	
	#5	
Cause:	#1	Meteorite bombardment, premature deployment, full retraction in orbit
	#2	Van Allen Belt Radiation & Solar Flares
	#3	Poor or damaged bonding
	#4	
	#5	
Effect on Components	#1	Degraded operation-time dependent
	#2	Degraded operation-time dependent
	#3	Loss of desired angle of inclination to sun
	#4	
	#5	
Present Compensating Provisions	#1	Meteorite impingement protection offered by glass filters
	#2	Filter glass over solar cells
	#3	
	#4	
	#5	
Remarks and Recommendations:		
Criticality		1 & 2 [III] 3 [I]

C-3

Program: 30W/# Rollup Solar Array   Prepared by: G. Borie

System: _____   Date: 18 June 69
Subsystem: _____
Module: _____

PART DESCRIPTION:		LEADING EDGE
QUANTITY:		1 per array
Assumed Failure:	#1 #2 #3 #4 #5	Loss of movement at attachment of boom to leading edge
Cause:	#1 #2 #3 #4 #5	Bearing seized
Effect on Components	#1 #2 #3 #4 #5	Adds undesirable loads to BLANKETS causing possible damage to cells or interconnections
Present Compensating Provisions	#1 #2 #3 #4 #5	
Remarks and Recommendations:		Lubrication and bearings chosen and tested to demonstrate compatibility of lubricant and bearing in their intended environment
Criticality		III

C-4

Program: 30W/# Rollup Solar Array   Prepared by: G. Borie

System: _____   Date: 6-18-69
Subsystem: _____
Module: _____

PART DESCRIPTION:		Outboard End Support Micro Switch (Not part of deliverable item, to be customer supplied)
QUANTITY:		2 per array
Assumed Failure:	#1 #2 #3 #4 #5	Fail Open
Cause:	#1 #2 #3 #4 #5	Broken roller
Effect on Components	#1 #2 #3 #4 #5	No indication of end support seperation.
Present Compensating Provisions	#1 #2 #3 #4 #5	Redundant switches exsist but they are connected to a single roller
Remarks and Recommendations:		
Criticality		III

Program: 30W/# Rollup Solar Array
System: _____
Subsystem: _____
Module: _____

PART DESCRIPTION:	Outboard end support

QUANTITY:	2 per array

Assumed Failure:	#1	Premature release
	#2	Failure to release
	#3	
	#4	
	#5	

Cause:	#1	Premature firing of explosive nuts, failed closed pyro switch S2 or S
	#2	Pyrotechniques fail to actuate
	2a	Hinge fails to release, hinge frozen or damaged
	2b	Pyro switch fails open (not part of deliverable equipment to be customer supplied)

Effect on Components	#1	Possible structural damage due to confined detonation
	#2	Cannot deploy solar array
	2a	Cannot deploy array
	2b	Cannot deploy array
	#5	

Present Compensating Provisions	#1	Pyro devices are assumed to be shorted to ground exterior to array SW 2 & 4 are in parallel it is assumed that they will be isolated from power source relays (N/O) external to the array.
	#2	Dual initiators with dual bridge wires and parallel switches
	2a	None
	2b	2 Pyro switches in parallel

Remarks and Recommendations:	Pyro devices must be shorted prior to activation to protect against sperious signals.

Criticality

1	2	2a	2b
II	III	I	II

C-6

Program: 30W/# Rollup Solar Array   Prepared by:___G. Bori____
  System: _____   Date:__6-18-69__
  Subsystem: _____
  Module: _____

PART DESCRIPTION:	Inboard/Outboard End Caps
QUANTITY:	2 per array

Assumed Failure:	#1	Loss of attachment bolt
	#2	
	#3	
	#4	
	#5	

Cause:	#1	Vibration
	#2	
	#3	
	#4	
	#5	

Effect on Components	#1	None
	#2	
	#3	
	#4	
	#5	

Present Compensating Provisions	#1	6 screws used to secure inboard and cap to drum. Only 4 of 6 required.
	#2	
	#3	
	#4	
	#5	

Remarks and Recommendations:	

Criticality	III

Program: 30W/# Solar Array
System: _____
Subsystem: _____
Module: _____

PART DESCRIPTION:		Center Support
QUANTITY:		1 per array
Assumed Failure:	#1	Loss of mechanical rigidity
	#2	Failure to rotate about its axis
	#3	
	#4	
	#5	
Cause:	#1	Broken weld, loose bolter nut
	#2	Bearing failure
	#3	
	#4	
	#5	
Effect on Components	#1	None
	#2	Introduction of excessive loads to blankets
	#3	
	#4	
	#5	
Present Compensating Provisions	#1	Multiple welds and nuts used
	#2	Compatability of lubricant and bearings
	#3	
	#4	
	#5	
Remarks and Recommendations:		Misalignment would require multiple failures
Criticality		III

Program: 30 W/# Rollup Solar Array

System: _____

Subsystem: _____

Module: _____

PART DESCRIPTION:		SLIP RING (POWER RINGS)
QUANTITY		4 per Array/2 per Blanket
Assumed Failure:	#1	Broken brush or Support Arm
	#2	High Resistance (Brush or Ring)
	#3	
	#4	
	#5	
Cause:	#1	Excessive loads
	#2	Contamination or Pitting
	#3	
	#4	
	#5	
Effect on Components	#1	Reduced current carrying capacity – reduced power transfer
	#2	Reduced current carrying capacity, excessive heat generation, reduced power transfer
	#3	
	#4	
	#5	
Present Compensating Provisions	#1	Redundant Brushes
	#2	Clean Assembly areas
	#3	
	#4	
	#5	
Remarks and Recommendations:		
Criticality		II/I

Program: 30 W/# Rollup Solar Array

System: _____
Subsystem: _____
Module: _____

PART DESCRIPTION:	SLIP RINGS (SIGNAL RINGS)
QUANTITY:	8 per Array/4 per Blanket

Assumed Failure:	#1	Broken Brush or Support Arm
	#2	High resistance (Brush or Ring)
	#3	
	#4	
	#5	

Cause:	#1	Excessive loads
	#2	Contamination or pitting
	#3	
	#4	
	#5	

Effect on Components	#1	Loss of thermistor signal
	#2	Reduced signal level
	#3	
	#4	
	#5	

Present Compensating Provisions	#1	None
	#2	Clean Assembly Area
	#3	
	#4	
	#5	

Remarks and Recommendations:	Loss of thermistor measurement does not degrade power output from Solar Cell Array

Criticality	III

C-10

FMECA WORK SHEET

Program: 30 W/# Rollup Solar Array

System: _____

Subsystem: _____

Module: _____

Prepared by: G. Borie

Date: 6-18-69

PART DESCRIPTION:		NEGATOR MOTOR
QUANTITY:		1 Per Array
Assumed Failure:	#1	Loss of required tension
	#2	
	#3	
	#4	
	#5	
Cause:	#1	Broken or stretched spring
	#2	
	#3	
	#4	
	#5	
Effect on Components	#1	Introduction of undesirable first mode resonant frequencies and possible incorrect solar angle of incidence.
	#2	
	#3	
	#4	
	#5	
Present Compensating Provisions	#1	
	#2	
	#3	
	#4	
	#5	
Remarks and Recommendations:		
Criticality		I

Program: 30 W/# Rollup Solar Array

System: _____

Subsystem: _____

Module. _____

Prepared by: G. Borie

Date: 6-18-69

PART DESCRIPTION:	FOAM BUTTONS (RTV 560)
QUANTITY:	
Assumed Failure: #1 #2 #3 #4 #5	Loss of adhesion to Kapton substrate
Cause: #1 #2 #3 #4 #5	Insufficient oven curing or contamination
Effect on Components #1 #2 #3 #4 #5	Possible damage to selected solar cells and glass coverings during deployment and retraction maneuvers.
Present Compensating Provisions #1 #2 #3 #4 #5	
Remarks and Recommendations:	These items undergo 100% inspection prior to blanket assembly.
Criticality	III

C-12

GENERAL ⊛ ELECTRIC

SPACE DIVISION

SPACE SYSTEMS ORGANIZATION

APPENDIX C

FAILURE MODE, EFFECT,

AND CRITICALITY ANALYSIS

WORK SHEETS